Journal of Environmental Chemical Engineering 14 (2026) 124571

Contents lists available at ScienceDirect

Journal of Environmental Chemical Engineering

journal homepage: www.elsevier.com/locate/jece

Recent advancements of bismuth-based materials in piezo-(photo)catalytic: Mechanism, advances, and applications

Jialin Jia [a], Xiaoyu Pu [a], Tianxin Wang [a], Xingang Wang [a,*], Dong Li [b,c,**]

[a] School of Environmental and Chemical Engineering, Jiangsu University of Science and Technology, Zhenjiang 212100, China
[b] Yantai Research Institute, Harbin Engineering University, Yantai 264006, China
[c] College of Materials Science and Chemical Engineering, Harbin Engineering University, Harbin 150001, China

ARTICLE INFO

Keywords:
Bismuth-based materials
Piezocatalysis
Piezo-photocatalysis
Modification
Application

ABSTRACT

Piezoelectric catalysis promotes redox reactions by using piezoelectric polarized charges induced by mechanical stress, while piezo-photocatalysis synergistically enhances carrier separation efficiency and catalytic activity by coupling the piezoelectric effect with the photoexcitation effect. Recent years, bismuth-based catalysts have shown broad application prospects in the fields of piezo-(photo)catalytic due to their unique electronic structure, environmental friendliness and intrinsic piezoelectricity and photocatalytic activity. Herein, this review systematically covers the fundamentals of bismuth-based catalysts mediated piezo-(photo)catalysis and the mechanisms, including the regulation of the built-in electric field, the optimization of the band structure and the interface charge transfer path. The design strategies and modification methods such as defect project, metal/nonmetal doping and constructing heterojunctions of bismuth-based piezo-(photo)catalysts were also summarized. The review then proceeds to outline significant advances in piezo-(photo)catalysis, spanning the fields of water environment restoration (removal of dyes, antibiotics, heavy/radioactive metal and bacteria), energy conversion (production of H_2 and H_2O_2, CO_2 reduction) and biomedical therapy (kill cancer cells and bacterial infection). Finally, the review culminates in a forward-looking perspective on the prevailing challenges and potential future trajectories.

1. Introduction

The accelerated pace of economic development has resulted in the discharge of substantial quantities of hazardous chemicals into the natural environment, causing a steady worsening of environmental issues. Simultaneously, the high rate of non-renewable energy consumption serves to intensify a multifaceted crisis encompassing energy supply, greenhouse gas levels, and environmental health. Consequently, as paramount challenges of the contemporary era, it is imperative that environmental pollution and the energy crisis are addressed with urgency [1]. It is widely recognized that catalytic technology serves as the fundamental driver of the modern chemical industry, with over 80% of global chemical manufacturing is facilitated by catalytic processes. Hence, the exploration and development of catalytic technologies powered by clean energy is of paramount importance to address environmental pollution and thereby mitigate the energy crisis.

Since Fujishima and Honda firstly reported the study of TiO_2 photoelectrodes in 1972, photocatalytic oxidation technology has received widespread attention since it exhibited outstanding ability which can convert solar energy into chemical energy, this endows it with growth potential and persistent vitality to solve energy and environmental pollution challenges [2]. Under light irradiation, semiconductor photocatalysts with an appropriate bandgap (Eg) can produce photogenerated electron (e^-)–hole (h^+) pairs, triggering a series of chemical reactions to generate active species for pollutant treatment and energy conversion, which has been widely investigated and attained considerable achievement [3,4]. Nevertheless, the relatively low quantum efficiency and lackluster response in the absence of light irradiation severely restricts the practical application of photocatalytic technology. The rapid recombination of photogenerated electron-hole (e^--h^+) pairs on the surface and in the bulk phase of photocatalysts is an important issue affecting the efficiency of photocatalysis, which can lower the photocatalytic efficiency [5]. Therefore, the key focus of the photocatalysis is how to accelerate the separation rate of photoinduced

* Corresponding author.
** Corresponding author at: Yantai Research Institute, Harbin Engineering University, Yantai 264006, China.
E-mail addresses: hofs@just.edu.cn (X. Wang), lidong890210@126.com (D. Li).

https://doi.org/10.1016/j.jece.2026.124571
Received 14 May 2026; Received in revised form 30 July 2026; Accepted 10 August 2026
Available online 11 August 2026

carriers. Additionally, another drawback of photocatalysis is that the reaction is highly dependent on light, as an intermittent energy, the uneven distribution and regional characteristics of sunlight result in its better application only in specific areas. And once the illumination ceases, the production of reactive species stop immediately, which make photocatalysis difficult to realize all-weather continuous reaction.

Recent years, piezoelectric catalysis has been demonstrated as an efficient catalytic strategy that complements and augments traditional sunlight-driven photocatalytic processes, since it can utilize the lattice of piezoelectric nanocrystals to generate a piezoelectric polarization field, which enhances charge carrier separation and facilitates redox reactions. In 1880, Jacques and Pierre Curie firstly discovered the piezoelectric effect. By applying an external force to the piezoelectric material along its asymmetric direction, the material will undergo deformation, and subsequently positive and negative charges will be generated on the opposite surfaces of piezoelectric material [6]. In this way, mechanical energy was successfully converted into chemical energy. Obviously, piezoelectric materials, which generate an electric field when undergoing deformation under external mechanical forces, are the core of piezoelectric technology. At present, piezoelectric materials mainly include ABO_3-type perovskites (where A represent alkaline/rare-earth metal, and B represent transition metal, such as lead zirconate titanate-based materials ($Pb(Zr_{1-x}Ti_x)O_3$, potassium niobate ($KNbO_3$), barium titanate ($BaTiO_3$)), nonperovskite-like wurtzite (GaN and ZnO), piezoelectric polymers (polyvinylidene fluoride (PVDF) and polytetrafluoroethylene (PTFE)), 2D layered transition-metal dichalcogenide--based piezocatalysts MX_2 (where M represent transition metal, e.g., W, Mo, and X represent S, Se, S, Te), and bismuth-based piezoelectric catalyst [1]. Owing to the proper band gap (Eg~2.4 eV) and the inherent ferroelectricity, some bismuth-based materials possess competitive piezoelectric properties and photocatalytic properties simultaneously, such as BiOX (X = Cl, Br, I), $BiVO_4$, Bi_2MoO_6, Bi_2WO_6, $Bi_4Ti_3O_{12}$, bismuth-based perovskite materials ($Na_{0.5}Bi_{0.5}TiO_3$), and et al. [7]. Research on bismuth-based materials in the fields of piezo-(photo) catalysis has received increasing attention. Particularly, bismuth-based materials which feature a distinctive layered architecture composed of alternating $[Bi_2O_2]^{2+}$ slabs and anionic species or groups [8,9]. This arrangement endows them with a unique crystalline framework, diverse atomic coordination environments, and a desirable hybrid electronic band structure [10,11]. Owing to this structural versatility, such materials can be readily tailored through crystal engineering to achieve specific crystallographic orientations. This facilitates precise control over exposed facets, band gap tuning, and defect manipulation—strategies that hold significant promise for applications in solar energy conversion catalysis. Moreover, the low tolerance factor in bismuth-based oxides induces a lattice mismatch among cations, which results in considerable spontaneous polarization and a high piezoelectric coefficient at room temperature [12]. Additionally, the narrow band gap, environmentally friendly and non-toxic characteristics have made bismuth-based materials a popular choice for research in the fields of piezo-(photo)catalysis for environmental remediation (such as the degradation of organic pollutants and sterilization [13–15]), energy conversion (such as splitting water to produce hydrogen and CO_2 reduction) [16–18], and recently, there have also been studies applying piezoelectric catalysis to biomedical therapy, which involves using the electric field and reactive oxygen species (ROS) generated by nano-piezoelectric materials under the action of ultrasound to sterilize human tissues or organs, as well as to kill cancer cells [19–21].

Despite there have been many studies on piezo-(photo)catalysis mediated by bismuth-based materials, comprehensive reviews systematically covering category, design, optimization, mechanism and application of bismuth-based materials in piezo-(photo)catalysis area remain scarce. For instance, Jia et al. [22] have conducted a review which comprehensively summarizes the piezoelectric catalysis and piezo-photocatalysis technologies from material design to application. However, the review covers a very wide range of catalytic material systems (including various inorganic and organic piezoelectric materials), and the discussion on bismuth-based materials is relatively scattered, failing to present the unique advantages and design paradigms of bismuth-based materials as an independent material family. The review of Cheng et al. [23] mainly focuses on the application of bismuth-based materials in the fields of piezoelectric catalysis, photocatalysis, and piezo-photocatalysis for the degradation of organic pollutants, while the review did not systematically discuss the structure-activity relationship of the materials. Chen et al. [24] mainly conducted a systematic summary of the piezoelectric catalytic of $BiFeO_3$. However, the material system covered in this review was limited (only $BiFeO_3$ and its modified forms), and its application is limited to water treatment only. In contrast, this review focuses on the relationship between the crystallography and piezoelectricity of bismuth-based materials (particularly, layered bismuth-based materials), conducted a detailed discussion on the decisive influence of the asymmetric polarization between the $[Bi_2O_2]^{2+}$ layers in the layered structure and the halogen/other anion layers on its piezoelectric response. The possible advanced piezo-(photo) catalysis mechanistic of bismuth-based materials have also been systematically summarized. Moreover, unlike the existing reviews on bismuth-based piezo-(photo)electric catalysis, which mainly focus on environmental remediation (degradation of organic pollutants), this review expands on this basis and systematically explores the applications of piezo-(photo)electric catalysis on energy conversion (H_2 and H_2O_2 production, CO_2 reduction) and biomedical therapy. The systematic review and mechanism analysis of these application directions are lacking in the existing reviews.

2. Piezoelectric effects

The conventional piezocatalytic process can typically be summarized in the following steps: under mechanical stimulation such as stirring or ultrasonic vibration, the piezoelectric material produces a built-in electric field, which propels free electrons (e^-) and holes (h^+) to migrate toward its surface. This process initiates redox reactions that generate ROS, thereby driving subsequent reactions such as pollutants degradation, water splitting, CO_2 reduction, and bacterial inactivation [25,26]. The piezoelectric effect can be categorized into two forms: the direct (positive) and the converse (inverse) piezoelectric effects. As illustrated in Fig. 1a, the direct effect occurs when mechanical energy is applied to a piezoelectric material, leading to electrode polarization and the transformation of mechanical energy into electrical energy [27]. While, in the inverse piezoelectric effect, the application of an external electric field induces a mechanical deformation in the material, effecting a conversion of electrical energy to mechanical energy [28,29].

Hong et al. first reported in 2010 that H_2 could be produced via water splitting driven by a piezopotential, which was created by $BaTiO_3$ microdendrites and ZnO microfibers under ultrasonic irradiation, and proposed the piezoelectrochemical (PZEC) effect as a mechanism for directly converting mechanical energy into chemical energy [30]. Under the action of ultrasonic, ZnO microfibers and $BaTiO_3$ microdendrites undergo deformation, then a strain-induced electric potential generated on their surface, triggered redox reactions through the transfer of free surface charges (Fig. 1b). In 2013, Starr et al. performed a comprehensive theoretical analysis of the piezocatalytic process based on frameworks from semiconductor physics, piezoelectricity, molecular orbitals, and electrochemistry. The study demonstrated that to achieve high electrochemical activity, piezoelectric materials should possess a low conductivity, high voltage coupling coefficient, and a suitable dielectric constant, thereby balancing piezoelectric and capacitive effects [31].

Among the three categories of piezoelectric materials (inorganic, organic and composite materials), inorganic piezoelectric materials are subdivided into piezoelectric crystals and ceramics, with piezoelectric crystals typically denoting single-crystal structures. Owing to its high cost and substantially inferior piezoelectric coefficient relative to piezoelectric ceramics, its application is confined exclusively to high-

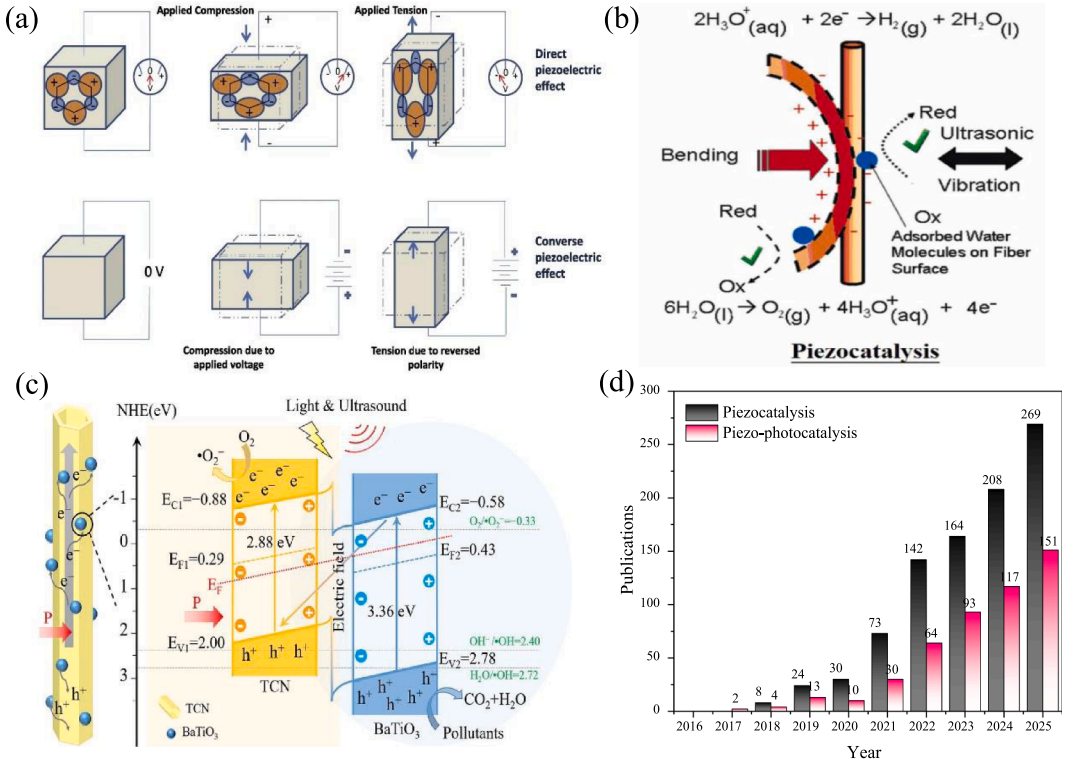

Fig. 1. (a) Schematic diagram of positive and inverse piezoelectric effect, Reproduced with permission from Ref. [27]. Copyright 2018 Elsevier. Possible Mechanisms of (b) piezocatalysis, Reproduced with permission from Ref. [31]. Copyright 2013 Nature. (c) piezo-photocatalysis, Reproduced with permission from Ref. [36]. Copyright 2023 Elsevier. (d) Publication statistics for piezocatalysis and piezo-photocatalysis covering the years 2016–2025. The data were sourced from the Web of Science based on keyword searches for "piezocatalysis" and "piezo-photocatalysis".

precision standard instruments or sensors. Piezoelectric ceramics, which are polycrystalline materials, include compounds such as ZnO, $KNbO_3$, barium titanate (BTO), and lead zirconate titanate (PZT) [32,33]. Despite exhibiting drawbacks like high brittleness, low fatigue resistance, and limited temperature stability, their outstanding piezoelectric properties ensure they remain highly important for applications in actuators, sensors and transducers. However, conventional piezoelectric ceramics like PZT contain lead (Pb), a substance detrimental to both environmental and human health. This not only violates environmental regulations but also restricts their broad applicability. There is a critical need for the extensive development and research of lead-free piezoelectric ceramics. In parallel, organic piezoelectric materials—commonly referred to as piezoelectric polymers—encompass polyamide (PA), cellulose, PVDF, polylactic acid (PLA) and their derivatives [34]. Piezoelectric composite materials are fabricated by integrating piezoelectric ceramics and polymers in specific configurations, with defined volume-to-mass ratios and spatial arrangements. These composites overcome the limitations associated with single-phase piezoelectric materials, significantly enhancing their piezoelectric performance and enabling a broader range of practical applications [35].

3. Piezo-photocatalysis technology

The integration of piezoelectric materials with photocatalysts is regarded as an effective strategy to facilitate the separation and transportation of photo-generated charge carriers. Piezoelectric materials are capable of producing an IEF when subjected to mechanical strain. This induced field acts as a driving force that facilitates the movement of photo-generated charge carriers within the bulk and across the surface of photocatalysts, thereby enhancing their separation rate. This novel catalytic approach, which harnesses both solar and mechanical energy concurrently, is termed 'piezo-photocatalysis'. Gong et al. constructed a $BaTiO_3$/g-C_3N_4 (TCN) piezo-photocatalyst and used it for the removal of tetracycline hydrochloride (TCH) under ultrasonic vibration and visible light (VL) illumination [36]. Under ultrasonic vibration, polarization electric fields were generated in both TCN and $BaTiO_3$. These fields sustained the built-in electric field strength at the heterojunction interfaces, greatly improved the migration of photogenerated carriers, resulting in a synergistic catalytic effect of the dual piezoelectric materials under VL irradiation (Fig. 1c).

Typically, piezo-photocatalysts are realized through piezoelectric/semiconductor composite structures, most commonly in core–shell configurations. In such designs, the core is made of piezoelectric materials such as $BaTiO_3$, ZnO or $NaNbO_3$, and the shell is formed from visible-light photocatalysts like FeS, CuS or Ag_2O. Some piezocatalysts featuring narrow bandgaps also exhibit photocatalytic capabilities (such as $BiFeO_3$) [37]. This means a single catalyst possesses both photocatalytic and piezoelectric properties simultaneously, enabling it to simultaneously produce photo-induced charges and piezopotential. Under light irradiation, not only are photogenerated e^--h^+ pairs produced, but a strain-induced polarization electric field is also formed. In this way, the photogenerated charge carriers are effectively separated, and the surface reduction and oxidation reactions are enhanced.

Study on piezo-(photo)catalysis remains in its early stages. The annual publication number for piezo-(photo)catalysis research between 2016 and 2025 is illustrate in Fig. 1d. The search period for the literature is from January 1st of one year to January 1st of the following year using the Web of Science Core Collection database. The search strategy employed the following query in the topic field of "bismuth + piezocatalysis" and "bismuth + piezo-photocatalysis", and the document types were restricted to "Article" and "Review" to ensure the inclusion of peer-reviewed original research and reviews. The data exhibits a sharp upward trend, indicating the growing prominence of piezo-(photo)catalysis in energy and environmental science amid the contemporary global energy predicament. Despite the relatively brief

period of investigation, significant advancements have been made in this field, and it has progressively emerged as a prominent research focus. Beyond conventional piezoelectric materials such as wurtzite, perovskite and piezoelectric polymer, some emerging novel piezoelectric materials are also demonstrating efficacy as efficient catalysts. The research on new piezoelectric catalysts is increasing year by year, reflecting the growing interest among researchers in exploring and developing new materials in this field.

4. Advanced mechanistic understanding beyond conventional piezo-(photo)catalysis

The mechanisms of piezocatalysis are still controversial, with the main theories being energy band theory and the screening charge effect [38]. In accordance with energy band theory, the redox reaction is governed primarily by the energy band levels, while the piezopotential is employed to trigger the reaction by modulating the band structure and steering the internal charge carriers to the catalyst surface. Analogous to photocatalysis, band theory grounds piezocatalytic activity in the band structure, while the screening charge effect stresses the piezoelectric potential–surface charge interaction. The main difference between these two theories lies in the source of the reactive charge carriers: intrinsic to the material in the first case, and externally adsorbed in the second. Apart from the two main mechanisms, recently, the ferroelectric domain effect and the flexoelectric effect have also been employed to explain the enhanced piezo-(photo)electric catalytic mechanism.

4.1. Energy band theory

According to energy band theory, piezocatalysis resembles photocatalysis, as the degradation of pollutants proceeds via redox reactions that are mediated by charge carriers. In photocatalysis, photon absorption excites electrons from the VB to the CB, leaving behind holes. These holes can either oxidize water to generate ·OH or directly attack organic pollutants. Meanwhile, the excited electrons reduce dissolved oxygen to yield $O_2^{\bullet-}$ [39]. Whereas photocatalysis uses light, piezocatalysis employs external mechanical energy for the excitation of charge carriers. For instance, at the catalyst/water interface, ultrasonic waves can induce local pressures greater than 10^8 Pa, which enables the excitation of electrons [40]. Cavitation—vapor bubble formation and collapse arising from rapid liquid pressure drops—in turn produces transient “hot spots” in water, enabling thermal excitation of e^- [41]. Fig. 2a shows e^- excitation from the VB to the CB under ultrasound, with h^+ left behind. Furthermore, intrinsic defects present in the catalyst also represent an important reservoir of free charge carriers. Upon introduction of anionic defects into the crystal lattice, the system counteracts the resultant charge imbalance through the redistribution of electrons, consequently generating surplus free e^- [24,42]. Cationic defects likewise increase the hole concentration, which is a frequent finding in doping studies [43]. These carriers, propelled by the piezopotential, move to the surface and improve catalytic reactivity (Fig. 2b) [24,44].

4.2. Screening charge effect

The screening charge effect, in contrast, focuses on the piezopotential and the dynamic redistribution of surface screening charges. These

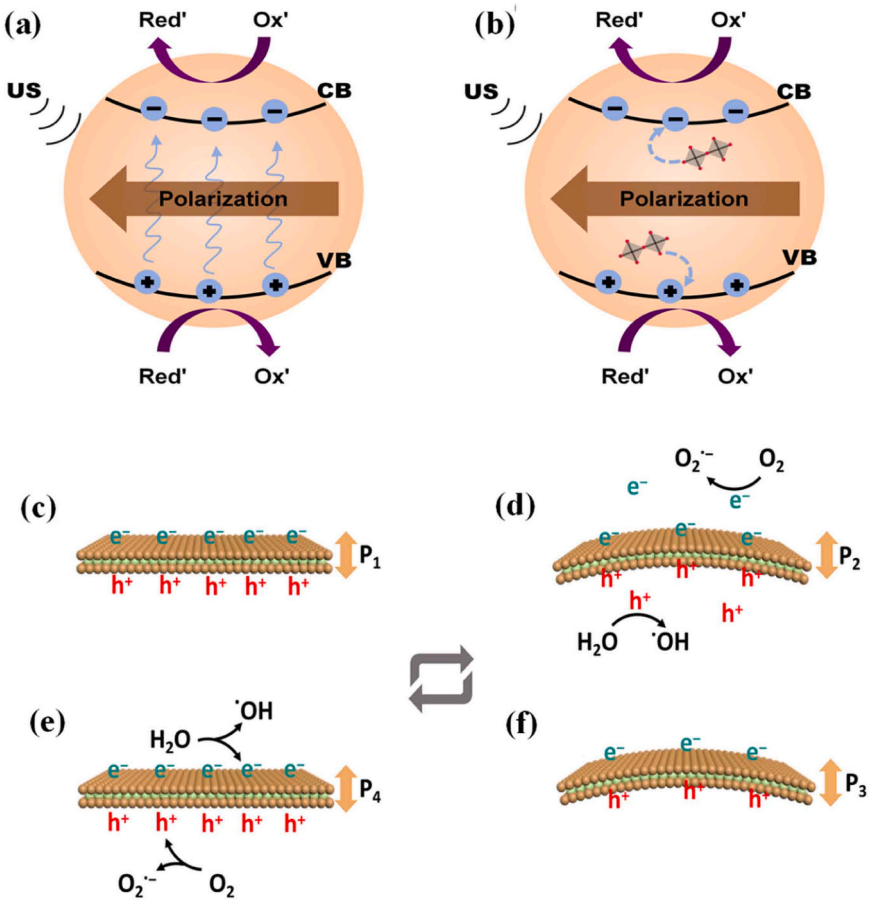

Fig. 2. Schematic illustration of (a-b) the energy band theory and (c-f) the screening charge effect. (a-f) Reproduced with permission from Ref. [24]. Copyright 2025 Elsevier.

charges are adsorbed species that offset the bound charges generated by spontaneous polarization in ferroelectric materials. Fig. 2c-f show how the piezocatalyst produces ROS under ultrasonic stimulation, with the dynamic process being governed by the screening charge effect [24]. Initially, piezoelectric materials are charge-compensated by the polarization-induced bound charges and their associated screening charges on both polar surfaces (Fig. 2c). Upon application of external stress, the material deforms, resulting in a polarization change driven by its asymmetric crystal structure. The screening charges on the surface are then discharged into the ambient solution to preserve charge balance, these charges engage in various reactions, one of which is the reduction of dissolved oxygen by electrons to generate $O_2^{\bullet-}$ (Eq. (1)), whereas oxidative holes either oxidize water to ·OH or directly assault organic pollutants (Eq. (2)) (Fig. 2d). These processes carry on until a new equilibrium is reached (Fig. 2e). Once the periodic stress is removed, the material regains its original polarization by re-adsorbing space charges from the electrolyte to replenish the bound charges, whereas opposite-polarity charges persist in the solution and remain active in redox processes (Fig. 2f).

$$e^- + O_2 \rightarrow O_2^{\bullet-} \quad (1)$$

$$h^+ + OH^- \rightarrow OH \quad (2)$$

The two mechanisms are commonly invoked to explain piezocatalysis. The energy band theory is substantiated by ultrasound-induced e^- excitation [40,45], but it lacks explanatory power for pollutant degradation under mild mechanical agitation, such as stirring [46]. By contrast, direct surface potential measurements verify the crucial role of screening charges [47].

A systematic comparative study was carried out by Boßl et al. [48] to investigate the degradation of Rhodamine B under simultaneous ultrasonic and mechanical stirring, employing three distinct piezocatalysts: ZnO, with its wide bandgap but low piezoelectricity, provides evidence for the energy band theory. In contrast, BF–KBT–PT, which exhibits strong piezoelectricity yet a narrow bandgap, supports the screening charge effect. Meanwhile, BTO, featuring both a wide bandgap and high piezoelectricity, is capable of supporting both mechanisms. The findings demonstrated that ZnO performed poorly because of insufficient piezoelectricity, whereas BF-KBT-PT was limited by its unfavorable band gap, which restricted its catalytic activity. Notably, only BTO achieved a far higher degradation efficiency. This key finding suggests that future work should prioritize quantifying the relative contributions of the two mechanisms rather than debating their dominance. This would provide clear guidance for catalyst design: when band processes prevail, focus on band structure optimization; when the screening charge effect takes over, emphasize polarization enhancement.

4.3. Ferroelectric domain engineering

Ferroelectric materials are distinguished by their ability to sustain spontaneous polarization below the Curie temperature. This behavior stems from the crystal's non-centrosymmetric ionic structure and the off-centering of certain ions, which creates stable charge separation and thus generates intrinsic electric dipole moments [49]. Once these dipole moments organize into domains featuring consistent polarization alignment, a net polarization intensity emerges across the entire domain area. The polarization of ferroelectrics can be reversibly switched by external fields. Specifically, when a reverse electric field of sufficient strength is applied, all domain polarizations flip in unison, leaving a remanent polarization (Pr) upon field removal. External mechanical forces can concurrently alter ionic displacements or induce domain wall motion in ferroelectric materials, thereby leading to tunable polarization intensity and a pronounced piezoelectric response [49]. The single-domain structure creates a spatially continuous internal electric field by virtue of the uniform alignment of polarization vectors, thereby guiding photogenerated e^--h^+ directly toward specific crystal facets through oriented migration. Conversely, the disordered polarization vectors in multi-domain grains lead to both a weakened overall electric field and the formation of recombination centers for charges at the domain walls [50]. Through the single-domain strategy, photogenerated e^--h^+ are directed toward the oppositely polarized surfaces. This creates a well-defined pathway that notably reduces the migration distance for charge carriers and thus lowers the likelihood of recombination during their movement.

4.4. Flexoelectric effects

The flexoelectric effect, ubiquitous in dielectrics, is an electromechanical coupling whereby strain (or field) gradients interact with polarization (or stress). Extensive studies confirm that ferroelectrics show much higher flexoelectric coefficients than other dielectrics, so their flexoelectric response is pronounced. Flexoelectricity in solids, also termed the flexoelectric effect, is a mechanism refers to the generation of polarization from a strain gradient (direct) or strain from an electric field gradient (converse). Unlike piezoelectricity, ferroelectricity, or ferroelasticity, flexoelectricity does not require any specific structural symmetry. Because of this, it can occur in all crystalline insulators, which gives it a clear advantage over the piezoelectric effect. The flexoelectric effect is often employed to enhance the piezoelectric effect. Shi et al. [51] designed BiO(Cl, Br) nanosheets with a radial-gradient architecture by emulating the radial gradient hierarchy of bamboo, the centrosymmetry of BiOCl is disrupted in this structure, which not only generates strong piezoelectricity but also enhances flexoelectricity due to the intrinsic mechanical heterogeneity. Owing to the triple-field synergy (built-in, piezo, flexoelectric), the BiO(Cl, Br) nanosheets boost H_2O_2 production to 742.2 μmol/g/h, a 4.23-fold increase over pristine BiOCl. Structural defects such as doping, grain boundaries, and dislocations are also known to significantly affect the flexoelectric effect. Zhou et al. [52] studied the effect of S-vacancies in defective bismuth sulfide (Bi_2S_{3-x}) on the generation of ROS and the degradation of organic pollutants under ultrasonic irradiation, and found it was S-vacancies break the centrosymmetric structure of pristine Bi_2S_3, thereby inducing piezoelectric behavior and raising the electrical energy in Bi_2S_{3-x}. The flexoelectric catalytic effect from nonuniform strain accounts for the nonzero catalytic efficiency of centrosymmetric Bi_2S_3.

5. Crucial parameters governing piezo-(photo)electric performance

Material parameters—particularly electronic structure, piezoelectricity, and charge transport—are closely intertwined in bi-based materials and collectively dictate the efficiency of piezo-(photo)catalytic processes. To maximize catalytic activity, selectivity and stability, it is essential to understand and optimize these parameters. The following subsections address three key factors: band structure, piezoelectric coefficients, and carrier dynamics.

5.1. Band structure

The band structure of the piezocatalyst critically influences its catalytic performance by regulating the energy levels of charge carriers, the migration efficiency, and the thermodynamic favorability of the redox reactions [53,54]. In piezocatalyst, the band structure both sets the intrinsic electronic properties and dynamically couples with the piezopotential from mechanical stress, adding a further dimension of control over catalysis [55]. Bi-based catalysts generally possess moderate bandgaps (2.0–3.5 eV) and asymmetric electronic structures that arise from the 6 s^2 lone-pair electrons of Bi^{3+} [56]. Bi-based piezoelectric catalysts have narrower bandgaps than most of conventional piezoelectric catalysts, which aids electron excitation, yet their band positions are often insufficient for the redox demands of water splitting and some pollutant degradation. In photocatalysis, narrower bandgaps improve

light absorption across a broad spectrum from UV to near-infrared, yet the electrochemical driving force may still be inadequate. By contrast, piezocatalysis involves a real-time modulation of the band structure by the piezopotential arising from mechanical strain. This modulation results in band tilting and bending, thereby enabling redox reactions that are thermodynamically forbidden under normal conditions [57]. Hence, the combination of a rationally tuned band structure and a pronounced piezoelectric response is critical for the realization of efficient Bi-based oxide piezo-(photo)catalysts.

5.2. Piezoelectric coefficient

The piezoelectric coefficient, often denoted by d (such as d_{33} and d_{31}), serves as a fundamental parameter that measures the electromechanical coupling in piezoelectric materials. The longitudinal piezoelectric coefficient d_{33} reflects polarization along the stress direction, while the transverse d_{31} corresponds to polarization perpendicular to it. A larger d value not only reflects a stronger piezoelectric response but also means a higher IEF can be generated under mechanical stimulation—a feature that is vital for effective charge separation in piezocatalysis [58]. The value of d depends on intrinsic lattice distortion, as well as extrinsic factors related to domain switching and the motion of domain walls. Consequently, doping, defect states, composite formation, crystal structure and domain configurations can effectively modulate it. Thus, boosting d is a key strategy in designing high-performance piezocatalysts, since it directly governs the piezopotential magnitude and the charge-separation efficiency under mechanical excitation.

5.3. Carrier density/mobility and lifetime

The catalytic efficiency of piezocatalysts is determined by carrier density, mobility, and lifetime, whose interplay governs charge generation, migration to active sites, and redox participation before recombination [59,60]. Carrier density refers to the quantity of e^- and h^+ that are accessible for catalytic reactions [61]. In piezocatalytic systems, it is governed by intrinsic factors such as dopant concentration, native defects, and electronic structure as well as extrinsic effects from piezoelectric polarization induced by mechanical stress [62]. A higher carrier density makes a large enough population of charge carriers accessible to engage in redox reactions at the surface of the catalyst [63]. However, the mere generation of charge carriers is insufficient unless they are effectively transported and have a long enough lifetime to avoid recombination [64]. Carrier mobility controls the efficiency of carrier transport to surface active sites before recombination occurs. Doping, heterostructure construction or defect modulation can improve carrier mobility. Moreover, the strengthened piezopotential not only promotes charge separation and suppresses recombination but also directs e^- and h^+ to separate active sites, which accelerates the overall reaction kinetics. Meanwhile, the carrier lifetime—the average time that carriers persist before recombination—determines whether they can effectively engage in surface reactions. The piezopotential not only significantly influences carrier concentration and separation, but also exerts a major effect on carrier lifetime, because it spatially separates e^- and h^+, thus suppressing recombination and prolonging their lifetime.

6. Differences from related catalytic processes

Piezocatalysis exhibits conceptual parallels with photocatalysis, sonocatalysis, and tribocatalysis, whereas it is fundamentally distinct with regard to the mechanisms of energy input and charge generation. Understanding the differences among these processes clearly is critical for both data interpretation and catalyst design. Photocatalysis uses light absorption to excite electrons from the VB to the CB, producing e^--h^+ pairs that then drive redox reactions [65]. Unlike photocatalysis, piezocatalysis requires no light and can work under dark conditions with mechanical energy as the sole driving force. Additionally, the generated piezopotential is maintained throughout the application of mechanical stress, which enhances the stability of charge separation. Sonocatalysis utilizes ultrasonic waves (20 kHz–1 MHz) in a liquid to induce cavitation bubbles, which subsequently collapse violently, giving rise to localized hot spots characterized by extreme temperature and pressure [66]. The transient microenvironments can promote the generation of radicals and increase chemical reactivity. Such extreme conditions are capable of breaking chemical bonds or producing reactive species. Physical cavitation, rather than the catalyst's electronic structure, is the main governing factor in sonocatalysis, although it remains effective. In piezocatalysis, ultrasonic vibration is employed not to induce cavitation, but rather to mechanically strain a piezoelectric catalyst and create an IEF, which makes the mechanism fundamentally different. Tribocatalysis originates from contact electrification induced by friction, whereby mechanical rubbing produces surface charges that subsequently initiate chemical reactions [67]. Tribocatalysis, though conceptually connected to mechanically driven charge generation, is driven by surface charge transfer, not by bulk lattice polarization. Thanks to its reliance on crystal deformation, piezocatalysis is more predictable, controllable, and reproducible, and its performance is closely linked to the material's intrinsic structure.

Establishing unambiguous experimental criteria for true piezocatalytic activity is crucial to distinguish it from other catalytic processes. Piezocatalysis can be broadly defined as the catalytic activity elicited by strain-induced polarization and piezopotential in non-centrosymmetric materials when subjected to mechanical force. Several experimental controls are routinely employed in practice as the minimum evidence required to substantiate a piezocatalytic mechanism. To exclude photocatalytic effects, experiments should be operated in the dark; simultaneously, control experiments without the catalyst under ultrasonic or mechanical stimulation are necessary to evaluate sonochemical influences. Moreover, it is useful to compare with non-piezoelectric analogues in order to verify that the catalytic activity is due to piezoelectric polarization rather than to purely mechanical effects, and thus to rule out friction-induced reactions. Finally, the activity's dependence on mechanical parameters like ultrasonic power and frequency further supports the link between performance and strain-induced piezopotential.

7. Bismuth-based piezo-(photo)catalysts

Some bismuth-based materials own both piezoelectric and photocatalytic properties simultaneously, which make it an attractive material for piezo-(photo)catalytic applications. Particularly, the unique crystal structure of layered bismuth-based materials results in diverse atomic coordination and a favorable hybrid electronic band structure. The peculiar structure enables the materials to be readily tailored through crystal design and facilitates crystallographic orientations that are ideal for facet control, band gap tuning, and defect engineering, and these approaches have demonstrated significant potential for the catalytic conversion of solar energy. This section systematically presents representative bi-based piezo-(photo)catalysts, with particular attention to their crystal structures, key physicochemical characteristics, and the relationships between structure and property that dictate piezocatalytic performance.

7.1. Sillén-type

7.1.1. BiOX

Sillén-structured bismuth-layered materials, including bismuth oxyhalides with the formula BiOX (X = Cl, Br, I) and bismuth-rich compounds such as $Bi_xO_yX_z$ (X = Cl, Br, I), as well as their related solid solutions, have been extensively employed in photocatalysis [68]. BiOX is composed of Bi_2O_2 layers alternating with double sheets of halogen atoms (as shown in Fig. 3a). These layers are stacked along the

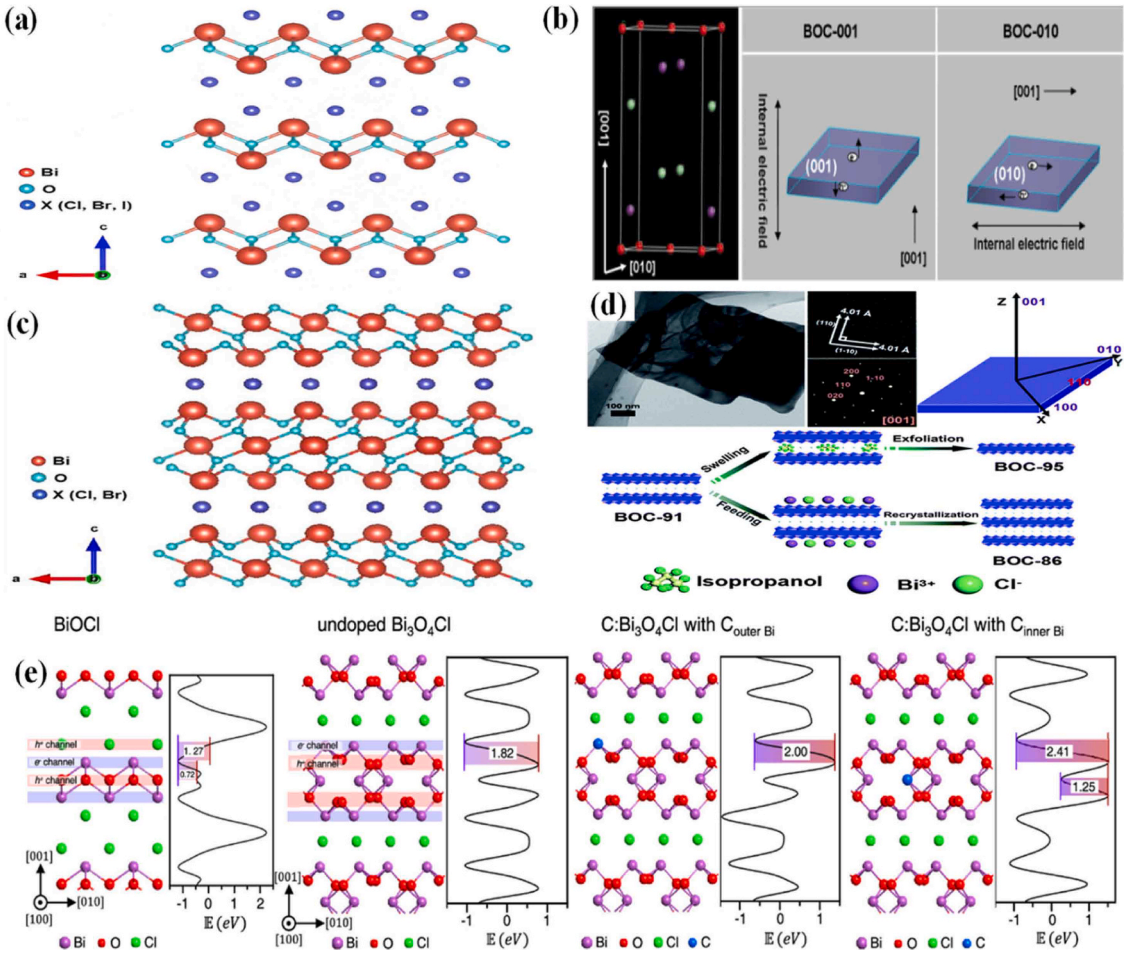

Fig. 3. (a) Crystal structure of BiOX (X = Cl, Br, I), Reproduced with permission from Ref. [68]. Copyright 2022 Elsevier. (b) Atomic model of BiOCl and the direction of the internal electric field, Reproduced with permission from Ref. [71]. Copyright 2012 American Chemical Society. (c) Crystal structure of Bi_3O_4X (X = Cl, Br), Reproduced with permission from Ref. [68]. Copyright 2022 Elsevier. (d) TEM image and schematic illustration of the liquid-exfoliation and hydrothermal-induced recrystallization process for tuning the facet percentages of Bi3O4Cl nanosheets, Reproduced with permission from Ref. [75]. Copyright 2014 Royal Society of Chemistry. (e) Interlayer energy barrier diagrams are for the BiOCl, undoped Bi_3O_4Cl, C:Bi_3O_4Cl with $C_{outerBi}$, and C:Bi3O4Cl with $C_{innerBi}$, respectively, Reproduced with permission from Ref. [76]. Copyright 2023 American Chemical Society.

c-axis and held together by nonbonding interactions—specifically van der Waals forces—acting through the halogen atoms. The unique layered structure results in an uneven charge distribution between the Bi_2O_2 layers and the halogen slabs. This asymmetry polarizes the associated atoms and orbitals, creating an IEF that facilitates the separation and transport of photogenerated charge carriers. The pronounced anisotropy in the structural, optical, electronic, and mechanical properties of BiOX arises from its strong intralayer covalent bonds and weak interlayer van der Waals interactions—a characteristic that has also been noted in other reviews [69,70]. These publications primarily addressed the synthesis, modification, photocatalytic applications, and reaction mechanisms of bismuth oxyhalides. More recently, growing research interest has shifted toward the IEF in these materials, with particular emphasis on how internal polarization influences photocatalytic behavior.

Jiang et al. were the first to demonstrate a facet-controllable method for preparing BiOCl single-crystalline nanosheets [71]. They successfully synthesized nanosheets with exposed [001] and [010] facets and conducted a comparative study of their photocatalytic properties. Due to its unique layered structure, internal static electric fields can form within BiOCl, oriented perpendicularly to the alternating Bi_2O_2 and halogen anionic layers (Fig. 3b). As illustrated in Fig. 3b, the self-induced IEFs are oriented perpendicularly to the BOC−001 nanosheets and parallel to the BOC−010 nanosheets. Under UV–vis irradiation, the BOC−001 film electrode exhibited a higher photocurrent response than BOC−010. This indicates that photo-induced charge separation and transfer are more efficient along the [001] direction in BOC−001 [72]. Due to the presence of favorable IEF, BiOCl nanosheets featuring exposed [001] facets demonstrated enhanced UV-light photodegradation activity. Meanwhile, photochemical labeling effectively confirmed the specific locations of holes and electrons on the [001] and [110] facets. Unlike the photocatalytic process, Shao et al. [73] employed ultrasonic excitation as the sole driving force for piezocatalysis, carrying out an oxygen reduction reaction (ORR) to produce H_2O_2 using BiOCl plates. Under ultrasonic excitation, an alternating electric field was generated across the BiOCl, which facilitated the movement of charge carriers (electrons) to react with O_2 and H_2O, leading to the formation of H_2O_2. In a study by Ismail et al. [74], the degradation efficiency of RhB using BiOCl microspheres was compared across three processes: photocatalysis (~72%), piezocatalysis (~26%), and piezo-photocatalysis (~99%). The significantly enhanced degradation under piezo-photocatalysis was attributed to the synergistic effect between piezoelectric and photocatalytic mechanisms. Specifically, the electric field generated by mechanical strain vibration promoted the separation of photogenerated e^--h^+ pairs, thereby improving the biocatalytic decomposition performance.

7.1.2. $Bi_xO_yX_z$

Bismuth-rich bismuth oxyhalides comprise compounds such as Bi_3O_4X (X = Cl, Br), $Bi_4O_5X_2$ (X = Br, I), Bi_5O_7X (X = Br, I), $Bi_7O_9I_3$, $Bi_{12}O_{15}Cl_6$, $Bi_{12}O_{17}X_2$ (X = Cl, Br) and $Bi_{24}O_{31}X_{10}$ (X = Cl, Br). Their structural arrangements are influenced by both the identity of the halide ion and the oxygen-to-halogen ratio. As an illustration, the structural model of Bi_3O_4X (X = Cl, Br) is presented in Fig. 3c. Additionally, these bismuth-rich oxyhalides possess a distinctive interlayer electric field that enhances the separation efficiency of photoinduced charge carriers. Through a combination of liquid-phase exfoliation and hydrothermal recrystallization, Li and colleagues [75] synthesized single-crystalline Bi_3O_4Cl nanosheets with varying percentages of exposed [001] facets-specifically 95%, 91%, and 86%, designated as BOC−95, BOC−91, and BOC−86, respectively. Their work further revealed a correlation between the magnitude of the IEF and the percentage of exposed [001] facets (Fig. 3d). A range of analytical techniques, including degradation rate, transient photocurrent response tests, electrochemical impedance spectroscopy and photoluminescence spectroscopy demonstrated that Bi_3O_4Cl nanosheets with higher percentages of exposed [001] facets generate a stronger IEF. This enhanced IEF promotes the separation and migration of photogenerated e^--h^+ pairs, leading to appreciable photocatalytic activity. Regulating the strength of the IEF through crystal facet engineering has also been proposed as an innovative approach to boost photocatalytic performance. The research conducted by Fu et al. has revealed that the IEF of Bi_3O_4Cl can be boosted through dual carbon substitutions at both the inner and outer bismuth positions [76]. They calculated the interlayer energy barriers ($\Delta\mathbb{E}$) from models representing BiOCl, undoped Bi_3O_4Cl, C-doped Bi_3O_4Cl with $C_{outerBi}$ (doped at the outer Bi site) and C-doped Bi_3O_4Cl with $C_{innerBi}$ (doped at the inner Bi site), as shown in Fig. 3e. In Bi_3O_4Cl, the outer bismuth layers act as electron channels while the oxygen layers serve as hole channels. Hence, the interlayer energy barrier ($\Delta\mathbb{E}$) presented here specifically corresponds to that between an outer bismuth layer and an adjacent oxygen layer, denoted as $\Delta\mathbb{E}_{outer\ Bi\ vs\ O}$. The $\Delta\mathbb{E}_{outer\ Bi\ vs\ O}$ value is approximately 10% higher for $C_{outerBi}$, and approximately 32% higher for $C_{innerBi}$, compared to that of undoped Bi_3O_4Cl. The IEF is calculated by dividing the interlayer energy barrier by the corresponding layer spacing. This yields $\Delta\mathbb{E}_{outer\ Bi\ vs\ O}$ values of 19.69 aV/nm for C-doped Bi_3O_4Cl with $C_{innerBi}$, 16.34 aV/nm for C-doped Bi_3O_4Cl with $C_{outerBi}$, 14.87 aV/nm for undoped Bi_3O_4Cl, and 5.6 aV/nm for BiOCl (between the Bi and O layers). In addition, a number of bismuth-rich oxyhalides and related composites—including Bi_3O_4Br [77] and CNT/$Bi_4O_5I_2$ [78]—have been utilized in piezocatalysis by taking advantage of their self-polarized IEF.

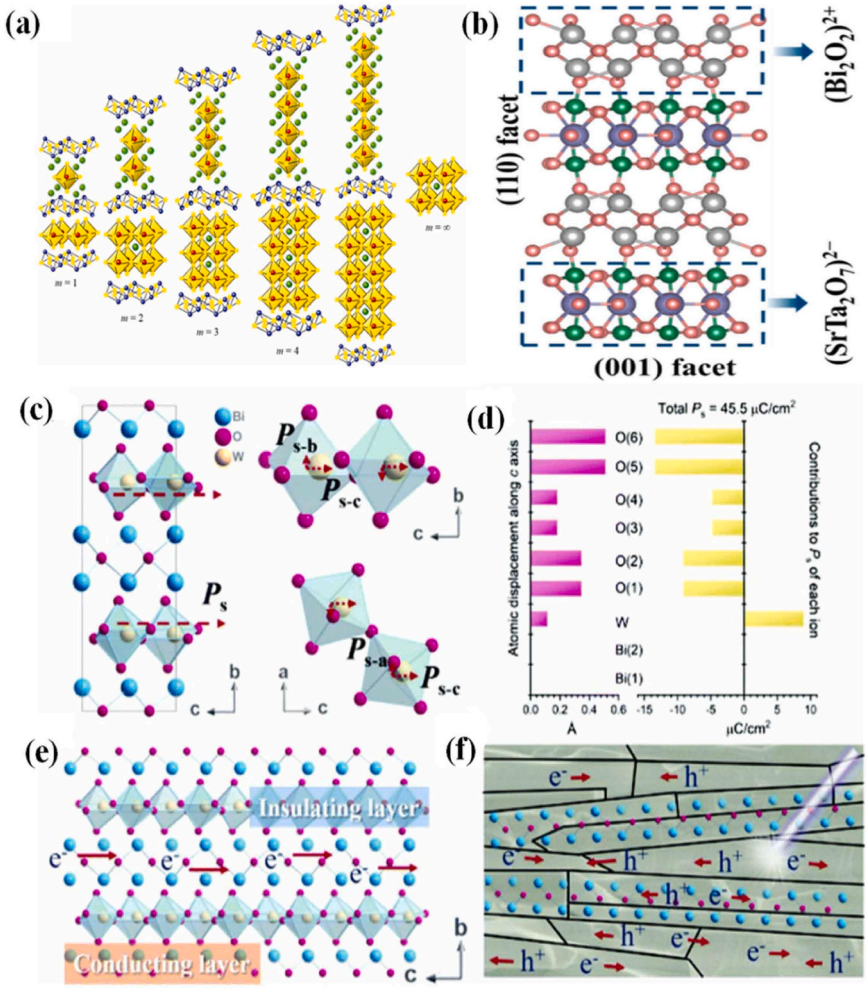

Fig. 4. (a) Schematic representations of the crystal structures for Aurivillius-type bismuth layer-structured materials with varying stacking numbers m, Reproduced with permission from Ref. [1]. Copyright 2024 Elsevier. (b) crystal structure of $SrBi_2Ta_2O_9$, Reproduced with permission from Ref. [93]. Copyright 2025 Elsevier. (c) Illustration of the Bi_2WO_6 unit cell structure along with its spontaneous polarization direction, (d) Calculated polarizations of individual constituent ions with respect to the c-axis, (e) Schematic view of the alternation between stacked Bi_2O_2 layers and WO_6 perovskite layers, (f) Schematic depicting the migration of photoexcited e^--h^+ pairs. (c-f) Reproduced with permission from Ref. [86]. Copyright 2021 Royal Society of Chemistry.

7.2. Aurivillius-type

7.2.1. Structure

Bismuth-layered perovskite ferroelectrics (BLSFs), also referred to as Aurivillius-phase materials, were first identified by Aurivillius in 1949 [79]. These compounds have garnered significant interest among researchers due to their distinctive layered crystal structures, the presence of asymmetric centers that give rise to spontaneous polarization, and their anisotropic physical characteristics [80–82]. BLSFs are generally represented by the chemical formula $(Bi_2O_2)^{2+}(A_{m-1}B_mO_{3m+1})^{2-}$. Their crystal structure consists of alternating layers: a fluorite-type $(Bi_2O_2)^{2+}$ sheet and a perovskite-type $(A_{m-1}B_mO_{3m+1})^{2-}$ block. Here, the integer 'm' indicates how many oxygen octahedra are stacked perpendicular to the layering direction [83–85]. The structure accommodates a wide variety of chemical substitutions at the A and B sites. The A site can be occupied by mono-, di-, or trivalent ions like Na^+, K^+, Sr^{2+}, Ba^{2+}, Pb^{2+}, or Bi^{3+}, while the B site is typically filled by smaller cations with tetra-, penta-, or hexavalent charges, such as Ti^{4+}, Ta^{5+}, Nb^{5+}, or W^{6+} [1,86,87] (Fig. 4a). This flexibility in ion substitution enables the tuning of a broad spectrum of physical properties. A wide range of BLSFs-including Bi_2WO_6 and Bi_2MoO_6 (corresponding to m=1); $BaBi_2Nb_2O_9$, $CaBi_2Nb_2O_9$, $SrBi_2Nb_2O_9$ and $SrBi_2Ta_2O_9$ (m=2); $Bi_4Ti_3O_{12}$ (m=3); $BaBi_4Ti_4O_{15}$, $CaBiTi_4O_{15}$, and $SrBiTi_4O_{15}$ (m=4); as well as $Pb_2Bi_4Ti_5O_{18}$ and $Sr_2Bi_4Ti_5O_{18}$ (m=5) have been extensively investigated for applications in piezoelectric/ferroelectric filed [88]. These materials are also regarded as effective catalysts for photodegradation of organic pollutants and water splitting [89].

BLSFs represent the most extensively researched materials for high-temperature ferroelectric and piezoelectric ceramic applications, owing to their high Curie temperatures (Te), distinctive spontaneous polarization, and remarkable resistance to thermal depoling [90,91]. Nevertheless, Aurivillius-type ceramics synthesized via conventional routes often exhibit low density—resulting from the anisotropic growth of lamellar grains—as well as poor piezoelectric performance, primarily due to spontaneous polarization being largely confined within the plane [92]. The fabrication of highly dense ceramics has traditionally relied on techniques such as hot pressing and spark plasma sintering. In contrast, Aurivillius-type bismuth-layered structure nano-catalyst are uniquely suited for catalytic applications as they can be utilized directly in their as-synthesized state, eliminating the sintering requirement. Furthermore, the hybridization between Bi 6 s and O 2p orbitals near the band edge is a common characteristic of BLSFs. This feature enables most BLSFs to absorb a portion of visible light, suggesting their potential suitability for photovoltaic, photoelectric and photocatalytic applications. Accordingly, Aurivillius-phase bismuth-layered structural materials have emerged as a major focus in piezo-(photo)catalysis research, owing primarily to their distinctive intrinsic electric field generated by polarization and their outstanding photo-absorption capability.

The spontaneous polarization in BLSFs is largely confined within the a-b plane. For instance, in $SrBi_2Ta_2O_9$, the crystal structure is composed of perovskite-like TaO_6 units alternating with $(Bi_2O_2)^{2+}$ layers, as illustrated in Fig. 4b. The TaO_6 octahedron exhibits a distorted shape, characterized by elongation along the c-axis and indicative of an associated dipole moment. A shorter Ta–O bond along the c-axis and a longer bond oriented toward the Bi_2O_2 layer are observed. Consequently, a net spontaneous polarization develops along the a-axis, in contrast to the absence of polarization along the pseudotetragonal c-axis [93]. Additionally, the direction of spontaneous polarization lies within the a–b plane of the perovskite-like layers for compounds with an even number of perovskite units (m), while for those with an odd m, a component of polarization also appears along the c-axis. For instance, in $Bi_4Ti_3O_{12}$ (where m=3), spontaneous polarization occurs along both the a-axis (50 $\mu C/cm^2$) and the c-axis (4 $\mu C/cm^2$) [94].

7.2.2. Applications in piezo-(photo)catalysis

A significant number of Aurivillius-type piezo-(photo)catalysts exhibit high performance in environmental treatment and energy conversion. Therefore, there is a need to explore new piezo-(photo)catalysts with Aurivillius structures to advance the fields of piezo-(photo)catalysis. This section presents an overview of currently reported Aurivillius-phase bismuth-layered materials used in piezo-(photo)catalytic applications, organized according to increasing values of m.

7.2.2.1. m= 1. Bi_2WO_6, which represents the simplest Aurivillius compound (with m=1), consists of alternating layers of fluorite-type $[Bi_2O_2]^{2+}$ and pseudoperovskite $[WO_4]^{2-}$ stacked along the c-axis. Bi_2WO_6 possesses a noncentrosymmetric crystal structure, which gives rise to macroscopic polarization. This spontaneous polarization occurs primarily along the c-axis and is concentrated in the WO_6 layers (parallel to the layers), resulting from distortions in the oxygen octahedra (Fig. 4c) [95]. He et al. [86] summarized the polarization contribution of each constituent ion along the c-axis (Fig. 4d). The total polarization is estimated to be approximately 45.5 $\mu C/cm^2$. In the crystal structure of Bi_2WO_6, the conductive Bi_2O_2 layers and the insulating WO_6 layers are alternately stacked along the b-axis (Fig. 4e). Finally, the spontaneous polarization of Bi_2WO_6 generates a polarization electric field, which acts as a driving force to separate e^- and h^+ by directing their movement in opposite directions (Fig. 4f). This mechanism highlights the applications potential of Bi_2WO_6 as a promising two-dimensional material for various catalytic area.

Kudo et al. [96] identified Bi_2WO_6 as a photocatalyst capable of evolving oxygen in 1999. Since then, it has attracted extensive research interest, particularly in the areas of morphology control and the development of its visible-light-induced photocatalytic properties [97–99]. Despite this, so far, a systematic investigation into the piezo-(photo) catalytic performance of Bi_2WO_6 has not been undertaken. In a pioneering study, Hao and co-workers [95] demonstrated the use of Bi_2WO_6 nanosheets as piezocatalyst for organic pollutants degradation. Under piezocatalytic conditions, approximately 96% of the pollutants were decomposed within 35 min, and the nanosheets exhibited excellent reusability and cycling stability. This remarkable performance was ascribed to two main factors: the piezoelectric effect, which promotes charge generation and accelerates carrier transport in redox reactions (Fig. 5a), and the tilting of the conduction and valence bands in piezocatalysts resulting from a strong piezoelectric potential (Fig. 5b). The high reaction kinetic rate constant (k) of the Bi_2WO_6 nanosheets surpasses that of many reported piezocatalysts (Fig. 5c), underscoring its competitive piezocatalytic performance and promising applications potential.

As another simplest Aurivillius phase compounds (m=1), Bi_2MoO_6 is also an active bismuth-based semiconductors, which features appropriate band structure and layered morphology with a crystal lattice formed by $(Bi_2O_2)^{2+}$ and $(MoO_4)^{2-}$ [100]. Cheng and colleagues [100] prepared Bi_2MoO_6 microspheres and nanoparticles using the hydrothermal method (HT-Bi_2MoO_6) and the co-precipitation method (CP-Bi_2MoO_6), respectively. It was found that the morphology has a certain influence on the piezoelectric properties of Bi_2MoO_6. Under vibration, the HT-Bi_2MoO_6 achieves a degradation rate of 98.4% for RhB, which is higher than that of CP-Bi_2MoO_6 (67.6%). This can be explained by that HT-Bi_2MoO_6 featuring a flower-like microsphere architecture of nanosheets with abundant surface defects, which is more conducive to promoting the piezoelectric generation and restraining e^--h^+ recombination than that of CP-Bi_2MoO_6.

Synergetic piezo-photocatalysis, which combines light irradiation with ultrasonic vibration, represents a promising approach for removing organic pollutants from wastewater. In a study by Sun et al. [101], the piezo-photocatalytic performance of 1 T/2H $MoSe_2/Bi_2WO_6$ hierarchical microspheres was evaluated under simultaneous exposure to ultrasonic vibration and sunlight. Results shown that the diclofenac (DCF) degradation rate constant for 1.5% 1 T/2H $MoSe_2/Bi_2WO_6$ (0.093 min^{-1}) is higher by factors of 1.1 and 1.3 than those of 1.5% 2 H

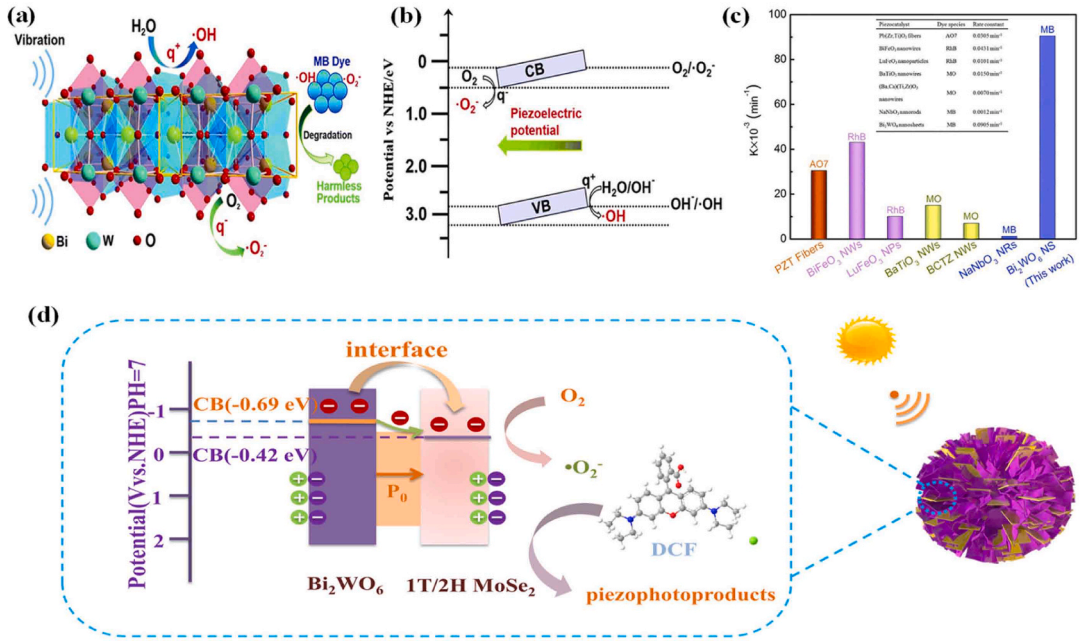

Fig. 5. (a) Schematic principle governing the piezocatalytic degradation of MB dye, (b) Diagram of piezoelectric-potential-induced energy band tilting, (c) Comparison of piezocatalytic reaction kinetics rate constants among representative piezocatalyst systems. Reproduced with permission from Ref. [95]. Copyright 2020 Royal Society of Chemistry. (d) Proposed mechanism for the piezoelectric-photocatalytic degradation of DCF by $MoSe_2/Bi_2WO_6$, Reproduced with permission from Ref. [101]. Copyright 2022 Elsevier.

$MoSe_2/Bi_2WO_6$ (0.037 min^{-1}) and pure Bi_2WO_6 (0.026 min^{-1}). According to PFM and ferroelectric analyzer results, the 1 T/2H MS/BWO composite produces a strong polarization electric field. This field acts as an effective driving force that accelerates the separation of carriers, thereby improving the piezo-photocatalytic performance (Fig. 5d). Li et al. [102] investigated the piezo-photocatalytic activity of the Bi_2MoO_6 nanosheets. It has been shown that, in the degradation of tetracycline (TC), Bi_2MoO_6 nanosheets exhibit piezo-photocatalytic activity that is significantly higher than either their individual photocatalytic or piezocatalytic activity, with a synergistic factor of 1.215.

7.2.2.2. m= 2. Li et al. [103] prepared a series of layered perovskite photocatalysts with the composition $ABi_2Ta_2O_9$ (where A represents Ba, Ca and Sr, corresponding to an increasing ionic radius of the A-site cation) using a conventional solid-state reaction approach as early as 2008, and evaluated the photocatalytic performance of these materials for water splitting under UV light. The photocatalytic H_2 evolution rate of $SrBi_2Ta_2O_9$ was significantly higher than that of both $CaBi_2Ta_2O_9$ and $BaBi_2Ta_2O_9$. This enhanced activity can be attributed to two structural factors: firstly, the bond angle between the corner-linked NbO_6 octahedra in $SrBi_2Nb_2O_9$ is closer to the ideal 180° compared to that in $CaBi_2Nb_2O_9$; secondly, the orthorhombic structure of $SrBi_2Nb_2O_9$ exhibits greater degree of lattice distortion than the tetragonal structure of $BaBi_2Nb_2O_9$ (Fig. 6a). It was also suggested that the crystalline structure and associated lattice distortions likely significantly influenced the separation of photogenerated charges, thereby ultimately determining the photocatalytic performance [104,105]. Wu et al. [106] successfully synthesized tetragonal $BaBi_2Nb_2O_9$ and single-phase orthorhombic $SrBi_2Nb_2O_9$ and photocatalysts. Results demonstrated that $SrBi_2Nb_2O_9$ exhibited stronger photocatalytic activity in the redox reaction of MO compared to $BaBi_2Nb_2O_9$, a difference they attributed to the presence of a dipole moment within the $SrBi_2Nb_2O_9$ crystal. As illustrated in Fig. 6b, the $BaBi_2Nb_2O_9$ crystal structure exhibits a tilt of the NbO_6 octahedra of less than 3° relative to the c-axis. In contrast, the octahedral tilt in $SrBi_2Nb_2O_9$ is approximately 6°. Moreover, due to the distortion within the perovskite layer framework, $SrBi_2Nb_2O_9$ develops a dipole moment along the c-axis, a feature deficiency in $BaBi_2Nb_2O_9$. This intrinsic dipole moment in $SrBi_2Nb_2O_9$ promotes the separation and migration of photogenerated electrons and holes, thereby enhancing its photocatalytic activity.

Senthil et al. [107] studied the photocatalytic water splitting performance of Y^{3+}-modified $SrBi_2Ta_2O_9$ ferroelectric materials with the composition $Sr_{1-x}Y_{2x/3}Bi_2Ta_2O_9$. Their findings indicated that the introduction of A-site vacancies promotes enhanced rotation of the octahedra, which leads to improved ferroelectric properties, as illustrated in Fig. 6c. Lattice distortion and the presence of a dipole moment improved photocatalytic water splitting performance by enabling the spontaneous separation of photogenerated charge carriers. Consequently, in ferroelectric photocatalysts, charge separation is facilitated by local electric fields generated by dipoles within noncentrosymmetric structural domains [108].

7.2.2.3. m= 3. Tu et al. [109] conducted a pioneer work on the piezocatalytic performance of $Bi_4Ti_3O_{12}$ for MO degradation under ultrasonic irradiation. It was found that when an ultrasonically applied pressure was employed, positive and negative charges were generated on opposite surfaces of the $Bi_4Ti_3O_{12}$. The non-centrosymmetric nature of $Bi_4Ti_3O_{12}$'s crystal structure is responsible for its piezoelectric behavior, leading to the separation of positive and negative charges on opposing sides. The piezocatalytic process generated a substantial amount of highly reactive ·OH and $O_2^{\bullet-}$ radicals, which led to effective degradation. Nevertheless, the overall dye degradation efficiency achieved by $Bi_4Ti_3O_{12}$ remained relatively low.

Wu and colleagues [110] hypothesized that the random orientation of nanocrystals could lead to the mutual cancellation of their spontaneous polarizations, thereby reducing the overall piezoelectric response. Using layered sodium titanate ($Na_2Ti_3O_7$) as a precursor, they synthesized several nanostructured forms of $Bi_4Ti_3O_{12}$—such as rectangular nanoplates, cross-arranged nanoplates, and slice-assembled microspheres—and examined how these morphological variations

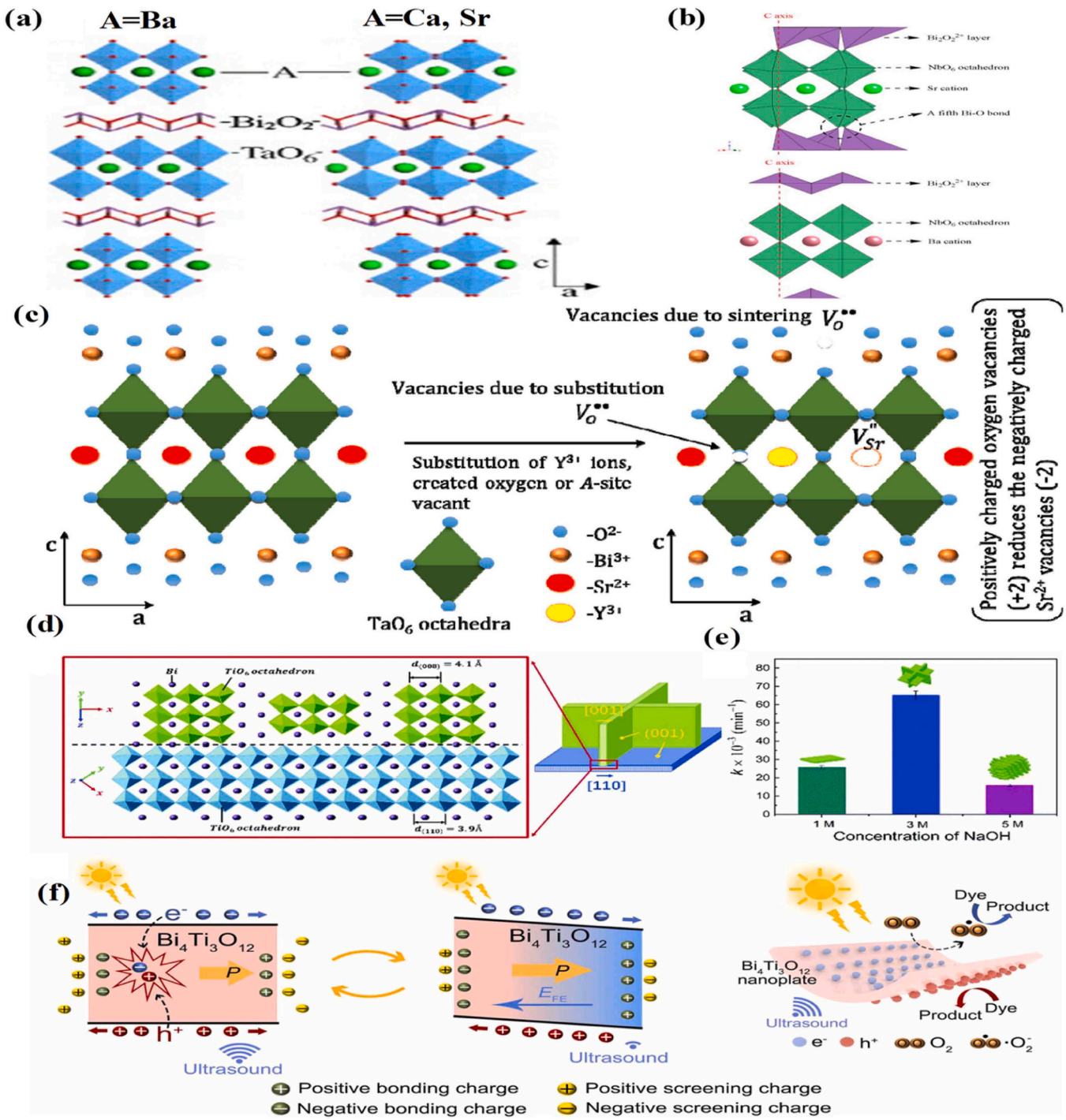

Fig. 6. (a) A schematic illustration depicting the crystal structure of $ABi_2Ta_2O_9$ (with A representing Ca, Sr, and Ba), Reproduced with permission from Ref. [103]. Copyright 2008 Elsevier. (b) A schematic representation of the crystal structures: $SrBi_2Nb_2O_9$ (upper) and $BaBi_2Nb_2O_9$ (lower), Reproduced with permission from Ref. [106]. Copyright 2011 Elsevier. (c) A schematic diagram depicting charge neutrality maintained by oxygen and strontium vacancies, Reproduced with permission from Ref. [107]. Copyright 2011 Elsevier. (d) Schematic representation of the vertical growth mode of $Bi_4Ti_3O_{12}$ nanoplates, (e) Comparison of the reaction rate constants among $Bi_4Ti_3O_{12}$ samples with distinct morphologies. (d-e) Reproduced with permission from Ref. [110]. Copyright 2019 Royal Society of Chemistry. (f) Schematic illustration of the piezo-photocatalytic mechanisms involved in the degradation of dye by $Bi_4Ti_3O_{12}$ nanoplates, Reproduced with permission from Ref. [112]. Copyright 2022 Elsevier.

affect piezocatalytic activity (Fig. 6d). The decussated $Bi_4Ti_3O_{12}$ nanoplates were found to exhibit higher piezocatalytic activity for the degradation of RhB under ultrasonic vibration compared to other morphological structures. This finding was determined to result from a greater piezoelectric potential difference and a reduced separation between their polar surfaces (Fig. 6e). By exploiting the rapid hydrolysis of inorganic titanium sources, Ji et al. [111] prepared hollow-sphere $Bi_4Ti_3O_{12}$ with enhanced spontaneous polarization using a simple hydrothermal route. It was found that the rate of its piezo-photocatalytic degradation of TC was 1.57 times and 5.29 times higher than that of the spherical and plate-like morphologies, respectively, with a rate constant of $k = 0.127$. The hollow spheres were found to contain a

moderate concentration of oxygen vacancies (Ov), as revealed by surface chemical analysis. Measurements of polarization and piezoelectric response indicated that they possess considerable spontaneous polarization and piezoelectric properties, and photoelectrochemical and carrier property tests confirmed that hollow-sphere $Bi_4Ti_3O_{12}$ offers superior charge transport and separation efficiency, which can be attributed to the synergistic effect of defects and polarization fields.

$Bi_4Ti_3O_{12}$ nanoplates produced via the molten-salt method demonstrated superior piezo-photocatalytic activity in RhB degradation when compared to the material which synthesized by solid-state reaction or hydrothermal methods. This enhancement can be attributed to the optimal combination of size, morphology, crystallinity, and specific surface area achieved in the nanoplates [112]. The significantly improved piezo-photocatalytic performance was also due to the efficient separation of photogenerated charge carriers driven by the built-in electric field. A schematic illustration of the proposed dye degradation mechanism via the piezo-photocatalytic process is presented in Fig. 6f.

7.3. Aurivillius- or Sillén-related

Layered bismuth-based materials related to the Aurivillius or Sillén families, including $BiOIO_3$, $Bi_2O_2CO_3$, and $Bi_2O_2(OH)(NO_3)$, have recently garnered significant attention. The crystal structure of these materials consistently consists of alternating layers of $[Bi_2O_2]^{2+}$ units with a fluorite-type arrangement and interstitial anionic slabs, which may be halide ions, perovskite-like blocks $(A_{m-1}B_mO_{3m+1})^{2-}$, or planar anionic groups such as CO_3^{2-}, BO_3^{3-}, or NO_3^-. The well-ordered layered structure is considered conducive to the formation of an IEF, promoting efficient charge separation. This capability enhances the photocatalytic performance of these materials and has generated considerable research interest, leading to a number of important scientific advances.

In 2011, Nguyen et al. [113] first characterized the structure of $BiOIO_3$, a new noncentrosymmetric polar material with an Aurivillius-type structure composed of alternating $[Bi_2O_2]^{2+}$ cation layers and $(IO_3)^-$ anions (Fig. 7a). The trigonal pyramidal geometry of the IO_3 units breaks the symmetry between positive and negative charge centers. This unique structural feature generates a local dipole moment, and the collective alignment of these dipoles within the IO_3 polyhedral layer results in macroscopic polarization along the c-axis (Fig. 7b). Wang et al. [114] demonstrated that the internal polar field within $BiOIO_3$ nanoplates efficiently separates photogenerated e^--h^+ pairs during photocatalysis. Density functional theory calculations verified that photooxidation takes place on the IO_3 surface layer, while photoreduction occurs at the edge of the nanoplate, driven by the IEF. The improved photocatalytic performance of $BiOIO_3$ nanoplates results from the combined effects of the internal polar field and heterolayered structure. Su et al. [115] synthesized a series of $BiOIO_3$ nanoplates with thicknesses of 25, 50, and 150 nm and assessed their performance in photocatalytic H_2 evolution. The rate of H_2 production was found to increase with nanoplate thickness, a trend attributed to the enhancement of the internal polar field effect in thicker nanoplates. Moreover, other study has confirmed the beneficial influence of this intrinsic polar field on the photocatalytic behavior of $BiOIO_3$ [116].

Zhang et al. [117] reported that $Bi_2O_2[BO_2(OH)]$ nanosheets featuring an internal polar field, resulting from the ordered alignment of $BO_2(OH)$ pyramids. The crystallographic analysis confirmed that this internal polar electric field is oriented along the ac plane due to the structured arrangement of the $BO_2(OH)$ units. Driven by the internal polar electric field, photoinduced charge carriers are selectively directed toward the Bi_2O_2 and $BO_2(OH)$ layers, respectively. This spatial separation of charge carriers enhances the photocatalytic performance of $Bi_2O_2[BO_2(OH)]$ under UV light irradiation.

Bi_4NbO_8X (X = Cl, Br), which adopts a Sillén/Aurivillius-type structure, consists of single-layered slices of NbO_6 octahedra alternating with $(Bi_2O_2)_2X$ blocks, as illustrated in Fig. 7c. Hu et al. synthesized Bi_4NbO_8X (X = Cl, Br) single-crystalline nanoplates via a flux method, leveraging their noncentrosymmetric structure and strong visible-light absorption. These nanoplates demonstrated outstanding piezo-photocatalytic performance [118]. The d_{33} of Bi_4NbO_8Cl and Bi_4NbO_8Br were measured for the first time using piezoresponse force microscopy (PFM), with values of approximately 128 and 214 pm/V, respectively. When subjected to simultaneous light and ultrasound irradiation, Bi_4NbO_8Br demonstrated notable oxygen reduction reaction (ORR) activity, which surpassed the combined effects of light and ultrasound applied individually. Besides promoting band bending and enriching reductive reactive sites, the markedly improved piezo-photocatalytic performance was also due to the efficient charge separation driven by the polarized electric field.

7.4. Perovskite-type ABO_3 ($BiFeO_3$ and $Bi_{0.5}Na_{0.5}TiO_3$)

Bi-containing perovskite have garnered significant interest because of their inherent ferroelectric properties, strong polarization, and good chemical stability. Among these, $BiFeO_3$ (BFO) and $Bi_{0.5}Na_{0.5}TiO_3$ (BNT) serve as two typical examples, displaying strong piezoelectric behavior and outstanding catalytic performance under mechanical activation.

BFO is a multiferroic perovskite featuring a rhombohedral R3c structure, which simultaneously shows ferroelectric and antiferromagnetic ordering at room temperature [119]. The stereochemically active Bi^{3+} 6 s^2 lone pairs enhance Bi–O hybridization and shift the Bi^{3+} ion against the FeO_6 octahedra along the pseudocubic axis, leading to spontaneous polarization (Fig. 8a) [120]. Ferroelectric polarization is further strengthened by the rhombohedral distortion, which is crucial for piezocatalysis. With a narrow bandgap (~2.1 eV) and a high remanent polarization (~100 μC/cm^2), BFO allows efficient coupling of its piezoelectric and semiconducting properties [121]. When subjected to mechanical stress, BFO generates a large piezopotential, which not only facilitates charge separation but also drives a range of redox processes

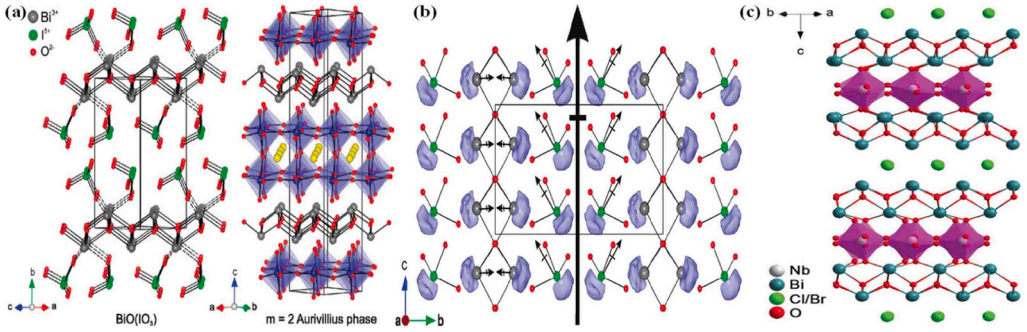

Fig. 7. (a) Crystal structure of $BiOIO_3$, (b) Net macroscopic polarization oriented along the c-axis (indicated by a large black arrow). Reproduced with permission from Ref. [113]. Copyright 2011 American Chemical Society. (c) Crystal structure of Bi_4NbO_8X (X = Cl, Br), Reproduced with permission from Ref. [118]. Copyright 2011 Wiley.

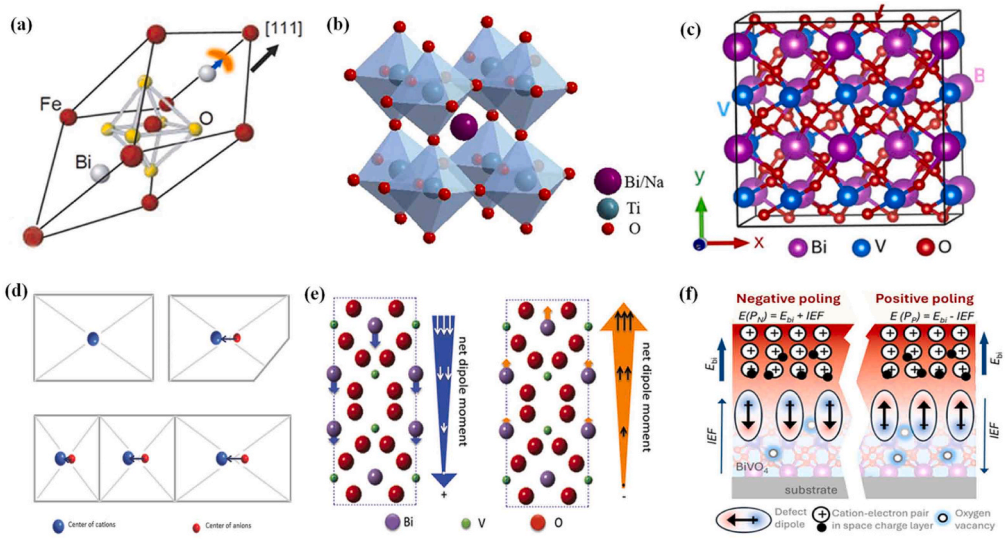

Fig. 8. (a) Schematic of the prototypical rhombohedral BFO unit cells, where the ordering of Bi^{3+} lone pairs is seen to contribute to the polarization, Reproduced with permission from Ref. [120]. Copyright 2003 Science. (b) The crystal structure of BNT, Reproduced with permission from Ref. [128]. Copyright 2022 Elsevier. (c) The structure of $BiVO_4$ crystal, Reproduced with permission from Ref. [130]. Copyright 2024 Nature. (d) Schematic of a strain-induced local polarization mechanism in $BiVO_4$, Reproduced with permission from Ref. [132]. Copyright 2018 Wiley. (e) Illustration of the atomic displacements that can lead to polar domains in BiVO4, Reproduced with permission from Ref. [133]. Copyright 2014 American Chemical Society. (f) The schematic illustration on how the IEF induced by external poling, Reproduced with permission from Ref. [130]. Copyright 2024 Nature.

[122]. BFO-based piezo-(photo)catalysts demonstrate robust performance for degrading organic pollutants [123], reducing heavy metal ions [124], converting CO_2 [125], producing H_2 and H_2O_2 [126], and enabling biomedical applications [127]. Defect engineering (particularly OVs) further boosts BFO performance via active sites, boosting carrier concentration, and reinforcing piezo-(photo)catalytic responses activity [125]. Additionally, doping strategies raise polarization and local electron density for improved catalytic efficiency [124]. Owing to Bi evaporation and the narrow phase stability, BFO is frequently accompanied by secondary phases during practical synthesis. Although these phases are often considered impurities, they can also form heterojunctions with BFO, which facilitate interfacial charge separation and curb recombination.

BNT is another Bi-based perovskite that exhibits either rhombohedral (R3c) or tetragonal symmetry, as illustrated in Fig. 8b [128]. The simultaneous presence of Bi^{3+} and Na^+ at the A-site leads to structural disorder and the formation of nanoscale ferroelectric domains. Being lead-free and environmentally benign, and also features a high piezoelectric coefficient and Curie temperature [129]. The ease of domain switching leads to enhanced local conductivity, which in turn enables efficient carrier migration and minimizes recombination under mechanical excitation. Owing to the suitable band structure and high deformability, BNT proves to be an excellent candidate for piezo-(photo) catalysis. BNT-based materials are highly active for pollutant degradation and water splitting. Their catalytic activity can be further enhanced by defect regulation to modify the band structure, while heterojunction strategies additionally promote carrier migration and separation, ultimately leading to superior piezo-photocatalytic performance.

7.5. Bismuth vanadates $BiVO_4$

BVO has three known polymorphs—tetragonal scheelite, tetragonal zircon, and monoclinic scheelite. Among which, the monoclinic scheelite phase (I2/b) exhibits the highest photocatalytic activity (Fig. 8c) [130,131]. Despite being centrosymmetric and consequently lacking intrinsic piezoelectricity, monoclinic BVO can still develop polarization under mechanical stress through other mechanisms. Particularly, flexoelectric effects from strain-gradient-induced local polarization at surfaces or interfaces can yield observable electromechanical responses (Fig. 8d-e) [132,133]. The introduction of OVs, as a common defect-engineering strategy, can lead to the formation of defect dipoles, thereby generating piezoelectric-like behavior when the material is mechanically deformed (Fig. 8f) [130]. Through these mechanisms, strain generates polarization fields that facilitate charge separation and thus contribute to the piezocatalytic activity observed in BVO systems, which are nominally centrosymmetric.

The piezocatalytic activity of BVO mainly originates from the separation of surface charges induced by mechanical stress. Ultrasound-induced lattice strain generates e^--h^+ pairs that drive redox reactions and promote ROS formation, thereby enabling organic oxidation and water splitting [134]. Additionally, BVO also absorbs visible light, the visible-light response of BVO, together with its piezocatalytic capability, enables synergistic piezo–photocatalytic systems where dual activation enhances charge separation and kinetics for efficient environmental and energy applications [135].

8. Enhancement of piezo-(photo)catalysis activity of the catalysts

Although the aforementioned bismuth-based materials possess piezo/-photocatalytic properties, their practical applications are still limited by the poor intrinsic carrier mobility and the inadequate utilization of solar energy (the response of most bismuth-based materials to visible light is not very ideal). The strategies for enhancing the piezo-(photo)catalysis activity of the catalysts of bismuth-based materials are summarized as follows:

8.1. Defect project

Defect engineering serves as an effective approach to enhance the degradation processes catalyzed by piezoelectric. In addition, defect engineering can also enhance the activity of semiconductor photocatalysts by deliberately modifying its crystal structure and electronic state. Oxygen vacancy (Ov)-a prevalent form of lattice defect—play a key role in determining the material's optical and piezoelectric properties. O_V serve as active reaction sites in catalytic processes, it not only facilitating reactant activation but also helping to lower the thermodynamic energy barrier [136–139]. From a band structure perspective, O_V

promote carrier separation by forming defect bands between the CB and VB [140–142]. Liu et al. [143] synthesized $Bi_4Ti_3O_{12}$ with tunable O_V for piezocatalytic H_2O_2 production (Fig. 9a). Results reveal a volcanic trend in piezocatalytic H_2O_2 production as a function of O_V concentration in pure water. This volcanic trend is due to the enhanced generation of $O_2^{\bullet-}$ by O_V, which is critical for H_2O_2 production. Despite their negative impact on piezoelectric properties, the boost in $O_2^{\bullet-}$ concentration ultimately governs the efficiency of the oxygen reduction pathway. Sha et al. [144] reported a strategy of using piezo-activated O_V to modulate the quantum well effect and p-band center in polar $BiOIO_3$ single crystals for exceptional photocatalysis. The introduction of the piezoelectric field serves to strengthen the local charge asymmetry distribution caused by O_V, which promotes the donation of electrons from the bulk to the surface iodine atoms, leading to favorable piezo-photocatalytic performance for various pollutant degradation (Fig. 9b). The presence of O_V in metal oxides leads to the formation of coordinatively unsaturated sites, which modifies both the surface acidity and electron affinity. These changes can enhance light absorption, thereby improving charge separation and increasing the accessibility of unsaturated coordination sites for catalytic processes.

As another type of defect project, sulfur vacancies can influence catalytic activity by creating coordinatively unsaturated sites on adjacent metal atoms, thereby increasing their acidity and electron affinity. The compounds containing sulfur vacancies have been widely investigated in photocatalysis, while their piezocatalytic applications are barely explored. Zhou et al. [145] explore the effect of sulfur vacancies in defective bismuth sulfide (Bi_2S_{3-x}) on the production of ROS under ultrasonic irradiation (Fig. 9c). They found that the introduction of sulfur vacancies breaks the centrosymmetric structure of pristine Bi_2S_3, thereby generating a piezoelectric effect and boosting the electrical energy within Bi_2S_{3-x}. By capturing electrons, the positively charged sulfur vacancies in Bi_2S_{3-x} facilitate the separation of electron-hole pairs generated by ultrasound. Consequently, Bi_2S_{3-x} exhibits pronounced performance under ultrasonic irradiation, with the rate of H_2O_2 formation and the RhB degradation rate constant being 1.9-fold and 37-fold greater than those of Bi_2S_3, respectively.

Along with non-metallic defect, metal defect engineering is another important strategy to enhance the piezo-(photo)catalytic performance of bi-based materials [146]. For example, Kang et al. [147] synthesized Bi_2WO_6 nanosheets featuring tunable bismuth vacancy (V_{Bi}) through ion exchange method (Fig. 9d). The high piezocatalytic efficiency (7.83×10^{-2} min^{-1}) of bi-defect-rich Bi_2WO_6 for RhB under ultrasound is facilitated by lattice-escaped bismuth ions, which promote charge carrier separation through the attraction of surrounding free electrons. Wang et al. [148] constructed Bi-deficient Bi_2O_2S (BOS) nanosheets for the decomposition of organic dyes and antibiotics. Under ultrasound, Bi_2O_2S (BOS−4) featuring abundant V_{Bi} achieved a remarkable degradation rate of 95.69% for RhB, which was roughly three times higher than that of BOS. The results can be largely attributed to the introduction of V_{Bi}, which not only narrow the band gap but also facilitate charge generation. Furthermore, these vacancies serve as centers that attract negative charges, guiding their migration in a specific direction and enabling effective charge separation, which collectively boosts the piezocatalytic efficiency (Fig. 9e). Recently, researchers have also combined the vacancy effect with heterojunctions, with the intention of leveraging the resulting synergistic effect to facilitate more efficient separation of charge carriers. Wang et al. [149] fabricated of V_{Bi}-enriched $BiOCl–Bi_2S_3$ heterojunctions via a novel light-induced deposition strategy (Fig. 9f). Under ultrasonic vibration in pure water, the optimal $BiOCl–Bi_2S_3$−40 composite exhibited a significantly enhanced hydrogen production rate of 678.67 μmol/g/h, representing a two-fold increase over that of pristine BiOCl (352.53 μmol/g/h). The enhanced performance is attributed to the strong built-in electric field from piezoelectric polarization that promotes charge separation, along with V_{Bi} that serve as electron traps to reduce interfacial charge-transfer barriers, as well as the synergistic interaction between heterojunction and V_{Bi} that enables efficient carrier migration. Defect engineering boosts piezoelectric potential and carrier migration via more active sites and larger surface area. However, the defect types (e.g., interstitial atoms and metal vacancies) and their distribution must be precisely regulated. On the one hand, an excessive number of vacancies can reduce crystallinity and impede charge separation. On the other hand, deep-lattice vacancies can

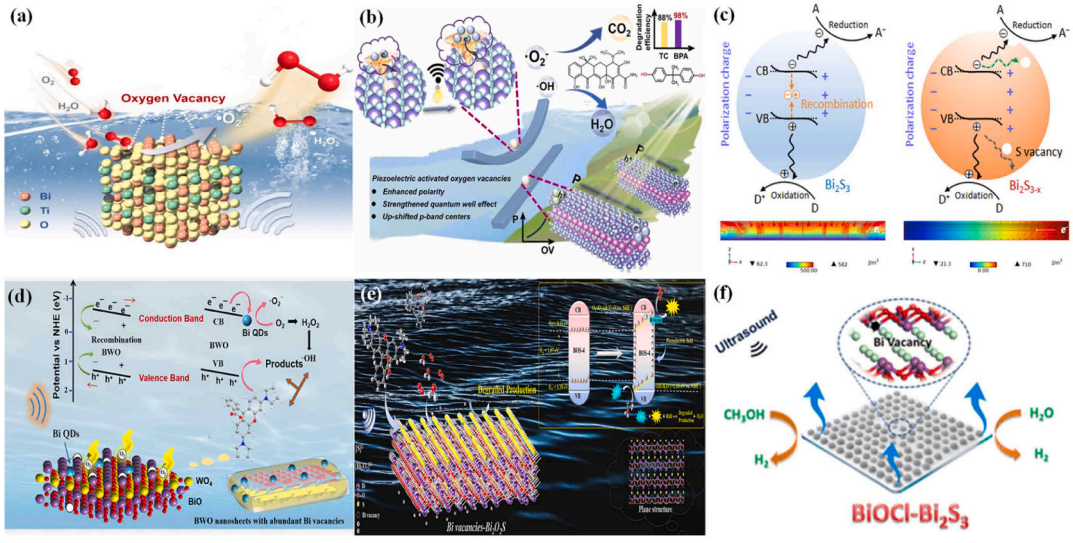

Fig. 9. Schematic of (a) $Bi_4Ti_3O_{12}$ with tunable OV for piezocatalytic H_2O_2 production, Reproduced with permission from Ref. [143]. Copyright 2025 Elsevier. (b) OV riched $BiOIO_3$ for piezo-photocatalytic degradation of pollutants, Reproduced with permission from Ref. [144]. Copyright 2025 Elsevier. (c) Schematic representations of the charge carrier activation and the simulated piezoelectronic energy distributions in Bi_2S_3 and Bi_2S_{3-x} subjected to mechanical force, Reproduced with permission from Ref. [145]. Copyright 2024 American Chemical Society. (d) Schematic representation of the catalytic reactions induced by piezopotential in Bi-defective BWO nanosheets subjected to mechanical force, Reproduced with permission from Ref. [147]. Copyright 2022 American Chemical Society. (e) Schematic of Bi-deficient Bi_2O_2S (BOS) nanosheets for the decomposition of organic dyes and antibiotics, Reproduced with permission from Ref. [148]. Copyright 2025 Elsevier. (f) Schematic of bismuth vacancy-engineered BiOCl–Bi2S3 heterojunctions piezoelectric catalytic mechanism, Reproduced with permission from Ref. [149]. Copyright 2026 Royal Society of Chemistry.

also act as recombination centers by trapping charge carriers. Future efforts should couple atomic layer deposition with other techniques to: (1) precisely control both the concentration and spatial distribution of vacancies; (2) build a predictive quantitative model for defect properties and synthesis parameters; and (3) elucidate the synergistic action of multiple defects (e.g., O and metal vacancies) and their stability under long-term operation, aiming at practical defect engineering and environmental robustness.

8.2. Doping modification

Doping strategy is an easy and effective method to elevate the carrier density and adjust the band gap of the catalyst. By incorporating foreign elements to the catalyst, the carrier density was greatly elevated, and the band gap was properly modulated, leading to an improvement in the piezo-(photo)catalysis activity [150,151].

Roy et al. [150] introduced Gd element into bismuth ferrite piezoelectric catalyst via a facile two-step solvothermal method, due to the much smaller ionic radius of Gd^{3+} (0.938 Å) compared to Bi^{3+} (1.17 Å), a significant lattice distortion occurs. This made the synthesized catalyst exhibited high polarization (0.92 μC/cm^2), which leading to a high piezoelectric activity for the degradation of RhB (97.6%) and EBT (91.3%). Moreover, the catalyst also exhibited remarkable antibacterial efficacy, with a bacterial mortality rate of approximately 99.33% within 30 min. In summary, the addition of Gd introduces structural distortion within the BFO matrix, this distortion leads to a heightened polarization effect, as polarization intensifies, the piezo response becomes increasingly prominent (Fig. 10a). In addition, bimetallic doping is also commonly used in the modification of piezoelectric materials. Guo et al. [124] prepared a bimetallic (Sm and Mn) co-doped $BiFeO_3$ (BFO) piezoelectric catalyst, results shown that the incorporation of Sm and Mn dopants reduced the band gap of BFO, alongside enhancements in the polarization electric field and piezoelectric coefficients, which collectively led to a significant improvement in piezocatalytic efficiency. The synthesized piezoelectric catalyst exhibited a significantly enhanced U (VI) removal rate of 94.8% over 120 min, which was about 3.2, 4.7 and 8.3 times higher than that of Sm doped BFO alone, Mn doped BFO alone and pure BFO, respectively, and simultaneously achieving a H_2 generation rate of 402 μmol/g/h. The findings reveal that doping substantially improves the piezocatalytic performance of BFO, presenting a viable strategy for wastewater remediation and sustainable energy generation (Fig. 10b).

Concurrently, piezo-photochemistry, as a derivative of traditional photocatalysis, has been receiving growing attention as an emerging field [152,153]. The fundamental principle of the piezoelectric effect involves converting external mechanical forces into a periodic stress applied to the photoelectrode, which in turn displaces the positive and negative charge centers within the material, thereby facilitating the efficient separation and migration of photogenerated electron-hole pairs [154]. Liu and co-workers [155] synthesized Cl^- modified $BiVO_4$ by a synthetic post-treatment method. Cl^- - modification can suppress surface charge recombination. Cl^- bonding with Bi^{3+} causing the distortion of the BiO_8 polar groups, this not only improves the piezoelectric response of the as-prepared catalyst, but also significantly enhances the piezo-photocatalytic performance for water oxidation (Fig. 10c). Without the use of any co-catalyst or sacrificial agent, the Cl^--embedded modified $BiVO_4$ achieved a photocurrent density of 0.268 mA/cm^2 at 1.23 V vs. RHE, which is 5 times higher than that of $BiVO_4$. Wang et al. [156] prepared Ce^{4+} doped Bi_2NdO_4Cl piezo-photocatalysts by a high-temperature solid-phase method, Ce^{4+} doping not only enhances

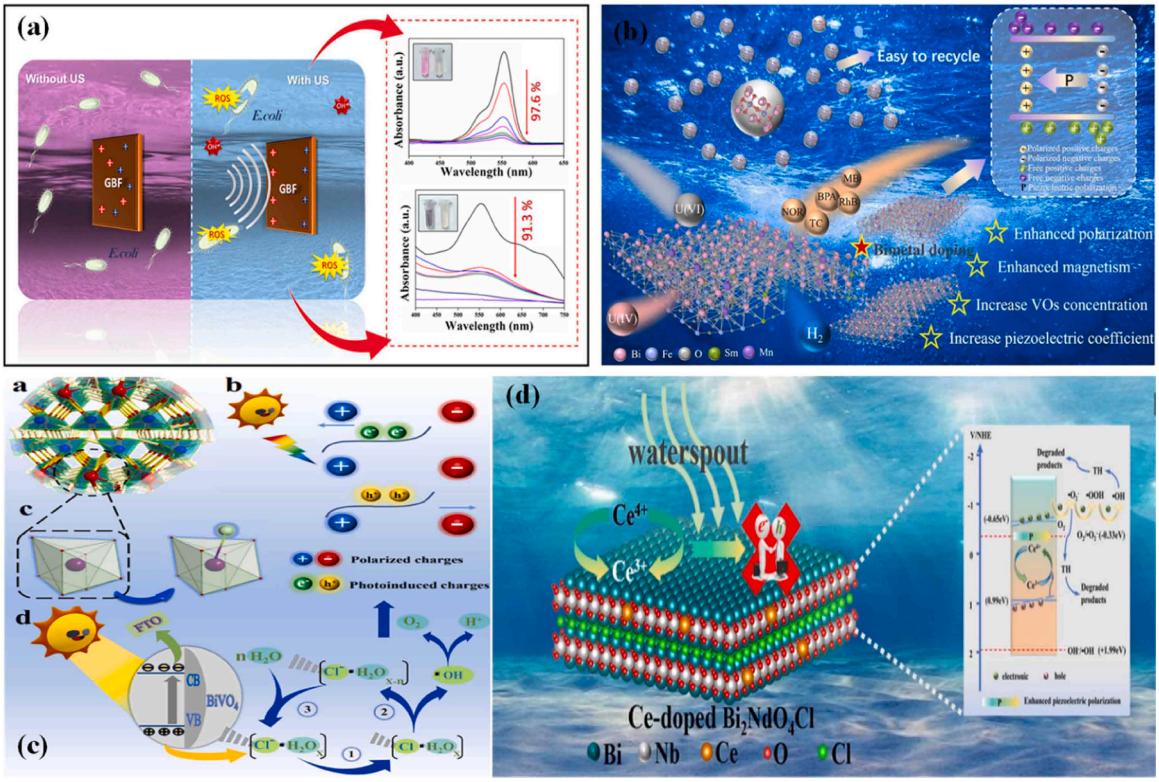

Fig. 10. Schematic diagram of (a) piezoelectric catalytic degradation of dyes and *E. coli* by Gd-doped bismuth ferrite, Reproduced with permission from Ref. [150]. Copyright 2024 Elsevier. (b) Sm and Mn co-doped $BiFeO_3$ for the reduction of uranium (U(VI)) and the production of hydrogen (H_2), Reproduced with permission from Ref. [124]. Copyright 2025 Elsevier. (c) a: the crystal structure of $BiVO_4$, b: polarization-driven bulk charge separation, c: Cl^- modified BiO_8 dodecahedron, d: ransfer of photogenerated holes and their subsequent reaction with water molecules for O_2 evolution on Cl^--modified $BiVO_4$, Reproduced with permission from Ref. [155]. Copyright 2024 Elsevier. (d) the mechanism of how Ce doping in Bi_2NdO_4Cl enhances its piezoelectric and photocatalytic properties, Reproduced with permission from Ref. [156]. Copyright 2025 Elsevier.

the piezoelectric performance of Bi_2NdO_4Cl by inducing the lattice distortion through the replacement of Nd^{3+} by Ce^{4+}, but also improves the separation efficiency of photogenerated electron-hole pairs where Ce^{4+} act as an electron trapping agent, leading an effectively synergistic enhancement for the degradation of TCH (Fig. 10d). Doping can tune the electronic structure of materials and boost the mechano–photocatalytic synergy. The current focus of research lies in rare-earth/transition-metal composite doping systems. Efforts are directed toward optimizing doping concentration and distribution, combined with precise techniques like atomic layer deposition, while also enhancing multiple properties synergistically through heterostructure design and defect engineering. Nevertheless, the doping kinetics and environmental adaptability remain poorly understood and impractical, posing obstacles to overcome.

8.3. Heterostructure construction

The construction of heterojunctions is another effective method to suppress the recombination of charge carriers, with proven efficacy in photocatalysis as well as in piezocatalysis. Many researchers have coupled bismuth-based piezoelectric crystals with other semiconductor materials to promote the separation efficiency of charge carriers. According to their band alignment, heterojunction structures can be categorized into Type I, Type II heterojunctions, Z-scheme, S-scheme and Schottky junctions [157].

Yue et al. [158] synthesized a 1 T@2H-MoS_2/Bi_2S_3 type-II heterojunction piezoelectric catalyst, under ultrasonic conditions, the 1 T@2H-MoS_2/Bi_2S_3 composite shows markedly enhanced performance in the piezoelectric degradation of methylene blue compared to 1 T@2H-MoS_2. The piezoelectric catalytic mechanism could be ascribed to: the incorporation of 1T-MoS_2 and Bi_2S_3 endows MoS_2/Bi_2S_3 with very low electrochemical impedance, which owing to the synergistic effect between the interfacial electric field. In addition, the highly conductive 1T-MoS_2 renders a high-speed pathway for free carrier transport. (Fig. 11a). Zhang et al. [159] fabricated Bi_2MoO_6-$BaTiO_3$ (BMO-BTO) Type-I heterojunction piezocatalyst for H_2 production. Under ultrasonic vibration, the BMO−0.1BTO heterojunction achieved a H_2 production rate of nearly 152.57 μmol/g/h. This performance surpasses that of the individual BMO (16.36 μmol/g/h) and BTO (34.16 μmol/g/h) samples by factors of approximately 9.33 and 4.47, respectively. The enhanced H_2 production could be explained by: under the action of ultrasonic, an intrinsic piezoelectric field can be induced within BTO, which facilitates the migration of charge carriers in opposite directions. Because of the energy level mismatch between the VB of BMO and the CB of BTO, the e^- in the CB of BTO tend to migrate to the lower-energy CB of BMO, while the h^+ in the VB of BTO are prone to transfer to the VB of BMO. Subsequently, a large number of charge carriers gathered in the CB and VB of BMO, they are then separated and migrate to the active sites. In aqueous environment, e^- reduce H^+ to H_2, while the h^+-scavenging agent MeOH enhances piezoelectric carrier separation, whose synergy delivers exceptional piezocatalytic H_2 production performance (Fig. 11b).

In the field of piezo-photocatalysis, constructing heterojunctions not only facilitates the separation and migration of photogenerated charge carriers but also harnesses the built-in electric field to synergistically couple the piezoelectric effect with photocatalysis. Bai et al. [160] prepared a Z-scheme $Bi_4Ti_{3-2n}Cr_nNb_nO_{12}$/x-g-$C_3N_4$ heterojunctions by using the molten salt method, under external ultrasound, the piezoelectric response of $Bi_4Ti_{3-2n}Cr_nNb_nO_{12}$ was activated, which enhanced the piezoelectric polarization electric field. The enhanced polarization field promoted band bending in $Bi_4Ti_{3-2n}Cr_nNb_nO_{12}$, thereby reducing the interfacial Schottky barriers and thus enabling a faster transfer of photogenerated e^- across the interface. Through a combination of energy band bending (induced by the piezoelectric polarization of $Bi_4Ti_{3-2n}Cr_nNb_nO_{12}$) and the Z-scheme heterojunction, the piezo-photocatalytic activity of $Bi_4Ti_{3-2n}Cr_nNb_nO_{12}$ was synergistically promoted (Fig. 11c). Liu et al. [161] prepared a type-II heterojunction $Bi_2MoO_6/KNbO_3$ piezo-photocatalyst using a simple solvothermal method, theoretical analysis indicates that under the synergistic effects of ultrasound and illumination, the construction of heterojunction

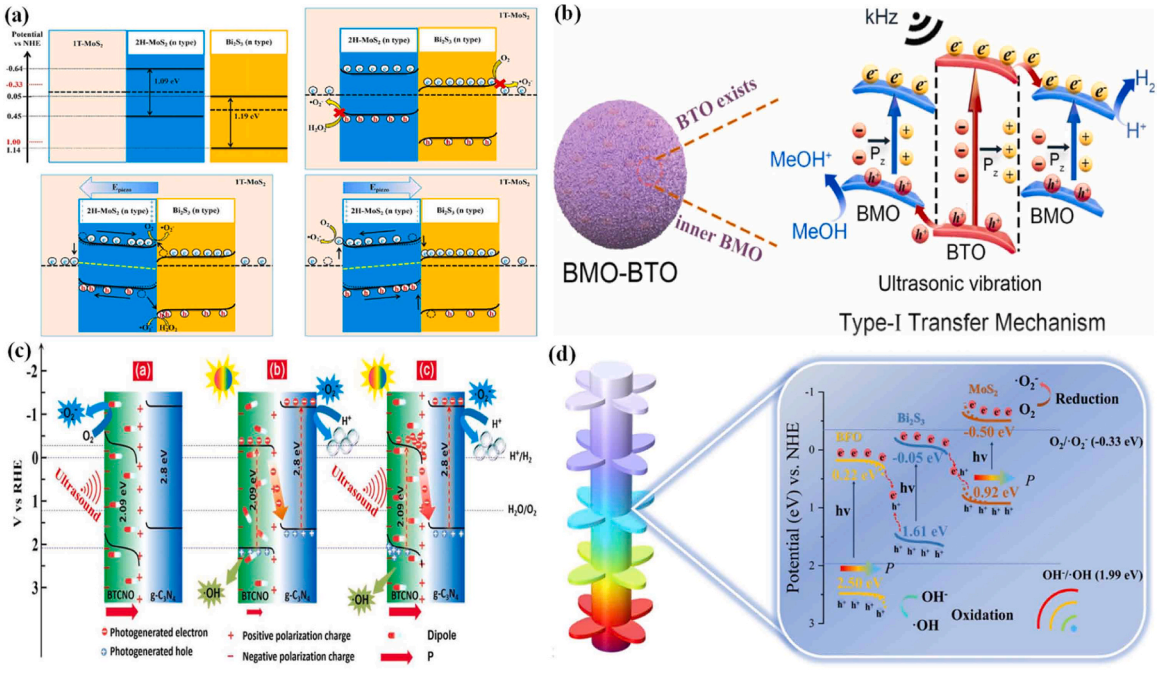

Fig. 11. Schematic diagram of (a) of the energy band structure of the 1T@2H-MoS_2/Bi_2S_3 heterojunction and the piezoelectric catalysis process under external mechanical force (dashed lines indicating the Fermi level), Reproduced with permission from Ref. [158]. Copyright 2023 Elsevier. (b) Bi_2MoO_6-$BaTiO_3$ Type-I heterojunction promotes piezocatalytic H2 production, Reproduced with permission from Ref. [159]. Copyright 2024 Elsevier. (c) piezocatalytic (a), photocatalysis (b) and piezo-photocatalytic (c) of $Bi_4Ti_{3-2n}Cr_nNb_nO_{12}$/x-g-$C_3N_4$ heterojunctions, Reproduced with permission from Ref. [160]. Copyright 2023 Elsevier. (d) piezo-photocatalytic mechanism of Fibrous $MoS_2/Bi_2S_3/BiFeO_3$ ternary heterojunction, Reproduced with permission from Ref. [163]. Copyright 2025 Elsevier.

composite greatly inhibited the recombination rate of photogenerated e^--h^+ pairs at the phase interface, resulting in notable oxidation ability towards methylene blue, TC and Congo red degradation. Yin et al. [162] synthesized $BiTi_5NbO_{14}$/BiOCl type II heterojunction piezo-photocatalyst, the lamellar structure $BiTi_5NbO_{14}$ and flower-spherical structure BiOCl provided a multitude of active site for catalytic reaction. Under the action of ultrasonic, an inherent electric field was formed via the piezoelectric effect, which triggered piezoelectric catalysis and greatly promoted the separation of photogenerated e^--h^+. Results indicated that the constructed heterojunction piezo-photocatalyst not only exhibited competitive oxidation efficiency towards a wide range of organic pollutants, but also showed good cycling stability. To further enhance the oxidation efficiency of piezo-photocatalysis, ternary composite system heterojunctions have also been synthesized. Zhou et al. [163] designed a novel MoS_2/-Bi_2S_3/$BiFeO_3$ piezo-photocatalyst, the catalyst exhibited enhanced piezoelectric properties, as evidenced by Kelvin probe force microscopy and piezoresponse force microscopy, which showed a surface potential difference of 66.50 mV and the maximum amplitude displacement of 395.51 pm under 9.91 V, respectively. Finite element simulations showed that the ternary heterojunction was capable of attain a larger piezoelectric potential. A high ciprofloxacin piezo-photocatalytic degradation efficiency of 96.6% within 75 min was achieved by the MoS_2/Bi_2S_3/BFO heterojunction, which was markedly surpassed that of single photocatalysis (60.5%) and piezoelectric catalysis (25.5%) (Fig. 11d). Heterojunction structures offer a promising avenue for boosting the piezo-(photo)catalytic activity of bi-based materials, as they effectively widen the range of absorbable light and enhance the efficiency of charge separation. However, the intricate fabrication, high cost, and variable performance of heterojunctions still pose significant challenges. In future work, research should prioritize new combinations of materials, such as coupling of diverse materials with bi-based materials to attain strong visible light harvesting, which can be accomplished through strategies like employing a visible-light sensitizer or harnessing surface plasmon resonance [164–167]. These efforts should aim at precise control of interfacial properties (roughness and contact area), interlayer modification, and band-gap engineering. Furthermore, optimization of the electronic structure and charge-transport mechanisms should be pursued through a combination of empirical analysis and theoretical modeling, ultimately overcoming the practical application bottleneck.

The above are the three common modification strategy of bismuth-based materials in the fields of piezo-(photo)catalysis, and the advantages and disadvantages of each strategy are summarized in Table 1. It is noteworthy that these strategies are not mutually exclusive; rather, they often exhibit synergistic effects. For instance, oxygen vacancies (defect engineering) and heterojunction construction could work cooperatively to regulate intrinsic vacancy concentrations while facilitating charge carrier separation. However, strategies such as polarization state regulation, heterojunction engineering, and defect engineering must balance multi-physical field synergy, lattice mismatch, and defect concentration to achieve optimal performance.

Table 1
Comparison of the modification strategies.

Strategies	Superiority	Limitation	Applicable scenarios
Defect project	Regulate band structure, create active sites	the concentration of defects must be precisely control	The systems that require the regulation of electronic structure
Element doping	Precisely control the properties of electrons and structures	The uniformity of doping is difficult to control, which may introduce lattice distortion.	Suitable for bandgap control and conductivity optimization
Heterostructure construction	Efficiently promoting carrier separation	Interface lattice mismatch problem	Applicable to scenarios where interface charge separation plays a dominant role

9. Application fields

9.1. Water pollution remediation

The technology of piezo-(photo)catalysis offers a promising solution for water treatment, demonstrating high effectiveness against a wide range of pollutants, such as organic dye, heavy/radioactive metal, antibiotics, etc [168]. Piezoelectric materials present key advantages of low energy consumption and minimal pollution compared to methods such as photocatalysis, electrocatalysis and chemical treatment. They accomplish this by utilizing diverse clean mechanical energy sources to drive or improve water purification, these catalytic processes produce abundant ROS. These reactive agents then attack pollutants through redox reactions and compromise the cellular integrity of harmful microbes, thus accomplishing water purification [169].

Since the pioneering work by Hong et al. in 2012, who first utilized ultrasonic vibration to achieve piezocatalytic degradation of Acid Orange II using $BaTiO_3$ fibers [170], the applications of piezo-(photo) catalysis have significantly broadened. These technologies are now employed to purify a wide range of pollutants in water. Du et al. [171] synthesized a Type-II n–n heterojunction piezocatalyst, $Bi_4Ti_3O_{12}$/MoS_2 (BTO/MS), by using a simple hydrothermal method. It was found that the 5%BTO/MS composite showed the highest removal efficiency toward ciprofloxacin (CIP). The 10 mg/L CIP removal reached 94.46% with a rate constant of 0.0539 min^{-1}, which is equivalent to 3.46 times that of pure MoS_2 and 17.39 times that of pure $Bi_4Ti_3O_{12}$. By forming an n–n Type-II heterojunction, the composite structure not only effectively alleviated MoS_2 nanosheet agglomeration but also suppressed charge recombination, thereby significantly boosting the piezocatalytic performance (Fig. 12a). Chang et al. [172] fabricated ZnO/BiOCl heterojunctions piezo-photocatalyst, the heterojunctions exhibit outstanding activity in the piezo-photocatalytic degradation of norfloxacin, with synergy factors of 1.92 versus piezocatalysis alone and 1.22 versus photocatalysis alone. Combined mechanistic investigations (in-situ XPS, KPFM, SPV, EPR, and DFT calculations) have revealed a direct Z-scheme charge transfer pathway, which is significantly promoted by the interfacial piezoelectric field. Oxygen vacancies in ZnO are recognized as crucial mediators that enable light-controlled reversal of the built-in electric field, thereby directing carrier flow (Fig. 12b).

In terms of heavy/radioactive metal removal, the piezo-(photo) catalysis technology has also achieved satisfactory results. Huang et al. [173] constructed a PVDF-HKUST−1/$BiVO_4$ piezo-photocatalytic membrane for Cr (VI) removal by combing Z-scheme HKUST−1/$BiVO_4$ and piezoelectric PVDF via electrospinning method. The novel flexible fiber piezo-photocatalytic membrane exhibited a high piezo-photocatalytic efficiency with the Cr (VI) removal rate of 85.33% within 120 min. This performance surpassed the photocatalysis and piezocatalytic alone by a factor of 1.35 and 2.19, respectively, which could be attributed to the synergistic effect of the piezoelectric field generated by PVDF and the heterojunction formed between HKUST−1 and $BiVO_4$ availably boosted the separation of photogenerated charges. Guo et al. [174] designed a $BiFeO_3$@In_2Se_3 heterojunction piezo-catalyst for uranium (U(VI)) removal from U(VI)-containing water. The system exhibited a U(VI) removal efficiency of 94.6% under ultrasonic vibration, with no sacrificial agents involved. They also found that with the help of auxiliary illumination, the free charges within the piezocatalyst would be accelerated, thereby promoting charge retention and leading to an improved U(VI) removal efficiency of 98.8% and a significantly higher reaction rate constant.

In addition, as a novel disinfection technology, piezoelectric water

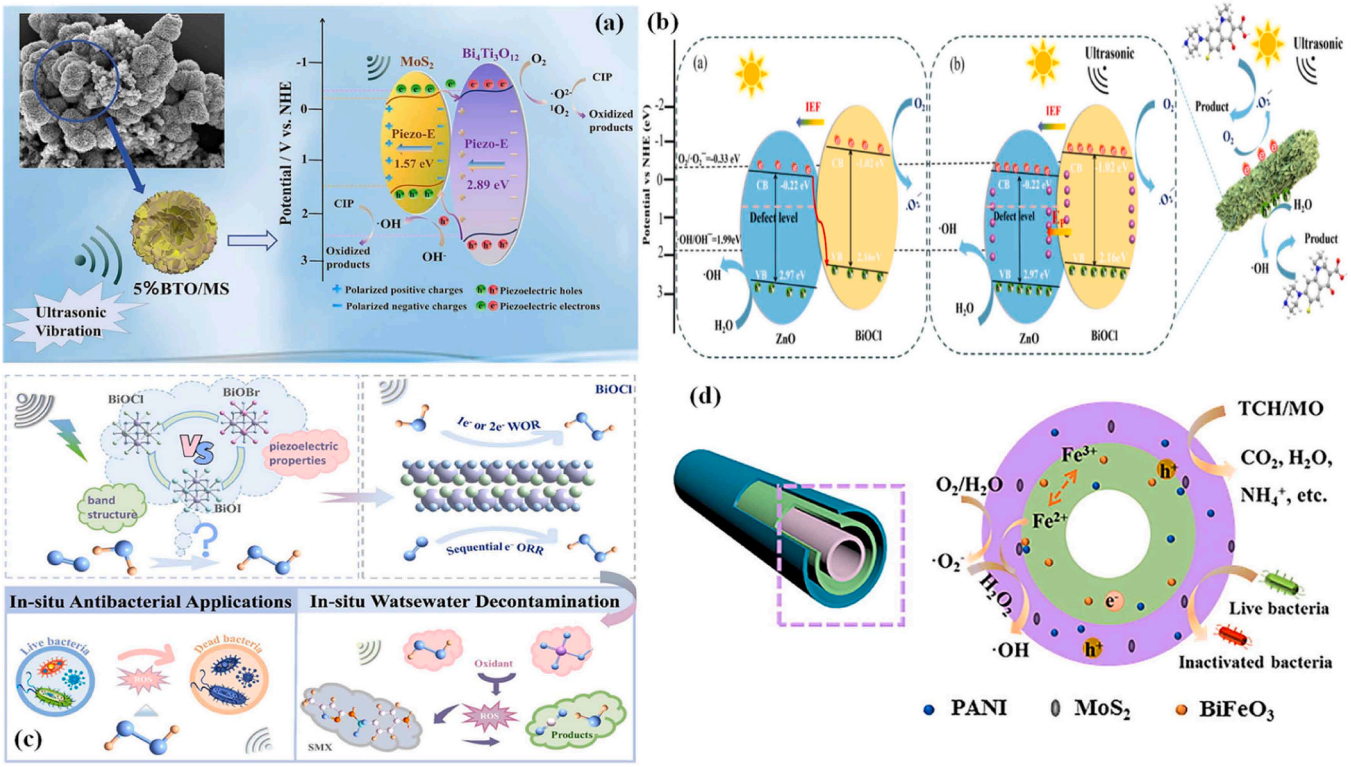

Fig. 12. Schematic diagram of (a) the mechanism of piezoelectric degradation of CIP by Bi4Ti3O12/MoS2, Reproduced with permission from Ref. [171]. Copyright 2026 Elsevier. (b) the charge transfer mechanism of ZnO/BiOCl under the exposure of (a) light and (b) both light and ultrasound, Reproduced with permission from Ref. [172]. Copyright 2026 Elsevier. (c) BiOX piezoelectric catalytic H2 production and its principle of simultaneously degrading organic pollutants in wastewater and sterilization, Reproduced with permission from Ref. [175]. Copyright 2026 Elsevier. (d) mechanism of piezo-photocatalytic degradation of organic pollutants and sterilization by MoS2/polyaniline (PANI)/polyacrylonitrile (PAN)@BiFeO3 bilayer hollow nanofiber membrane, Reproduced with permission from Ref. [176]. Copyright 2023 Elsevier.

disinfection has garnered much attention since it can overcome some limits in other disinfection methods, such as the restricted light energy utilization in photocatalysis, suboptimal efficacy in pyrocatalysis and low material utilization in contact-electro-catalysis. Xie et al. [175] employed BiOX (X = Cl, Br, I) to develop a system that integrates the production of H_2O_2 with its efficient in-situ utilization for organic wastewater disinfection. Through dual pathways—namely the water oxidation reaction (WOR) and oxygen reduction reaction (ORR)—the system achieved an exceptional piezocatalytic H_2O_2 production rate of over 710 μmol/g/h, the integrated system proved capable of good wastewater disinfection, as evidenced by an antibacterial efficiency of 70.7% (Fig. 12c). Lin et al. [176] designed a MoS_2/polyaniline (PANI)/polyacrylonitrile (PAN)@$BiFeO_3$ bilayer hollow piezoelectric nanofiber membrane (PPBMH) by coaxial electrospinning method. The fiber incorporated $BiFeO_3$ nanoparticles in the middle layer and MoS_2 nanosheets in the outer layer, forming a spatially separated type II heterojunction that markedly enhances charge separation during photocatalysis. Under ultrasonic excitation and visible light irradiation, PPBM-H exhibits a sterilization efficacy against nearly 100% of *E. coli* within 60 min, while under the same conditions, PPM only achieves an

Table 2
Summary of application of bismuth-based materials in piezo/-photocatalysis for water treatment.

Type	Catalysts and concentration	Reaction conditions	Target initial concentration	k (min^{-1})	Ref.
Piezo-photo	La/$BiFeO_3$ (0.2 g/L)	Ultrasonic (40 kHz, 100 W) + a simulated solar light 300 W Xenon lamp	CBZ (5 mg/L)	0.101 min^{-1}	[10]
Piezo	SnS_2-Bi_2S_3-BiOCl (0.2 g/L)	Ultrasonic (55 kHz, 100 W)	TCH (10 mg/L)	0.108 min^{-1}	[13]
Piezo	Bi-deficient Bi_2O_2S (0.3 g/L)	Ultrasonic (40 kHz, 100 W)	TCH (20 mg/L)	0.00401 min^{-1}	[148]
Piezo-photo	$Bi_2O_2OHNO_3$/$BiFeO_3$ (0.75 g/L)	Ultrasonic (100 W) + 300 W Xenon lamp	LEV (20 mg/L)	0.0569 min^{-1}	[164]
Piezo-photo	$Sr_2Bi_4Ti_5O_{18}$/BiOCl (0.4 g/L)	Ultrasonic (40 kHz, 120 W) + 300 W Xenon lamp (400 nm < λ < 780 nm)	CIP (20 mg/L)	0.015 min^{-1}	[167]
Piezo	$Bi_4Ti_3O_{12}$/MoS_2 (0.15 g/L)	Ultrasonic (40 kHz, 100 W)	CIP (10 mg/L)	0.0539 min^{-1}	[171]
Piezo-photo	ZnO/BiOCl (1 g/L)	Ultrasonic (60 kHz, 60 W) + 300 W Xenon lamp	norfloxacin (10 mg/L)	0.176 min^{-1}	[172]
Piezo-photo	PVDF-HKUST−1/$BiVO_4$ (Not given)	Ultrasonic (40 kHz, 150 W) + 300 W Xenon lamp (λ≥420 nm)	Cr (VI) (10 mg/L)	0.01420 min^{-1}	[173]
Piezo-photo	$BiFeO_3$@In_2Se_3 (1 g/L)	Ultrasonic (40 kHz, 120 W) + 300 W Xenon lamp	U(VI) (50 mg/L)	0.00922 min^{-1}	[174]
Piezo	BiOCl (0.5 g/L)	Ultrasonic (40 kHz, 280 W)	*E. coli* (Not given)	70.7% in 30 min	[175]
Piezo-photo	MoS_2/polyaniline/polyacrylonitrile @$BiFeO_3$ (1 g/L)	Ultrasonic (40 kHz, 300 W) + visible light	*E. coli* (10^7 CFU/mL)	100% in 30 min	[176]

inactivation level of approximately 3.88 log. Bacteriostatic cycle tests confirm that the high sterilization efficacy of PPBM-H against *E. coli* remains highly stable over five cycles, further indicating the recyclable stability and practical potential of PPBM-H (Fig. 12d). Other examples of bismuth-based piezo-(photo)catalysis for water treatment mentioned in this study are summarized in Table 2.

Although the piezo-(photo)catalysis technique has experienced explosive growth over the past decade (increasing nearly thirtyfold) and is expected to remain a significant research focus, its application in water treatment, especially for disinfection purposes, is still in its early stages. Future research should prioritize overcoming the bottlenecks of low mechanical energy utilization efficiency and material stability in complex water matrices. Key focuses will likely include the rational design of heterostructures with synergistic piezo-(photo)catalytic interfaces, the development of scalable reactor systems that effectively couple light and fluidic mechanical forces.

9.2. Energy conversion

The accelerated pace of industrialization has led to the heavy consumption of non-renewable fossil fuels, precipitating a worsening energy crisis. This situation urgently requires the development of alternative energy sources and the design of functional materials in sustainable energy technologies [177,178]. Piezo-(photo)catalysis are emerging technologies that utilize the piezoelectric effect to enable the highly efficient conversion of mechanical and solar energy into chemical energy. Bismuth-based piezo-(photo)catalysts have shown great potential in energy conversion, especially in capturing ambient mechanical energy and transforming it into useful chemical energy. Because of their multifunctionality, diverse structural chemistry, and advantageous electronic properties, some bismuth-based materials have emerged as highly adaptable piezo-(photo)catalysts for H_2 evolution, H_2O_2 synthesis, and CO_2 conversion.

Given its green credentials and high efficiency, hydrogen energy is considered a promising 'ultimate energy source' in the 21st century. As a promising sustainable energy conversion route, piezocatalytic H_2 production harnesses mechanical energy to drive redox reactions, relying on the piezoelectric properties of semiconductors. During this process, mechanical forces (e.g., ultrasound, fluid flow, or pressure) strain the piezoelectric material, creating an internal piezopotential [179]. The polarization field promotes the separation of charge carriers: e^- are directed to reduction sites for the reduction of H^+ to H_2, whereas h^+ move to oxidation sites for the oxidation of sacrificial agents or H_2O [180]. Wang et al. [181] developed Bi_5O_7Br ultrafine hollow nanotubes (HNTs), featuring a wall thickness of approximately 1 nm, as a highly sensitive piezocatalyst for water splitting. Unlike symmetric $[Bi_2O_2]$--based BiOBr, the Bi_5O_7Br HNTs are constructed from axially oriented, asymmetric polar $[Bi_5O_7]$ units. Attributed to this structural anisotropy, they exhibit high chemical bond anisotropy and a larger local electrostatic potential difference (ΔU) across all [-Bi-Br-], [-Bi-O-], and [-Br-Br-] regions, which collectively give rise to a strong piezoelectric response and IEF. Bi_5O_7Br exhibits enhanced H_2 evolution activity due to its more favorable Bi active sites that enable easy H* desorption, a feature originating from the upshifted p-band center (ε_p) of the Bi 6p orbital. Accordingly, Bi_5O_7Br HNTs yield an ultrahigh H_2 production rate of 2456.48 μmol/g/h (0.28% mechanical-to-H_2 efficiency) from pure water without sacrificial agents, with comparable efficacy in seawater and tap water (Fig. 13a). Moreover, piezo-photocatalysis, which couples piezoelectric activation with photoexcitation, has drawn increasing attention as a promising strategy to enhance H_2 production. In certain photoresponsive and piezoresponsive catalysts, polarized electric fields serve as a direct driving factor. Due to the charge shielding effect, these fields can direct e^- to positive regions and h^+ to negative regions [182]. Ma et al. [183] fabricated a Z-scheme $BiFeO_3$/CdS heterojunction piezo-photocatalyst for H_2 production. Owing to the piezoelectric effect, materials such as $BiFeO_3$ and CdS can develop spontaneous polarization moments under applied external forces. Piezoelectric polarization markedly improves charge redistribution in the catalyst's bulk phase, while also enabling the efficient separation and further migration of photogenerated carriers at the interface by means of a Z-scheme heterojunction. Under the action of ultrasound and visible light irradiation, the composite with 20 wt% CdS achieves a H_2 evolution rate of 3.58 mmol/g/h, which is 116.64 times higher than that of sole $BiFeO_3$ photocatalysis (Fig. 13b).

As an environmentally benign oxidant, H_2O_2 finds broad application in water treatment, disinfection, and green chemical synthesis, which

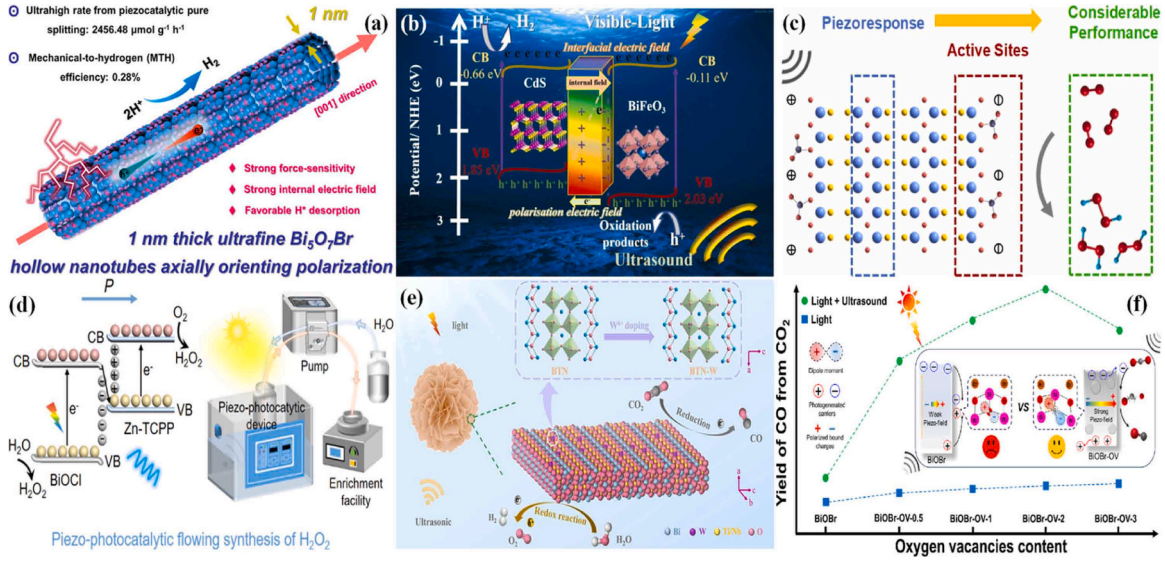

Fig. 13. Schematic diagram of (a) the piezocatalysis of H2 production using Bi5O7Br ultrafine hollow nanotubes, Reproduced with permission from Ref. [181]. Copyright 2011 American Chemical Society. (b) the piezo-photocatalysis of H2 production mechanism by BiFeO3/CdS, Reproduced with permission from Ref. [183]. Copyright 2025 Elsevier. (c) carbon modified BiOCl nanosheets for piezocatalytic H2O2 production, Reproduced with permission from Ref. [186]. Copyright 2023 Elsevier. (d) piezo-photocatalytic of H2O2 production by BiOCl/Zn-TCPP, Reproduced with permission from Ref. [187]. Copyright 2025 American Chemical Society (e) the mechanism of piezo-photocatalytic CO2 reduction by W doping in Bi3TiNbO9 nanosheets, Reproduced with permission from Ref. [190]. Copyright 2025 Elsevier. (f) the mechanism of pie.zo-photocatalytic CO2 reduction by Ov-BiOBr, Reproduced with permission from Ref. [191]. Copyright 2025 Elsevier.

makes its sustainable production a key research priority. However, traditional industrial methods, like the anthraquinone process, require high energy consumption and the use of hazardous organic solvents [184,185]. Piezocatalysis provides a promising alternative route for direct H_2O_2 synthesis from water under mechanical agitation, with no requirement for an external electric field or sacrificial agents. When a piezoelectric semiconductor is mechanically deformed, a polarization field is generated, thereby promoting charge separation. The piezoelectric field facilitates the migration of e^- and h^+ toward the catalyst surface, thus enabling the redox reactions essential for H_2O_2 formation. The dominant pathway is the two-electron oxygen reduction reaction ($2e^-$ ORR) (Eq. (3)):

$$O_2 + 2H^+ + 2e^- \rightarrow H_2O_2 \quad (3)$$

Zhou et al. [186] fabricated a carbon modified BiOCl nanosheets for piezocatalytic H_2O_2 production. Results shown that a high piezocatalytic H_2O_2 production rate of 2110 μmol/g/h was attained in pure water with carbon-modified BiOCl nanosheets. Mechanistic investigations indicated that while the carbon modification reduced the piezoelectricity of BiOCl, the contributions of the carbon species—which increase charge carrier density and act as oxygen activation sites—more than compensate for this, leading to enhanced H_2O_2 production. Thus, the diminished piezoresponse is more than offset by the enhanced surface reactivity, resulting in elevated piezocatalytic performance of C-BiOCl compared to the pristine nanosheets (Fig. 13c). The combination of piezocatalysis and photocatalysis can further boost performance, as the piezopotential not only suppresses e^--h^+ recombination but also benefits from the extra carriers supplied by photoexcitation. Zhang et al. [187] constructed BiOCl/Zn-TCPP heterojunction piezo-photocatalyst, under light irradiation, photogenerated e^--h^+ are generated on BiOCl/Zn-TCPP, and then separated by the interfacial IEF. The application of ultrasonic established an interfacial built-in electric field between BiOCl and Zn-TCPP, accompanied by the formation of bound surface charges driven by piezoelectric polarization. Specifically, the piezo-polarized charges cause band bending at the BiOCl/Zn-TCPP interface, which facilitates the migration of photogenerated e^--h^+ in opposite directions, resulting in more e^- accumulating on Zn sites for the reduction of O_2 to $O_2^{\bullet-}$. Subsequently, $O_2^{\bullet-}$ reacts with protons in the solution to form H_2O_2. Concurrently, photogenerated h^+ at bi sites oxidize OH^- from water molecules to yield ·OH. Following that, the coupling of two ·OH produces H_2O_2. Additionally, the electron density distribution of BiOCl/Zn-TCPP indicates that the distinctive π–π conjugated framework of Zn-TCPP greatly facilitates efficient e^- transport across the BiOCl/Zn-TCPP composite. As a result, BiOCl/Zn-TCPP achieves a piezo-photocatalytic H_2O_2 production rate of 202,200 μM/g/h, which is 44 times higher than the sole photocatalysis activity and superior to most conventional photocatalysts. It is noteworthy that under operational conditions of a continuous-flow setup with sunlight and air, it produces H_2O_2 at a rate of 407 μM/h, reaching a concentration of 1.38 wt% after 10 h (Fig. 13d).

To enhance the performance of piezo-photocatalytic water splitting for producing H_2 and H_2O_2, sacrificial agents such as methanol, triethanolamine, sodium sulfide, and lactic acid are commonly employed. These agents function by scavenging holes or positive charges, thereby facilitating the effective separation of polarized charges or charge carriers. Therefore, the careful selection of sacrificial agents plays a key role in advancing piezo/-photocatalytic water splitting toward practical application. However, from the perspectives of green chemistry and energy conservation, in the field of piezo-(photo)catalytic H_2 and H_2O_2 production using bismuth-based materials, efficient systems that avoid the use of sacrificial agents should be developed.

The burning of non-renewable energy releases significant amounts of CO_2, which causes environmental issues like the greenhouse effect. As a result, converting captured CO_2 into high-value-added chemicals to reduce its atmospheric concentration has become a valuable and active area of research. The photocatalytic reduction of CO_2 typically relies on photosensitizers and sacrificial electron agents. However, it suffers from a high recombination rate of photogenerated charge carriers, leading to limited conversion efficiency. Despite its advantages of a relatively simple design and the selective production of various high-value products, electrocatalytic CO_2 reduction suffers from multiple reaction paths. This often leads to a mixture of products and substantial energy demands [188,189]. By leveraging the piezoelectric effect to convert mechanical energy into chemical driving force, piezo-(photo)catalysis can directly initiate reactions or boost photocatalysis for efficient, low-energy CO_2 conversion. Yu et al. [190] prepared a series of W-doped Bi_3TiNbO_9 piezo-photocatalyst nanosheets via a one-pot hydrothermal method. Research found that the introduction of W^{6+} as a substitute for Ti^{4+} in the perovskite-like layers of Bi_3TiNbO_9 induces lattice distortion. This enhancement in macroscopic polarization effectively promotes the separation and transport of photogenerated charge carriers, and the strong built-in electric field induced by mechanical stress can further suppress the recombination of e^--h^+. After corona poling, the optimized W-doped Bi_3TiNbO_9 (5% W) achieved a CO generation rate of 36.67 μmol/g/h, a 3.88-fold increase over the pristine material, and this was accomplished without any co-catalyst or sacrificial agent (Fig. 13e). Li and colleagues [191] found that the introduction of a moderate level of O_V could induce changes in Bi-Br stretching, creating strong local dipoles in BOB-O_V. Under simultaneous ultrasonic and light stimulation, the weak piezoelectric field of BOB led to easy recombination of photogenerated carriers. In contrast, the as-prepared BOB-O_V can generate a strong piezoelectric field that drives photogenerated e^- and h^+ toward opposite directions on the surface, enabling efficient catalytic reactions. Then, CO_2 molecules were abundantly adsorbed onto the defect sites of BOB-O_V, where bi atoms served as both active sites and electron-enrichment centers, enabling the activation of CO_2 by e^-. Attacked by CB-excited e^-, the activated CO_2 molecules distort geometrically to ease C═O bond cleavage, finally yielding CO as the major reduction product. Results exhibited that the CO_2 piezo-photocatalytic reduction efficiency of the modified material (BOB-O_V) surpassed pure BOB, reaching a CO production rate of 54.4 μmol/g/h. This represented a durable process with high selectivity of 92% (Fig. 11f). Table 3 presents a comparative summary of the recent applications of bi-based materials mediated piezo-(photo)catalysis on energy conversion.

Nevertheless, the development of piezoelectricity-driven photocatalytic CO_2 reduction is hampered by several unresolved issues, such as the alignment between the band edges of piezoelectric materials and the redox potentials for CO_2 reduction, the investigation of the underlying charge transfer mechanism for photogenerated charge carriers in piezo-photocatalyst, strategies for maintaining a persistent and stable piezoelectric field, and a deeper understanding of the CO_2 reduction reaction mechanism. Therefore, dedicated efforts are necessary to drive the development of piezoelectric materials and pave the way for their more effective application in piezo-(photo)catalytic CO_2 reduction.

9.3. Biomedical therapy

Piezocatalytic therapy is gaining significant attention as a promising new field of research. The application of ultrasound induces polarization and a built-in electric field within the piezoelectric material. This field, in turn, acts to continuously separate and draw the charge carriers toward opposing surfaces [192]. The charge carriers migrating to the surface interact with water and dissolved oxygen in the solution, thereby producing ROS that serve as the key therapeutic agents against cancer cells as well as bacterial infection [193]. Furthermore, ultrasound irradiation demonstrates deep tissue penetration (≈10 cm), precise targeting of deep-seated tumors, and non-invasiveness. These attributes establish it as a promising external activation source for medical applications.

Jing et al. [194] synthesized Fe-doped ultrathin $Bi_4Ti_3O_{12}$

Table 3
Summary of application of bismuth-based materials in piezo/-photocatalysis for Energy Conversion.

Type	Catalysts and concentration	Reaction conditions	Reaction solution	Applications	Performance	Ref.
Piezo	$Bi_4Ti_3O_{12}$ (0.5 g/L)	Ultrasonic (40 kHz, 300 W)	alcohol and water (volume ratio 1:9)	H_2O_2 generation	1611.2 μmol/h	[11]
Piezo	$Bi_2Fe_4O_9$ (0.2 g/L)	Ultrasonic (40 kHz, 200 W)	pure water	H_2 evolution	1058 μmol/g/h	[18]
Piezo	BiOCl (0.5 g/L)	Ultrasonic (53 kHz, 150 W)	pure water	H_2O_2 generation	28 μmol/h	[73]
Piezo	$Bi_4Ti_3O_{12}$ (0.5 g/L)	Ultrasonic (40 kHz, 150 W)	deionized water	H_2O_2 generation	147.2 μmol/h	[143]
Piezo	BiOCl–Bi_2S_3 (0.5 g/L)	Ultrasonic (45 kHz, 120 W)	deionized water	H_2 evolution	678.67 μmol/g/h	[149]
Piezo	Bi_2MoO_6-$BaTiO_3$ (0.17 g/L)	Ultrasonic (180 W, 240 W, and 300 W)	10 vol% MeOH	H_2 evolution	152.57 μmol/g/h	[159]
Piezo-photo	Cr/Nb modified $Bi_4Ti_3O_{12}$/g-C_3N_4 (0.38 g/L)	Ultrasonic (45 kHz) + 300 W Xenon lamp	0.15 M Na_2S solution	H_2 evolution	696 μmol/g/h	[160]
Piezo	Bi_5O_7Br ultrafine hollow nanotubes (0.1 g/L)	Ultrasonic (40 kHz, 240 W)	pure water	H_2 evolution	2456.48 μmol/g/h	[181]
Piezo-photo	$BiFeO_3$/CdS (0.2 g/L)	Ultrasonic (40 kHz, 100 W) + 300 W Xenon lamp (λ≥420 nm)	0.35 M Na_2S/0.25 M Na_2SO_3 solution	H_2 evolution	3.58 mmol/g/h	[183]
Piezo	C-BiOCl (0.2 g/L)	Ultrasonic (40 kHz, 100 W)	deionized water	H_2O_2 generation	2110 μmol/g/h	[186]
Piezo-photo	BiOCl/Zn-TCPP (0.5 g/L)	Ultrasonic (40 kHz, 300 W) + 300 W LED lamp	pure water	H_2O_2 generation	407 μmol/g/h	[187]
Piezo-photo	W-doped Bi_3TiNbO_9 (0.1 g/L)	Ultrasonic (40 kHz, 240 W) + 300 W Xenon lamp	deionized water	CO_2 reduction	36.67 μmol/g/h	[190]
Piezo-photo	OVs/BiOBr (1 g/L)	Ultrasonic (40 kHz, 120 W) + 300 W Xenon lamp	deionized water	CO_2 reduction	54.4 μmol/g/h	[191]

nanosheets (Fe-UBTONSs) piezoelectric catalyst for the treatment of cutaneous melanoma, targeting both tumor cells and bacteria under the action of ultrasound. The introduction of Fe doping establishes a piezo-chemocatalytic system, where piezocatalysis facilitates the

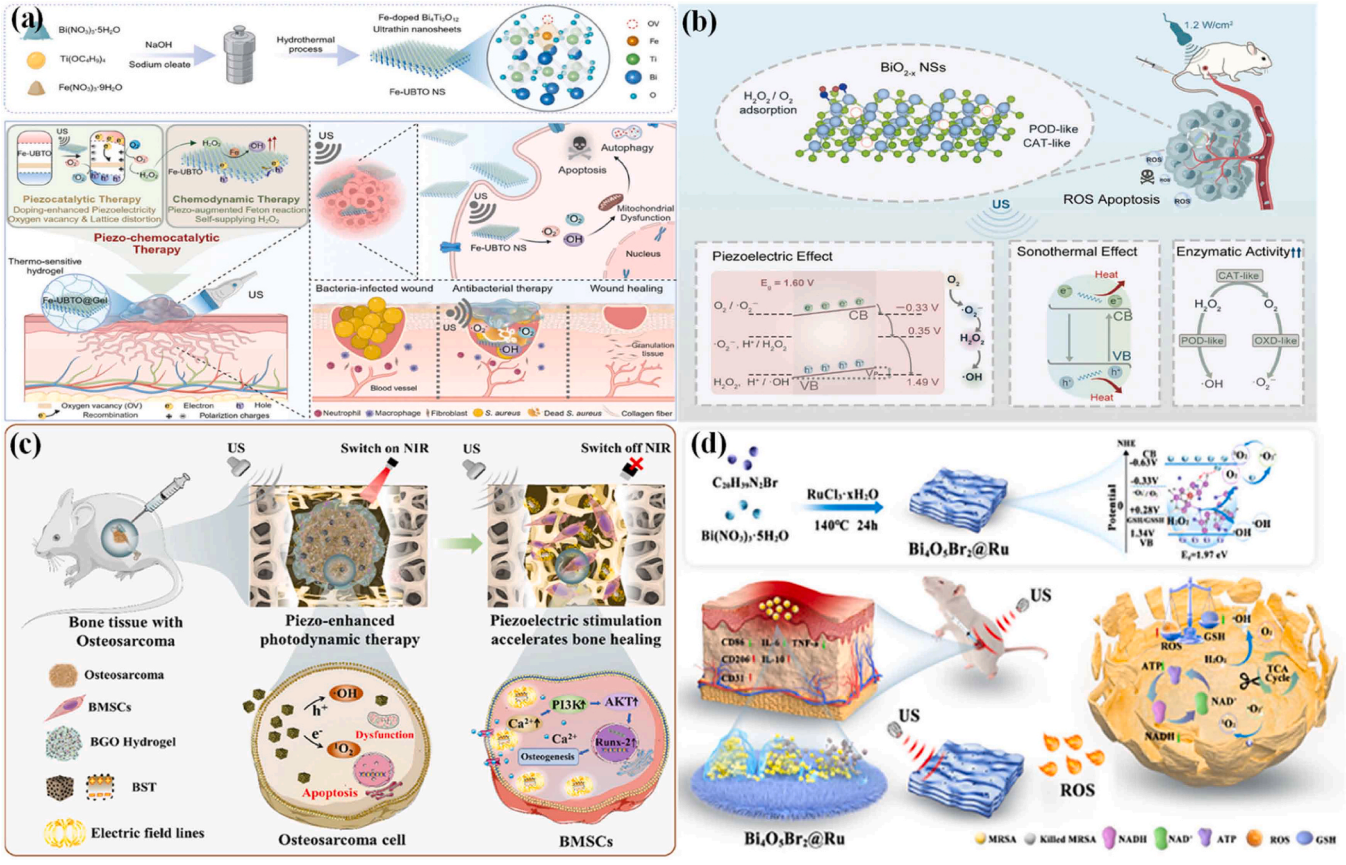

Fig. 14. Schematic diagram of (a) Fe-doped ultrathin $Bi_4Ti_3O_{12}$ nanosheets preparation process and the mechanism of piezocatalytic treatment of cutaneous melanoma, Reproduced with permission from Ref. [194]. Copyright 2024 Wiley. (b) the mechanism of piezocatalytic treatment of tumor by O_v-rich BiO_{2-x} nanosheets, Reproduced with permission from Ref. [195]. Copyright 2023 Wiley. (c) piezo-photocatalytic therapy anti-osteosarcoma and osteogenesis combination by Bi/SrTiO3, Reproduced with permission from Ref. [196]. Copyright 2024 Elsevier. (d) defect-Promoted Synergistic Piezoelectric and Nanozymatic Catalysis toward Deep Bacterial Abscess Therapy by Ru-doping $Bi_4O_5Br_2$, Reproduced with permission from Ref. [198]. Copyright 2025 American Chemical Society.

self-generation of H_2O_2 and promotes electron transfer in Fenton reactions, resulting in enhanced ·OH production. By inducing intracellular oxidative stress, the Fe-UBTO-based piezo-chemocatalytic therapy triggers tumor cell apoptosis and excessive autophagy, while concurrently accelerating wound healing via sterilization, angiogenesis, and enhanced collagen deposition (Fig. 14a). Yang et al. [195] synthesized O_V-rich BiO_{2-x} nanosheets (NSs). Ultrasonic excitation induces a 0.25 V piezo-potential on the as-obtained NSs, endowing them with peroxidase- and oxidase-like activities to elevate ROS yields, and this favorable effect is prominent in H_2O_2-overproduced tumor microenvironments. Moreover, the rapid movement of electrons facilitates a remarkable sonothermal effect. This effect is demonstrated by a swift temperature increase to approximately 65 °C under low-power ultrasound (1.2 W cm^{-2}) within a short duration of 96 s. The study achieved a synergistic integration of piezocatalytic, enzymatic, and sonothermal therapeutic modalities, representing a novel direction in tumor therapy (Fig. 14b). Xiao et al. [196] developed ultrasmall bismuth/strontium titanate nanocubes (Bi/$SrTiO_3$), the prepared piezoelectric material generated ROS efficiently by synergizing the rapid charge separation from the piezoelectric field and the surface plasmon resonance effect. When integrated into an injectable biopolymer hydrogel, these hybrid nanotherapeutics yield remarkable anticancer effects, enabling a potent anticancer response under dual NIR and ultrasound activation (Fig. 14c). The hydrogel demonstrated considerable filling and retention within the bone defect. Moreover, under mild ultrasound radiation, it facilitated bone repair by polarizing and delivering electrical stimuli to the resident cells.

As an innovative non-invasive antimicrobial approach, piezocatalytic therapy that employs lattice-asymmetric sonosensitizers provides flexible spatiotemporal selectivity and the capacity to penetrate deep into tissues. Chen et al. [197] constructed a piezocatalytic bio-heterojunction (P-bioHJ) which composed of BiOI and few-layered MXene for antibacterial application. The engineered P-bioHJ achieves rapid sterilization through a burst of radicals, a result of not only its relatively narrow bandgap, which responds to sonoluminescence from sonocavitation, but also its ability to induce interfacial polarization and O_V for effective carrier separation. Transcriptomic analysis points to P-bioHJ disruption of the bacterial electron transport chain as the mechanism of sterilization, undermining both bacterial metabolism and energy synthesis. The P-bioHJ exhibits good cytocompatibility in vitro, which is further corroborated by its outstanding in vivo antimicrobial performance in a cutaneous infection model. Moreover, when decorated with naringin, it demonstrates the additional functionality of promoting angiogenesis and osteogenesis in an infectious bone defect model. Peng et al. [198] fabricated a Ru-doping $Bi_4O_5Br_2$ ($Bi_4O_5Br_2$@Ru), the Ru dopants function as dual promoters of lattice distortion and O_V to simultaneously enhance the piezoelectric response and confer POD- and CAT-like enzymatic activities. Ultrasound excitation creates a piezoelectric field that optimizes the conduction band alignment of the prepared piezocatalyst. This enhanced alignment amplifies its POD-like activity, leading to the production of a series of ROS (·OH, $^1O_2$, and $O_2^{\bullet-}$). The mixed Ru (III/IV) valence states in $Bi_4O_5Br_2$@Ru function to deplete glutathione, resulting in a consequential enhancement of oxidative stress capacity for more effective biofilm eradication. The boosted CAT-like activity serves to ameliorate the hypoxic conditions within the biofilm microenvironment, and the RNA transcriptomic analysis points to the disruption of the tricarboxylic acid cycle as the mechanism by which $Bi_4O_5Br_2$@Ru impairs bacterial energy metabolism (Fig. 14d). Other studies about bi-based materials mediated piezo-(photo)catalysis on biomedical therapy are summarized in Table 4.

Despite the broad exploration of bi-based materials piezo-(photo) catalysis in biomedicine for disinfection, antibacterial purposes, and tumor therapy, substantial advancements in both efficiency and safety remain to be addressed. The biosafety of bismuth-based materials is key to their clinical translation. Generally, Bismuth-based nanomaterials possess good biocompatibility and low cytotoxicity [199]. For instance, $BiFeO_3$ nanoparticles maintain 85% cell viability even at concentrations as high as 75 μM [200]. The toxicity of Bismuth-based materials is predominantly determined by their physicochemical characteristics, including shape, size, chemical composition and surface chemistry [201]. Owing to their small size, Bi NPs can intimately interact with cellular components, including organelles, cell membranes, proteins and DNA, thereby giving rise to potential biological or cytotoxic effects. Although reports have shown low cytotoxicity of Bi NPs both in vitro and in vivo [202], data on toxic effects remain insufficient for clinical use thus far, and their pharmacokinetics, biodistribution, and clearance pathways in animal models call for systematic evaluation. Furthermore, the degradation behavior of Bi-based materials under physiological conditions is a key determinant of their long-term biocompatibility. The low solubility of bismuth compounds in biological fluids is a major contributing factor to their relatively non-toxic nature. Nonetheless, the long-term fate of Bi-based nanomaterials in vivo—including their degradation products and clearance routes—remains still poorly understood. Consequently, despite considerable progress made in preclinical studies, the clinical translation of bi-based piezo-(photo) catalysts faces great challenges: (1) lack of standardized toxicity evaluation protocols; (2) insufficient understanding of long-term biosafety and biodegradation; (3) complexity of large-scale synthesis with consistent quality; and (4) regulatory hurdles for nanomedicine approval. Future research should prioritize the development of safe-by-design strategies and comprehensive in vivo evaluations to bridge the gap between fundamental research and clinical applications.

Moreover, the early stage of this technology in biomedicine presents considerable obstacles for its subsequent development and clinical application. However, rapid technological progress is poised to enable piezo-(photo)catalytic therapy to make a substantial impact on medical innovation and the improvement of human health.

10. Summary and outlook

This review summarizes the types of bismuth-based materials in the fields of piezo-(photo)catalysis, the methods for enhancing the piezo-

Table 4
Summary of application of bismuth-based materials in piezo/-photocatalysis for biomedical therapy.

Type	Catalysts	Reaction conditions	Applications	Performance	Ref.
Piezo	$BiFeO_3$	1.0 W/cm^2	Tumor therapy	Promoting the activation of anticancer immunity	[20]
Piezo	Fe-doped $Bi_4Ti_3O_{12}$	Ultrasonic (40 kHz, 80 W)	Antitumor and Antibacterial Therapies	Tumor inhibition rate of 76.2%	[194]
Piezo	Ov riched BiO_{2-x}	Ultrasonic (1.2 W/cm^2)	Tumor therapy	Tumor tissue undergone severe apoptosis	[195]
Piezo-photo	Bi/$SrTiO_3$	Ultrasonic (1.0 MHz, 2.0 W/cm^2) + near-infrared light (808 nm, 1.0 W/cm^2)	Anti-osteosarcoma and osteogenesis combination therapy	Tumor suppression for xenograft and tibial osteosarcoma were 98.6% and 67.6% respectively	[196]
Piezo	BiOI/Mxene	Ultrasonic (40 kHz, 80 W) + 80 W Xenon lamp (λ≥420 nm)	Bacterial Infection	S. aureus inactivation rate of 99.85%	[197]
Piezo	$Bi_4O_5Br_2$@Ru	Ultrasonic (1 MHz)	Bacterial Abscess Therapy	E. coli removal rates of 74.2%	[198]

(photo)catalysis activities of catalysts, the advanced mechanistic beyond conventional piezo-(photo)catalysis and applications in various areas. Despite the publication of outstanding research on novel bi-based piezo-(photo)catalysis materials, the field remains in its nascent stages and requires continued development. For instance, the synthesis techniques for novel bi-based piezo-(photo)catalysts are confined to a narrow range, primarily centered around the hydrothermal method. Variations in experimental conditions, including catalyst dosage, pollutant concentration, and ultrasonic parameters, due to a lack of standardization, prevent meaningful comparison of piezo-(photo)catalysis performance. The catalytic mechanism remains a subject of debate. Current applications are largely confined to organic pollutants degradation and H_2 production; others, including CO_2 reduction, N_2 fixation, and sterilization, have received much less attention. Therefore, this gap offers vast potential for enriching the role of piezoelectric materials in catalysis. Given that persistent fundamental issues remain, we propose the following strategies for advancement:

(1) For layered bi-based piezoelectric catalyst, the piezoelectric effect occurred only confined to single or odd-numbered layers, and rapidly diminishing as the layer count increases, despite the natural coexistence of both odd and even layers. Moreover, the current synthesis methods—including hydrothermal, exfoliation, and CVD techniques—pose a significant challenge for accurately controlling monolayer number and scaling up production. Therefore, higher demands on current synthesis methods, particularly in enhancing the yield of monolayer bi-based piezoelectric catalyst.

(2) The primary techniques currently used to verify the piezoelectric properties of materials are piezoelectric force microscopy (PFM), second-harmonic generation (SHG), and theoretical simulation. However, there are extremely few documents that simultaneously contain the value of piezoelectric coefficients, polarization values, band gaps and charge-separation efficiencies, the simultaneous optimization of these three parameters and the associated mechanism still require further exploration. In addition, while the piezoelectric coefficients are not thoroughly detailed in some of the reviewed literature, it has been established through past experiments that mechanical vibration can enhance their piezo-photocatalytic performance. Nevertheless, these processes not only accelerate mass transfer but also enhance overall catalytic activity: ultrasonic vibration and mechanical stirring improve transfer, while ultrasonic cavitation induces sonocatalysis. Clarifying the role of piezoelectric effect in boosting catalytic activity requires performing piezoelectric tests and precise control of experimental variables.

(3) Understanding the dynamic evolution of piezoelectric polarization, charge carrier behavior, and surface reactive species under operational conditions is essential for elucidating the true catalytic mechanisms. It is an urgent need to develop operando characterization setups tailored specifically for piezo-(photo)catalytic reactions. Advanced in situ techniques—including operando EPR, Raman spectroscopy, and PFM—enable real-time monitoring of the piezoelectric response, charge separation dynamics, and ROS generation under simultaneous mechanical stimulation and light irradiation. Therefore, future research should prioritize the construction of integrated operando platforms that combine multiple spectroscopic and electrochemical probes to capture the full complexity of piezo-photocatalytic processes.

(4) First-principles calculations, particularly density functional theory (DFT), have become indispensable for predicting piezo-(photo)catalytic performance and elucidating reaction mechanisms at the atomic level. DFT calculations can effectively predict piezoelectric coefficients, band structures, charge density distributions, and adsorption energies of key intermediates, thereby guiding the rational design of high-performance piezo-(photo)catalysts. Moreover, future theoretical efforts should focus on developing machine-learning-accelerated high-throughput screening frameworks to rapidly identify promising bismuth-based piezo-(photo)catalyst candidates from the vast compositional space, as well as multi-scale modeling approaches that bridge atomic-scale piezoelectric responses with macroscopic catalytic performance.

(5) Current literature exhibits wide variations in experimental conditions—including ultrasonic frequency and power, catalyst dosage, pollutant concentration, temperature, pH, and mechanical energy input—making it extremely difficult to compare the catalytic performance of different materials reported by different research groups. At present, there is no universally standardized testing protocols for evaluating piezo-(photo)catalytic activity of bismuth-based materials. Thus, the community should work toward establishing standardized reference materials and benchmark reaction systems, as well as consensus guidelines for reporting key parameters such as mechanical energy input per unit volume, reaction temperature control, and the use of appropriate control experiments to distinguish piezocatalysis from sonocatalysis and tribocatalysis. Such standardization efforts will be essential for enabling meaningful cross-study comparisons and accelerating the translation of laboratory findings into practical applications.

(6) Despite the remarkable progress achieved at the laboratory scale, most piezo-(photo)catalysts are still synthesized through small-scale methods that are not readily transferable to industrial production. For bismuth-based materials, scalable synthesis must address not only production yield but also batch-to-batch consistency, phase purity, and morphological control, all of which critically influence piezocatalytic performance. Future research should explore continuous-flow synthesis and industry-relevant production scales to bridge the gap between academic research and industrial application.

(7) Translating piezo-(photo)catalysts from powder-form laboratory studies to practical devices represents a significant step toward practical applications. Future research should focus on the design of immobilized piezo-(photo)catalysts systems (e.g., films, membranes, and 3D porous frameworks) that enable easy recovery and reuse, as well as the integration of energy harvesting devices with piezocatalytic reaction systems. Future device development should consider flow-through reactor configurations, membrane-based separation, and hybrid systems that combine piezocatalysis with other advanced oxidation processes to maximize treatment efficiency. The development of self-powered piezocatalytic devices that harvest ambient mechanical energy (e.g., from water flow, wind, or vibration) represents an exciting frontier that could enable off-grid operation in remote or resource-limited settings.

(8) Piezo-(photo)catalysis offers a promising alternative to conventional methods for industrial wastewater treatment, enhancing the effectiveness of degrading organic pollutants and reducing heavy metal ions. Therefore, it has broad prospects for industrial applications. However, substantial barriers remain, including elevated operational costs, scalability limitations, and the need for integration with existing industrial infrastructure. Future study should focus on: (i) pilot-scale demonstrations to validate laboratory findings under real conditions; (ii) life-cycle assessment and techno-economic analysis to evaluate the economic viability of piezocatalytic technologies; and (iii) development of durable and stable piezo-(photo)catalysts that can withstand long-term operation in harsh industrial environments.

In summary, through the dedicated efforts of researchers, a diverse array of bi-based piezo-(photo)catalysts exhibiting high catalytic efficiency has been developed. This review may provide a useful reference for the future development of more novel materials with desirable piezo-(photo)catalytic performance, thereby contributing to a better comprehension of their mechanisms. This review may also provide impetus for advancements in related disciplines, including piezoelectric sensors and actuators, ultimately fostering the development of innovative piezoelectric materials for sustainable science and enhancing their potential for real-world applications. The investigation of novel piezoelectric materials is crucial for deepening our comprehension of the mechanisms underlying piezo-(photo)catalytic processes. It is anticipated that this research will support the future design and development of more innovative bi-based piezo-(photo)electric materials.

CRediT authorship contribution statement

Xingang Wang: Supervision, Methodology. **Dong Li:** Writing – review & editing, Supervision, Funding acquisition. **Xiaoyu Pu:** Methodology, Data curation. **Tianxin Wang:** Project administration, Methodology, Investigation. **Jialin Jia:** Writing – review & editing, Writing – original draft, Resources, Methodology, Formal analysis, Conceptualization.

Declaration of Competing Interest

The authors declare that they have no known competing financial interests or personal relationships that could have appeared to influence the work reported in this paper.

Acknowledgments

This work was supported by funds from the Natural Science Foundation of Jiangsu Province (Grant No BK20241535), National Natural Science Foundation of China (Grant No. 22306101), and Fundamental Research Funds for the Central Universities (Grant No. 3072026ZX2709).

Data availability

No data was used for the research described in the article.

References

[1] H.J. Zheng, Y.L. Wang, J.S. Liu, J. Wang, K. Yan, K.J. Zhu, Recent advancements in the use of novel piezoelectric materials for piezocatalytic and piezo-photocatalytic applications, Appl. Catal. B Environ. 341 (2024) 123335, https://doi.org/10.1016/j.apcatb.2023.123335.

[2] A. Fujishima, K. Honda, Electrochemical photolysis of water at a semiconductor electrode, Nature 238 (1972) 37–38, https://doi.org/10.1038/238037a0.

[3] J. Schneider, M. Matsuoka, M. Takeuchi, J. Zhang, Y. Horiuchi, M. Anpo, D. W. Bahnemann, Understanding TiO_2 photocatalysis: mechanisms and materials, Chem. Rev. 114 (2014) 9919–9986, https://doi.org/10.1021/cr5001892.

[4] W. Wang, M.O. Tadé, Z. Shao, Research progress of perovskite materials in photocatalysis- and photovoltaics-related energy conversion and environmental treatment, Chem. Soc. Rev. 44 (2015) 5371–5408, https://doi.org/10.1039/C5CS00113G.

[5] M. Ge, J. Cai, J. Iocozzia, C. Cao, J. Huang, X. Zhang, J. Shen, S. Wang, S. Zhang, K.Q. Zhang, Y. Lai, Z. Lin, A review of TiO_2 nanostructured catalysts for sustainable H_2 generation, Int. J. Hydrog. Energy 42 (2017) 8418–8449, https://doi.org/10.1016/j.ijhydene.2016.12.052.

[6] M. Gill, M.T. Máthé, P. Salamon, J.T. Gleeson, A. Jákli, From solid to liquid piezoelectric materials, Mater. Horiz. 12 (2025) 8920–8942, https://doi.org/10.1039/D5MH00917K.

[7] Y. Cheng, Y. Zhang, Z. Wang, R. Guo, J. You, H. Zhang, Review of Bi-based catalysts in piezocatalytic, photocatalytic and piezo-photocatalytic degradation of organic pollutants, Nanoscale 15 (2023) 18571–18580, https://doi.org/10.1039/d3nr05016e.

[8] P. Xia, Y. Song, Y.Z. Liu, M.X. Long, C. Yang, X.Y. Zhang, T. Zhang, Advances in the optical and electronic properties and applications of bismuth-based semiconductor materials, J. Mater. Chem. C. 12 (2024) 1609–1624, https://doi.org/10.1039/D3TC03329E.

[9] S. Li, Y. Li, H. Huang, Solar-driven selective oxidation over bismuth-based semiconductors: from prolific catalysts to diverse reactions, Adv. Funct. Mater. (2024) 2313883, https://doi.org/10.1002/adfm.202313883.

[10] S. Lan, C. Yu, F. Sun, Y. Chen, D. Chen, W. Mai, M. Zhu, Tuning piezoelectric driven photocatalysis by La-doped magnetic $BiFeO_3$-based multiferroics for water purification, Nano Energy 93 (2022) 106792, https://doi.org/10.1016/j.nanoen.2021.106792.

[11] C. Wang, F. Chen, C. Hu, T. Ma, Y. Zhang, H. Huang, Efficient piezocatalytic H_2O_2 production of atomic-level thickness $Bi_4Ti_3O_{12}$ nanosheets with surface oxygen vacancy, Chem. Eng. J. 431 (2022) 133930, https://doi.org/10.1016/j.cej.2021.133930.

[12] H.Q. Ma, W.Y. Yang, S. Gao, W.R. Geng, Y.L. Lu, C.L. Zhou, J.K. Shang, T. Shi, Q. Li, Superior photopiezocatalytic performance by enhancing spontaneous polarization through post-synthesis structure distortion in ultrathin Bi_2WO_6 nanosheet polar photocatalyst, Chem. Eng. J. 455 (2023) 140471, https://doi.org/10.1016/j.cej.2022.140471.

[13] W.M. Li, H. Zhang, J.L. Yao, X.T. Xuan, H.L. Wang, C.M. Dai, One-step hydrothermal synthesis of ternary heterostructure stannic sulfide -bismuth sulfide - bismuth oxychloride (SnS_2-Bi_2S_3-BiOCl) composite loaded on carbon felt for highly efficient piezocatalytic degradation of organic dyes and antibiotics, Surf. Interf. 54 (2024) 105198, https://doi.org/10.1016/j.surfin.2024.105198.

[14] M.S. Chen, Z.H. Kang, J.J. Ning, Q. Ni, D.H. Bao, Multilayer structured bismuth silicate inverse opal film with improved piezo-photocatalytic performance for wastewater purification and dyes removal, Surf. Interf. 55 (2024) 105378, https://doi.org/10.1016/j.surfin.2024.105378.

[15] F. Yang, Y. Zhao, Piezoelectric water disinfection: mechanisms, applications, and emerging prospects, Nano Energy 131 (2024) 110270, https://doi.org/10.1016/j.nanoen.2024.110270.

[16] C.Y. Wang, F. Chen, E. Chen, T. Chen, T.Y. Ma, H.W. Huang, Unveiling strong electric fields of ultrafine hollow nanotubes axially orienting asymmetric polar $[Bi_5O_7]$ units for efficient piezocatalytic water splitting, ACS Nano 19 (2025) 22387–22401, https://doi.org/10.1016/j.nanoen.2024.110270.

[17] Y. Wu, P.F. Wang, H.N. Che, W. Liu, C.M. Tang, Y.H. Ao, TriggerinG Dual Two-electron Pathway For H_2O_2 generation by multiple [Bi−O]n interlayers in ultrathin $Bi_{12}O_{17}Cl_2$ towards efficient piezo-self-Fenton catalysis, Angew. Chem. Int. Ed. 63 (2024) e202316410, https://doi.org/10.1002/ange.202316410.

[18] Y.M. Du, T. Lu, X.N. Li, Y. Liu, W.P. Sun, S.J. Zhang, Z.X. Cheng, High-efficient piezocatalytic hydrogen evolution by centrosymmetric $Bi_2Fe_4O_9$ nanoplates, Nano. Energy 104 (2022) 107919, https://doi.org/10.1016/j.nanoen.2022.107919.

[19] G.Y. Wang, Y.X. Qi, Z. Liu, R.W. Wang, Emerging piezoelectric sonosensitizer for ROS-driven sonodynamic cancer therapy, Inorganics 13 (2025) 71, https://doi.org/10.3390/inorganics13030071.

[20] Y.Y. Pu, B.G. Zhou, J.H. Bing, L. Wang, M.Q. Chen, Y.C. Shen, S. Gao, M. Zhou, W. C. Wu, J.L. Shi, Ultrasound-triggered and glycosylation inhibition-enhanced tumor piezocatalytic immunotherapy, Nat. Commun. 15 (2024) 9023, https://doi.org/10.1038/s41467-024-53392-1.

[21] J. Feng, Y. Fu, X. Liu, S. Tian, S. Lan, Y. Xiong, Significant improvement and mechanism of ultrasonic inactivation to Escherichia coli with piezoelectric effect of hydrothermally synthesized t-$BaTiO_3$, ACS Sustain. Chem. Eng. 6 (2018) 6032–6041, https://doi.org/10.1021/acssuschemeng.7b04666.

[22] P.W. Jia, J.M. Li, H.W. Huang, Piezocatalysts and Piezo-Photocatalysts: From Material Design to Diverse Applications, Adv. Funct. Mater. 34 (2024) 2407309, https://doi.org/10.1002/adfm.202407309.

[23] Y. Cheng, Y.B. Zhang, Z.B. Wang, R. Guo, J.H. You, H.Z. Zhang, Review of Bi-based catalysts in piezocatalytic, photocatalytic and piezo-photocatalytic degradation of organic pollutants, Nanoscale 15 (2023) 18571, https://doi.org/10.1039/d3nr05016e.

[24] S.B. Chen, C. Chen, J.J. Zhu, Piezoelectric catalysis of $BiFeO_3$ for water pollutant degradation: a review from mechanisms to engineering solutions, Environ. Res. 286 (2025) 122849, https://doi.org/10.1016/j.envres.2025.122849.

[25] S. Lan, J. Feng, Y. Xiong, S. Tian, S. Liu, L. Kong, Performance and mechanism of piezo-catalytic degradation of 4-chlorophenol: finding of effective piezo-dechlorination, Environ. Sci. Technol. 51 (2017) 6560–6569, https://doi.org/10.1021/acs.est.6b06426.

[26] S. Kumar, M. Sharma, A. Kumar, S. Powar, R. Vaish, Rapid bacterial disinfection using low frequency piezocatalysis effect, J. Ind. Eng. Chem. 77 (2019) 355–364, https://doi.org/10.1016/j.jiec.2019.04.058.

[27] B. Tandon, J.J. Blaker, S.H. Cartmell, Piezoelectric materials as stimulatory biomedical materials and scaffolds for bone repair, Acta Biomater. 73 (2018) 1–20, https://doi.org/10.1016/j.actbio.2018.04.026.

[28] D. Kim, S.A. Han, J.H. Kim, J.H. Lee, S.W. Kim, S.W. Lee, Biomolecular Piezoelectric Materials: From Amino Acids to Living Tissues, Adv. Mater. 32 (14) (2020), https://doi.org/10.1002/adma.201906989.

[29] J. Wu, N. Qin, D.H. Bao, Effective enhancement of piezocatalytic activity of $BaTiO_3$ nanowires under ultrasonic vibration, Nano Energy 45 (2018) 44–51, https://doi.org/10.1016/j.nanoen.2017.12.034.

[30] K.S. Hong, H. Xu, H. Konishi, X. Li, Direct water splitting through vibrating piezoelectric microfibers in water, J. Phys. Chem. Lett. 1 (2010) 997–1002, https://doi.org/10.1021/jz100027t.

[31] M.B. Starr, X.D. Wang, Fundamental analysis of piezocatalysis process on the surfaces of strained piezoelectric materials, Sci. Rep. 3 (2013) 2160, https://doi.org/10.1038/srep02160.

[32] Z.X. Huang, L.W. Li, Y.Z. Huang, W.X. Rao, H.W. Jiang, J. Wang, H.H. Zhang, H. Z. He, J.P. Qu, Self-poled piezoelectric polymer composites *via* melt-state energy implantation, Nat. Commun. 15 (1) (2024), https://doi.org/10.1038/s41467-024-45184-4.

[33] J.K. Yang, Z.M. Li, X.D. Xin, X.Y. Gao, X.T. Yuan, Z.H. Wang, Z.H. Yu, X.H. Wang, J. Zhou, S.X. Dong, Designing electromechanical metamaterial with full nonzero piezoelectric coefficients, Sci. Adv. 5 (11) (2019), https://doi.org/10.1126/sciadv.aax1782.

[34] S. Chen, X. Tong, Y. Huo, S. Liu, Y. Yin, M.-L. Tan, K. Cai, W. Ji, Piezoelectric Biomaterials Inspired by Nature for Applications in Biomedicine and Nanotechnology, Adv. Mater. 36 (35) (2024), https://doi.org/10.1002/adma.202406192.

[35] M. Habib, I. Lantgios, K. Hornbostel, A review of ceramic, polymer and composite piezoelectric materials, J. Phys. D. -Appl. Phys. 55 (42) (2022), https://doi.org/10.1088/1361-6463/ac8687.

[36] S.X. Gong, W.X. Zhang, Z.R. Liang, Y.J. Zhang, T. Gan, H.Y. Hu, Z.Q. Huang, Construction of a $BaTiO_3$/tubular g-C_3N_4 dual piezoelectric photocatalyst with enhanced carrier separation for efficient degradation of tetracycline, Chem. Eng. J. 461 (2023) 141947, https://doi.org/10.1016/j.cej.2023.141947.

[37] W. Amdouni, M. Fricaudet, M. Otoničar, V. Garcia, S. Fusil, J. Kreisel, H. Maghraoui-Meherzi, B. Dkhil, $BiFeO_3$ Nanoparticles: The "Holy-Grail" of

Piezo-Photocatalysts? Adv. Mater. 35 (2023) 2301841 https://doi.org/10.1002/adma.202301841.
[38] K. Wang, C. Han, J.Q. Li, J.S. Qiu, J. Sunarso, S.M. Liu, The mechanism of piezocatalysis: energy band theory or screening charge effect? Angew. Chem. Int. Ed. 61 (2022) 202110429 https://doi.org/10.1002/anie.202110429.
[39] K. Wang, C. Han, Z.P. Shao, J.S. Qiu, S.B. Wang, S.M. Liu, Perovskite oxide catalysts for advanced oxidation reactions, Adv. Funct. Mater. 31 (2021) 2102089, https://doi.org/10.1002/adfm.202102089.
[40] J.D. Shi, W. Zeng, Z.H. Dai, L. Wang, S.P. Lin, Y. Xiong, S. Yang, S.M. Shang, W. Chen, L.Y. Zhao, X.J. Ding, X.M. Tao, Y. Chai, Piezocatalytic foam for highly efficient degradation of aqueous organics, Small Sci. 1 (2021) 2000011, https://doi.org/10.1002/smsc.202000011.
[41] V.T. Nguyen, H.J. Sagar, O. Moctar, W.G. Park, Understanding cavitation bubble collapse and rebound near a solid wall, Int. J. Mech. Sci. 278 (2024) 109473, https://doi.org/10.1016/j.ijmecsci.2024.109473.
[42] P.L. Wang, X.Y. Li, S.Y. Fan, X. Chen, M.C. Qin, D. Long, M.O. Tadé, S.M. Liu, Impact of oxygen vacancy occupancy on piezo-catalytic activity of $BaTiO_3$ nanobelt, Appl. Catal. B Environ. 279 (2020) 119340, https://doi.org/10.1016/j.apcatb.2020.119340.
[43] N. Bagheri, M.H. Ara, M.H. M, N. Ghazyani, Characterization and doping effects study of high hole concentration Li-doped ZnO thin film prepared by sol–gel method, J. Mater. Sci Mater. Electron. 27 (2016) 1293–1298, https://doi.org/10.1007/s10854-015-3888-0.
[44] J.M. Wu, W.E. Chang, Y.T. Chang, K. C, Piezo-catalytic effect on the enhancement of the ultra-high degradation activity in the dark by Single- and fewlayers MoS_2 nanoflowers, Adv. Mater. 28 (2016) 3718–3725, https://doi.org/10.1002/adma.201505785.
[45] W.R. Tian, J.H. Qiu, N.J. Li, D.Y. Chen, Q.F. Xu, H. Li, J.H. He, J.M. Lu, Efficient piezocatalytic removal of BPA and Cr (VI) with SnS_2/CNFs membrane by harvesting vibration energy, Nano Energy 86 (2021) 106036, https://doi.org/10.1016/j.nanoen.2021.106036.
[46] D.T. You, L. Liu, Z.Y. Yang, X.X. Xing, K.W. Li, W.J. Mai, T. Guo, Z.G. Xiao, C. X. Xu, Polarization-induced internal electric field to manipulate piezo-photocatalytic and ferro-photoelectrochemical performance in bismuth ferrite nanofibers, Nano Energy 93 (2022) 106852, https://doi.org/10.1016/j.nanoen.2021.106852.
[47] R. Su, Z.P. Wang, L.N. Zhu, Y. Pan, D.W. Zhang, H. Wen, Z.D. Luo, L.L. Li, F.T. Li, M. Wu, L.Q. He, P. Sharma, J. Seidel, Strain-engineered nano-ferroelectrics for high-efficiency piezocatalytic overall water splitting, Angew. Chem. Int. Ed. 60 (2021) 16019–16026, https://doi.org/10.1002/anie.202103112.
[48] F. Bößl, I. Tudela, Piezocatalysis: can catalysts really dance? Curr. Opin. Green. Sustain. Chem. 32 (2021) 100537 https://doi.org/10.1016/j.cogsc.2021.100537.
[49] Z.X. Zhang, Y.Y. Zhang, G.R. Chen, D.P. Hong, L.W. Shan, H.Y. Xu, H.T. Wu, X. L. He, S.Y. Qi, L.M. Dong, Mater. Chemphys 346 (2025) 131348, https://doi.org/10.1016/j.matchemphys.2025.131348.
[50] Y.J. Chen, L.Q. He, Y.J. Wang, Y.M. Li, X.H. Wang, D.P. Hong, H.T. Wu, Z. Wu, L. W. Shan, Polarization mechanism and piezo-photocatalytic application of ferroelectric materials, Mol. Catal. 585 (2025) 115338, https://doi.org/10.1016/j.mcat.2025.115338.
[51] K.Q. Shi, C.C. Jin, J.H. Sun, Z.Y. Gui, Y.X. Cai, D.M. Liu, X.T. Qiu, L. li, L.X. Zhang, Z. Chen, Q. Wu, Breaking Symmetry via Bamboo-Inspired Gradient Engineering for Triple-Field Synergistic H_2O_2 Production, Adv. Mater. 38 (2026) 73536, https://doi.org/10.1002/adma.73536.
[52] X.F. Zhou, J.Z. Liu, S. Ali, B. Shen, J.W. Zhai, N. Hedin, J.Y. Yuan, Efficient Catalytic Production of Reactive Oxygen Species through Piezoelectricity in Bismuth Sulfide Rich in Sulfur Vacancies, Nano Lett. 24 (2024) 13153–13161, https://doi.org/10.1021/acs.nanolett.4c02795.
[53] L. Zhang, J. Zhang, J. Yu, H. García, Charge-transfer dynamics in S-schemevphotocatalyst, Nat. Rev. Chem. 9 (2025) 328–342, https://doi.org/10.1038/s41570-025-00698-3.
[54] Q. Xu, J. Han, F. Tian, X. Zhao, J. Rong, J. Zhang, P. She, J.S. Qin, H. Rao, Synergistic bifunctional covalent organic framework for efficient photocatalytic CO_2 reduction and water oxidation, J. Am. Chem. Soc. 147 (2025) 10587–10597, https://doi.org/10.1021/jacs.5c00432.
[55] X. Yu, L. Wang, Z. Zhu, X. Han, J. Zhang, A. Wang, L. Ding, J. Liu, Piezoelectric effect modulates nanozyme activity: underlying mechanism and practical application, Small 19 (2023) 2304818, https://doi.org/10.1002/smll.202304818.
[56] R. He, D. Xu, B. Cheng, J. Yu, W. Ho, Review on nanoscale Bi-based photocatalysts, Nanoscale Horiz. 3 (2018) 464–504, https://doi.org/10.1039/c8nh00062j.
[57] S. Tu, Y. Wang, H. Huang, J. Zhang, H. Li, J. Sun, T. Chen, Y. Zhang, Band shifting triggered ·OH evolution and charge separation enhanced H_2O_2 generation in piezo-photocatalysis of Sillén-Aurivillius-structured $Bi_4W_{0.5}Ti_{0.5}O_8Cl$, Chem. Eng. J. 465 (2023) 142777, https://doi.org/10.1016/j.cej.2023.142777.
[58] X. Ma, B. Ding, Z. Yang, S. Liu, Z. Liu, Q. Meng, H. Chen, J. Li, Z. Li, Pa Ma, J. Lin, Sulfur-vacancy-engineered two-dimensional Cu@SnS_{2-x} nanosheets constructed via heterovalent substitution for high-efficiency piezocatalytic tumor therapy, J. Am. Chem. Soc. 146 (2024) 21496–21508, https://doi.org/10.1021/jacs.4c04385.
[59] S. Li, Z. Zhao, J. Zhao, Z. Zhang, X. Li, J. Zhang, Recent advances of ferro-, piezo-, and pyroelectric nanomaterials for catalytic applications, ACS Appl. Nano Mater. 3 (2020) 1063–1079, https://doi.org/10.1021/acsanm.0c00039.
[60] Y. Jiang, J. Liang, F. Zhuo, H. Ma, S.S. Mofarah, C.C. Sorrell, D. Wang, P. Koshy, Unveiling mechanically driven catalytic processes: beyond piezocatalysis to synergetic effects, ACS Nano 19 (2025) 18037–18074, https://doi.org/10.1021/acsnano.5c02660.
[61] J. Dai, Z. Fan, Y. Long, W. Yue, F. Huang, Y. Jiao, Y. Deng, Y. Chang, D. Wang, Remarkably boosting piezocatalytic performance of $Sr_{0.5}Ba_{0.5}Nb_2O_6$ piezoceramics via size optimization and oxygen vacancy engineering, Adv. Funct. Mater. 34 (2024) 2408754, https://doi.org/10.1002/adfm.202408754.
[62] X. Liu, M. Wang, Y. Zhou, T. Li, H. Duan, J. Li, L. Wang, Y. Li, S. Yang, J. Wu, C. Wang, X. Feng, F. Li, Ultrahigh piezocatalytic performance of perovskite ferroelectric powder via oxygen vacancy engineering, Small 19 (2023) e2303129, https://doi.org/10.1002/smll.202303129.
[63] Z. Kang, E. Lin, N. Qin, J. Wu, D. Bao, Bismuth vacancy-mediated quantum dot precipitation to trigger efficient piezocatalytic activity of Bi_2WO_6 nanosheets, ACS Appl. Mater. Interfaces 14 (2022) 11375–11387, https://doi.org/10.1021/acsami.1c23282.
[64] A. Shu, C. Qin, M. Li, L. Zhao, Z. Shangguan, Z. Shu, X. Yuan, M. Zhu, Y. Wu, H. Wang, Electric effects reinforce charge carrier behaviour for photocatalysis, Energy Environ. Sci. 17 (2024) 4907–4928, https://doi.org/10.1039/d4ee01379d.
[65] A. Kubacka, M. Fernández-García, G. Colón, Advanced nanoarchitectures for solar photocatalytic applications, Chem. Rev. 112 (2011) 1555–1614, https://doi.org/10.1021/cr100454n.
[66] Q.T. Trinh, N. Golio, Y. Cheng, H. Cha, K.U. Tai, L. Ouyang, J. Zhao, T.S. Tran, T. K. Nguyen, J. Zhang, H. An, Z. Wei, F. Jerome, P.N. Amaniampong, N.T. Nguyen, Sonochemistry and sonocatalysis: current progress, existing limitations, and future opportunities in green and sustainable chemistry, Green. Chem. 27 (2025) 4926–4958, https://doi.org/10.1039/d5gc01098e.
[67] L. Xiao, X. Xu, Z. Wu, T. Sun, X. He, X. Xu, L. Qin, D. Chen, Recent progress and prospect of friction-driven-tribocatalysis: from basic principle to material design, Surf. Interfaces 56 (2025) 105557, https://doi.org/10.1016/j.surfin.2024.105557.
[68] N. Tian, C. Hu, J. Wang, Y. Zhang, T. Ma, H. Huang, Layered bismuth-based photocatalysts, Coord. Chem. Rev. 463 (2022) 214515, https://doi.org/10.1016/j.ccr.2022.214515.
[69] J. Li, Y. Yu, L. Zhang, Bismuth oxyhalide nanomaterials: layered structures meet photocatalysis, Nanoscale 6 (2014) 8473–8488, https://doi.org/10.1039/C4NR02553A.
[70] L. Ye, Y. Su, X. Jin, H. Xie, C. Zhang, Recent advances in BiOX (X = Cl, Br and I) photocatalysts: synthesis, modification, facet effects and mechanisms, Environ. Sci. Nano 1 (2014) 90–112, https://doi.org/10.1039/C3EN00098B.
[71] J. Jiang, K. Zhao, X. Xiao, L. Zhang, Synthesis and facet-dependent photoreactivity of BiOCl single-crystalline nanosheets, J. Am. Chem. Soc. 134 (2012) 4473–4476, https://doi.org/10.1021/ja210484t.
[72] L. Zhang, W. Wang, S. Sun, D. Jiang, E. Gao, Selective transport of electron and hole among {001} and {110} facets of BiOCl for pure water splitting, Appl. Catal. B Environ. 162 (2015) 470–474, https://doi.org/10.1016/j.apcatb.2014.07.024.
[73] D. Shao, L. Zhang, S. Sun, W. Wang, Oxygen reduction reaction for generating H_2O_2 through a piezo-catalytic process over bismuth oxychloride, Chem. Sus. Chem. 11 (2018) 527–531, https://doi.org/10.1002/cssc.201702405.
[74] M. Ismail, Z. Wu, L. Zhang, J. Ma, Y. Jia, Y. Hu, Y. Wang, High-efficient synergy of piezocatalysis and photocatalysis in bismuth oxychloride nanomaterial for dye decomposition, Chemosphere 228 (2019) 212–218, https://doi.org/10.1016/j.chemosphere.2019.04.121.
[75] J. Li, L. Zhang, Y. Li, Y. Yu, Synthesis and internal electric field dependent photoreactivity of Bi_3O_4Cl single-crystalline nanosheets with high {001} facet exposure percentages, Nanoscale 6 (2014) 167–171, https://doi.org/10.1039/C3NR05246J.
[76] M.H. Fu, H.B. Dou, W.B. Zhai, B.S. Hou, C.C. Wu, W. Meng, N. Wu, Z. Zhang, T. C. Weng, Y. Yu, H.T. Wang, Enhancing UV-C Photoelectron Lifetimes for Avalanche-like Photocurrents in Carbon-Doped Bi_3O_4Cl Nanosheets, ACS Appl. Mater. Interfaces 15 (2023) 32525–32537, https://doi.org/10.1021/acsami.3c03331.
[77] Q. Zhou, J. Jiang, Bi_3O_4Br nanoplates as an efficient piezo-photocatalyst for organic dye degradation, Mod. Phys. Lett. B 35 (2021) 2150119, https://doi.org/10.1142/S0217984921501190.
[78] Y. Wang, D. Yu, Y. Liu, X. Liu, Y. Shi, Boosting piezo/photo-induced charge transfer of CNT/$Bi_4O_5I_2$ catalyst for efficient ultrasound-assisted degradation of rhodamine B, Materials 14 (2021), Materials 14 (2021), https://doi.org/10.3390/ma14164449.
[79] B. Aurivillius, Mixed bismuth oxides with layer lattices I. The structure type of $CaNb_2Bi_2O_9$, Ark. Kemi 1 (48) (1949) 463–480.
[80] B.H. Park, B.S. Kang, S.D. Bu, T.W. Noh, J. Lee, W. Jo, Lanthanum-substituted bismuth titanate for use in non-volatile memories, Nature 401 (1999) 682–684, https://doi.org/10.1038/44352.
[81] S. Supriya, Tailoring layered structure of bismuth-based aurivillius perovskites: Recent advances and future aspects, Coord. Chem. Rev. 479 (2023) 215010, https://doi.org/10.1016/j.ccr.2022.215010.
[82] M.R. Li, H.R. Sun, Y.Q. Ruan, C. Cao, P. Zhou, Y.J. Qi, T.J. Zhang, High-performance self-powered ultraviolet photodetector based on bismuth layered perovskite $Bi_{3.15}Nd_{0.85}Ti_3O_{12}$ ferroelectric thin films, Appl. Surf. Sci. 618 (2023) 156665, https://doi.org/10.1016/j.apsusc.2023.156665.
[83] L.W. Zhang, Y.J. Wang, H.Y. Cheng, W.Q. Yao, Y.F. Zhu, Synthesis of Porous Bi_2WO_6 Thin Films as Efficient Visible-Light-Active Photocatalysts, Adv. Mater. 21 (2009) 1286–1290, https://doi.org/10.1002/adma.200801354.
[84] L. Liang, F. Lei, S. Gao, Y. Sun, X. Jiao, J. Wu, S. Qamar, Y. Xie, Single Unit Cell Bismuth Tungstate Layers Realizing Robust Solar CO_2 Reduction to Methanol,

Angew. Chem. Int. Ed. Engl. 54 (2015) 13971–13974, https://doi.org/10.1002/anie.201506966.
[85] M.M. Seyfouri, Q.L. Liu, J. Yang, Y.L. Sun, X.C. Dai, J.J. Shi, X. Tan, S. Li, T. Wu, D.Y. Wang, New insights on the substantially reduced bandgap of bismuth layered perovskite oxide thin films, J. Mater. Chem. C. 9 (2021) 3161–3170, https://doi.org/10.1039/D0TC05300G.
[86] X. He, C. Chen, Y. Gong, H. Zeng, Z. Yi, Bi_2WO_6 lead-free ferroelectrics: microstructure design, polar behavior and photovoltaic performance, J. Mater. Chem. C. 9 (2021) 7539–7544, https://doi.org/10.1039/D1TC01156A.
[87] V.K. Yanovskii, V.I. Voronkova, Polymorphism and Properties of Bi_2WO_6 and Bi_2MoO_6, Phys. Status Solidi A 93 (1986) 57–66, https://doi.org/10.1002/pssa.2210930106.
[88] C.A.P. de Araujo, J.D. Cuchiaro, L.D. McMillan, M.C. Scott, J.F. Scott, Fatigue-free ferroelectric capacitors with platinum electrodes, Nature 374 (1995) 627–629, https://doi.org/10.1038/374627a0.
[89] J. Yu, J. Xiong, B. Cheng, Y. Yu, J. Wang, Hydrothermal preparation and visible light photocatalytic activity of Bi_2WO_6 powders, J. Solid. State Chem. 178 (2005) 1968–1972, https://doi.org/10.1016/j.jssc.2005.04.003.
[90] H. Djani, P. Hermet, P. Ghosez, First-principles characterization of the P21ab ferroelectric phase of aurivillius Bi_2WO_6, J. Phys. Chem. C. 118 (2014) 13514–13524, https://doi.org/10.1021/jp504674k.
[91] H. Takeda, J.S. Han, M. Nishida, T. Shiosaki, T. Hoshina, T. Tsurumi, Growth and piezoelectric properties of ferroelectric Bi_2WO_6 mono-domain crystals, Solid. State Commun. 150 (2010) 836–839, https://doi.org/10.1016/j.ssc.2010.02.011.
[92] A. Moure, A. Castro, L. Pardo, Aurivillius-type ceramics, a class of high temperature piezoelectric materials: Drawbacks, advantages and trends, Prog. Solid. State Chem. 37 (2009) 15–39, https://doi.org/10.1016/j.progsolidstchem.2009.06.001.
[93] H. Ma, W.T. Li, B. Liu, H.N. Hu, Y.H. Li, W. Xu, R.M. Fang, F. Dong, Oxygen vacancies induced intrinsic electric field attenuation for superior molecular oxygen activation and NO oxidation, Chem. Eng. J. 505 (2025) 159421, https://doi.org/10.1016/j.cej.2025.159421.
[94] J.F. Dorrian, R.E. Newnham, D.K. Smith, M.I. Kay, Crystal structure of $Bi_4Ti_3O_{12}$, Ferroelectrics 3 (1972) 17–27, https://doi.org/10.1080/00150197108237680.
[95] A. Hao, X. Ning, Y. Cao, J. Xie, D. Jia, Boosting the piezocatalytic performance of Bi_2WO_6 nanosheets towards the degradation of organic pollutants, Mater. Chem. Front. 4 (2020) 2096–2102, https://doi.org/10.1039/D0QM00179A.
[96] A. Kudo, S. Hijii, H_2 or O_2 evolution from aqueous solutions on layered oxide photocatalysts consisting of Bi^{3+} with $6s^2$ configuration and d^0 transition metal ions, Chem. Lett. 28 (1999) 1103–1104, https://doi.org/10.1246/cl.1999.1103.
[97] Z.G. Chen, W. Zhang, X.J. Qu, Y.F. Zhang, Piezoelectric Heterojunction-driven Biomedical Revolution: From Construction Principles to Diagnostic and Therapeutic Applications, Theranostics 16 (2026) 3136–3172, https://doi.Org/10.7150/thno.126489.
[98] X.L. Cai, B.Q. Jing, R. Li, B.W. Cao, J.B. Cao, Y.H. Xu, Ni/Cu co-doped modified Bi_2WO_6 microsphere for enhanced photocatalytic reduction of CO_2 toward CO, Chem. Eng. J. 543 (2026) 178316, https://doi.org/10.1016/j.cej.2026.178316.
[99] R. Chaharmahali, A. Fattah-alhosseini, M. Karbasi, D. Dastan, S. Giannakis, Synergistic effects of PEO and hydrothermal post-treatment on the photocatalytic behavior of TiO_2/Bi_2WO_6 coatings: Distinguishing between Type II and Z-Scheme heterojunctions, J. Environ. Chem. Eng. 13 (2025) 116583, https://doi.org/10.1016/j.jece.2025.116583.
[100] L.L. Cheng, D.Y. Huang, Y. Zhang, Y. Wu, Preparation and piezoelectric catalytic performance of HT-Bi_2MoO_6 microspheres for dye degradation, Adv. Powder Technol. 32 (2021) 3346–3354, https://doi.org/10.1016/j.apt.2021.07.021.
[101] G.F. Sun, N. Li, S.X. Zuo, W.J. Shen, M.M. Wu, Q.F. Li, M.H. Shi, J.Q. Ma, Piezo-photocatalysis over phase-engineered $MoSe_2$ modified Bi_2WO_6 hierarchical microspheres: Utilizing piezoelectric effect to enhance photocatalytic performance, Ceramint 48 (2022) 37242–37252, https://doi.org/10.1016/j.ceramint.2022.08.302.
[102] K. Hu, R. Wang, M. Maimaitituersun, H. Sun, X. Liu, Y. Zhang, Synergetic piezophotocatalytic effect in ultrathin Bi_2WO_6 nanosheets for decomposing organic dye, J. Mater. Sci. Mater. Electron. 33 (2022) 9845–9857, https://doi.org/10.1007/s10854-022-07966-8.
[103] Y. Li, G. Chen, H. Zhang, Z. Li, J. Sun, Electronic structure and photocatalytic properties of $ABi_2Ta_2O_9$ (A=Ca, Sr, Ba), J. Solid. State Chem. 181 (2008) 2653–2659, https://doi.org/10.1016/j.jssc.2008.05.020.
[104] Y. Li, G. Chen, H. Zhang, Z. Lv, Band structure and photocatalytic activities for H_2 production of $ABi_2Nb_2O_9$ (A=Ca, Sr, Ba), Int. J. Hydrog. Energy 35 (2010) 2652–2656, https://doi.org/10.1016/j.ijhydene.2009.04.021.
[105] Z.H. Fang, Z.H. Yu, M.S. Chen, Q.J. Xiang, Modulating Carrier Dynamics in Halide Perovskites through Lattice Strain Engineering of $CsPb_{1-x}Cu_xBr_3$ for Improved Photocatalytic CO_2 Reduction, ACS Nano 19 (2025) 34264–34272, https://doi.org/10.1021/acsnano.5c11198.
[106] W. Wu, S. Liang, X. Wang, J. Bi, P. Liu, L. Wu, Synthesis, structures and photocatalytic activities of microcrystalline $ABi_2Nb_2O_9$ (A=Sr, Ba) powders, J. Solid. State Chem. 184 (2011) 81–88, https://doi.org/10.1016/j.jssc.2010.10.033.
[107] V. Senthil, S. Panigrahi, Dielectric, ferroelectric, impedance and photocatalytic water splitting study of Y^{3+} modified $SrBi_2Ta_2O_9$ ferroelectrics, Int. J. Hydrog. Energy 44 (2019) 18058–18071, https://doi.org/10.1016/j.ijhydene.2019.05.064.
[108] J. Zhang, Y. Liu, T. Dittrich, Z. Wang, P.X. Ji, M.R. Li, N. Ta, H.Y. Zhang, C. Zhen, Y.J. Xu, D.F. Li, Z.D. Feng, Z. Li, Y.L. Luo, J.H. Cui, D. Su, Y.X. Weng, G. Liu, X. L. Wang, F.T. Fan, C. Li, Unveiling charge utilization mechanisms in ferroelectric for water splitting, Nat. Commun. 16 (2025) 1515, https://doi.org/10.1038/s41467-025-56359-y.
[109] S. Tu, H. Huang, T. Zhang, Y. Zhang, Controllable synthesis of multi-responsive ferroelectric layered perovskite-like $Bi_4Ti_3O_{12}$: Photocatalysis and piezoelectriccatalysis and mechanism insight, Appl. Catal. B Environ. 219 (2017) 550–562, https://doi.org/10.1016/j.apcatb.2017.08.001.
[110] J. Wu, N. Qin, E. Lin, B. Yuan, Z. Kang, D. Bao, Synthesis of $Bi_4Ti_3O_{12}$ decussated nanoplates with enhanced piezocatalytic activity, Nanoscale 11 (2019) 21128–21136, https://doi.org/10.1039/C9NR07544E.
[111] B.C. Ji, X.C. Li, S. Gao, Z.P. Qin, C.Z. Wang, Q. Wang, C.C. Wang, Polarization-enhanced piezo-photocatalysis over hollow-sphere $Bi_4Ti_3O_{12}$: Structure-property relationship and degradation mechanism, Chin. J. Catal. 76 (2025) 133–145, https://doi.org/10.1016/S1872-2067(25)64758-9.
[112] Z. Xie, X. Tang, J. Shi, Y. Wang, G. Yuan, J.-M. Liu, Excellent piezo-photocatalytic performance of $Bi_4Ti_3O_{12}$ nanoplates synthesized by molten-salt method, Nano Energy 98 (2022) 107247, https://doi.org/10.1016/j.nanoen.2022.107247.
[113] S.D. Nguyen, J. Yeon, S.-H. Kim, P.S. Halasyamani, $BiO(IO_3)$: a new polar iodate that exhibits an aurivillius-type $(Bi_2O_2)^{2+}$ layer and a large SHG response, J. Am. Chem. Soc. 133 (2011) 12422–12425, https://doi.org/10.1021/ja205456b.
[114] W. Wang, B. Huang, X. Ma, Z. Wang, X. Qin, X. Zhang, Y. Dai, M.-H. Whangbo, Efficient separation of photogenerated electron-hole pairs by the combination of aheterolayered structure and internal polar field in pyroelectric $BiOIO_3$ nanoplates, Chem. A Eur. J. 19 (2013) 14777–14780, https://doi.org/10.1002/chem.201302884.
[115] Y. Su, L. Zhang, W. Wang, Internal polar field enhanced H_2 evolution of $BiOIO_3$ nanoplates, Int. J. Hydrog. Energy 41 (2016) 10170–10177, https://doi.org/10.1016/j.ijhydene.2016.04.236.
[116] W. Wang, H. Cheng, B. Huang, X. Liu, X. Qin, X. Zhang, Y. Dai, Hydrothermal synthesis of C_3N_4/$BiOIO_3$ heterostructures with enhanced photocatalytic properties, J. Colloid Interface Sci. 442 (2015) 97–102, https://doi.org/10.1016/j.jcis.2014.11.061.
[117] R. Zhang, Y. Dai, Z. Lou, Z. Li, Z. Wang, Y. Yang, X. Qin, X. Zhang, B. Huang, Layered photocatalyst $Bi_2O_2[BO_2(OH)]$ nanosheets with internal polar field enhanced photocatalytic activity, Cryst. Eng. Comm. 16 (2014) 4931–4934, https://doi.org/10.1039/C4CE00162A.
[118] C. Hu, H. Huang, F. Chen, Y. Zhang, H. Yu, T. Ma, Coupling piezocatalysis and photocatalysis in Bi_4NbO_8X (X = Cl, Br) polar single crystals, Adv. Funct. Mater. 30 (2020) 1908168, https://doi.org/10.1002/adfm.201908168.
[119] A. Khorsand Zak, A.M. Hashim, Recent advances in $BiFeO_3$-based nanostructures: Properties and applications, Coord. Chem. Rev. 523 (2025) 216297, https://doi.org/10.1016/j.ccr.2024.216297.
[120] J. Wang, J.B. Neaton, H. Zheng, V. Nagarajan, S.B. Ogale, B. Liu, D. Viehland, V. Vaithyanathan, D.G. Schlom, U.V. Waghmare, N.A. Spaldin, K.M. Rabe, M. Wutting, R. Rameth, Epitaxial $BiFeO_3$ Multiferroic Thin Film Heterostructures, Science 299 (2003) 1719–1722, https://doi.org/10.1126/science.1080615.
[121] J. Dai, Z. Fan, H. Xie, Y. Jiao, F. Huang, A.A. Mohamad, Y. Chang, Y. Long, D. Wang, Versatile $BiFeO_3$ shining in piezocatalysis: from materials engineering to diverse applications, J. Adv. Ceram. 14 (2025) 9221046, https://doi.org/10.26599/JAC.2025.9221046.
[122] W. Amdouni, M. Otoničar, D. Alamarguy, E. Erdem, P. Gemeiner, F. Mazaleyrat, H. Maghraoui-Meherzi, J. Kreisel, S. Glinsek, B. Dkhil, Enhancement of the piezocatalytic response of La-doped $BiFeO_3$ nanoparticles by defects synergy, Small 20 (2024) 2406425, https://doi.org/10.1002/smll.202406425.
[123] X. Liu, J. Chao, F. Guo, L. Chang, X. Zhang, W. Long, Z. Xi, Gd and Zr Co-doped $BiFeO_3$ magnetic nanoparticles for piezo-photocatalytic degradation of ofloxacin, Nanomaterials 15 (2025) 792, https://doi.org/10.3390/nano15110792.
[124] R.S. Guo, L.H. Jin, X.Y. Zhang, Y. Zhang, Bimetal doping enhanced polarization electric field in $BiFeO_3$ for piezocatalytic U(VI) reduction and hydrogen production, Appl. Catal. B Environ. 367 (2025) 125113, https://doi.org/10.1016/j.apcatb.2025.125113.
[125] Q. Xu, J. Jiang, X. Sheng, Q. Jing, X. Wang, L. Duan, H. Guo, Understanding the synergistic effect of piezoelectric polarization and the extra electrons contributed by oxygen vacancies on an efficient piezo-photocatalysis CO_2 reduction, Inorg. Chem. Front. 10 (2023) 2939–2950, https://doi.org/10.1039/d3qi00405h.
[126] P. Su, D. Zhang, X. Yao, T. Liang, N. Yang, D. Zhang, X. Pu, J. Liu, P. Cai, Z. Li, Enhanced piezo-photocatalytic performance in $ZnIn_2S_4$/$BiFeO_3$ heterojunction stimulated by solar and mechanical energy for efficient hydrogen evolution, J. Colloid Interface Sci. 662 (2024) 276–288, https://doi.org/10.1016/j.jcis.2024.02.058.
[127] Y. Pu, B. Zhou, J. Bing, L. Wang, M. Chen, Y. Shen, S. Gao, M. Zhou, W. Wu, J. Shi, Ultrasound-triggered and glycosylation inhibition-enhanced tumor piezocatalytic immunotherapy, Nat. Commun. 15 (2024) 1–20, https://doi.org/10.1038/s41467-024-53392-1.
[128] Z. Liu, Y. Zheng, S. Zhang, J. Fu, Y. Li, Y. Zhang, W. Ye, 1- x) $Bi_{0.5}Na_{0.5}TiO_{3-x}BiFeO_3$ solid solutions with enhanced piezocatalytic dye degradation, Sep. Purif. Technol. 290 (2022) 120831, https://doi.org/10.1016/j.seppur.2022.120831.
[129] S. Supriya, A review on lead-free-$Bi_{0.5}Na_{0.5}TiO_3$ based ceramics and films: Dielectric, piezoelectric, ferroelectric and energy storage performance, J. Inorg. Organomet. Polym. Mater. 32 (2022) 3659–3676, https://doi.org/10.1007/s10904-022-02418-6.
[130] X. Li, Z. Wang, A. Sasani, A. Baktash, K. Wang, H. Lu, J. You, P. Chen, P. Chen, Y. Bao, S. Zhang, G. Liu, L. Wang, Oxygen vacancy induced defect dipoles in $BiVO_4$ for photoelectrocatalytic partial oxidation of methane, Nat. Commun. 15 (2024) 9127, https://doi.org/10.1038/s41467-024-53426-8.

[131] S. Wang, C. Li, Y. Qi, J. Zhang, N. Wang, M. Liu, B. Zhang, X. Cai, H. Zhang, S. H. Wei, G. Ma, J. Yang, S. Chen, F. Zhang, Etched $BiVO_4$ photocatalyst with charge separation efficiency exceeding 90, Nat. Commun. 16 (2025) 3776, https://doi.org/10.1038/s41467-025-59076-8.
[132] X. Liu, F. Zhang, P. Long, T. Lu, H. Zeng, Y. Liu, R.L. Withers, Y. Li, Z. Yi, Anomalous photovoltaic effect in centrosymmetric ferroelastic $BiVO_4$, Adv. Mater. 30 (2018) e1801619, https://doi.org/10.1002/adma.201801619.
[133] R. Munprom, P.A. Salvador, G.S. Rohrer, Polar domains at the surface of centrosymmetric $BiVO_4$, Chem. Mater. 26 (2014) 2774–2776, https://doi.org/10.1021/cm501087j.
[134] D. Liu, J. Zhang, L. Tan, C. Jin, M. Li, B. Chen, G. Zhang, Y. Zhang, F. Wang, Enhanced piezocatalytic hydrogen evolution performance of bismuth vanadate by the synergistic effect of facet engineering and cocatalyst engineering, J. Colloid Interface Sci. 646 (2023) 159–166, https://doi.org/10.1016/j.jcis.2023.05.040.
[135] Q. Ma, J. Ma, X. Sun, X. Chen, G. Liu, H. Yang, Theoretical and experimental elucidation of synergistic enhanced piezo-photocatalysis and mechanism of $BiVO_4$ for organic pollutant degradation, Mater. Res. Bull. 170 (2024) 112559, https://doi.org/10.1016/j.materresbull.2023.112559.
[136] S. Zhao, Y.Y. Wan, L. Han, B.C. Tian, Z.Y. Duan, R.D. Su, X.B. Li, Advances in ferroelectric and piezoelectric photocatalysts with oxygen vacancy, Carbon Lett. 35 (2025) 287–308, https://doi.org/10.1007/s42823-024-00794-2.
[137] X. Cheng, T. Yu, X.F. Lei, B. Wang, W.N. Mu, X.W. Liu, R. Guo, Regulation of oxygen vacancy by in-situ piezoelectric synthesized $BiVO_4$ to induce spin polarization for boosting the piezo-photocatalytic activity, Chem. Eng. J. 504 (2025) 158900, https://doi.org/10.1016/j.cej.2024.158900.
[138] Y.F. Cui, W. Liu, L.L. Chang, C.C. Wang, S. Pal, J. Briscoe, Z. Wang, Oxygen Vacancy-Mediated Microflower-like Bi_5O_7I for Reactive Oxygen Species Generation through Piezo-Photocoupling Effect, Inorg. Chem. 64 (2025) 1498–1510, https://doi.org/10.1021/acs.inorgchem.4c04751.
[139] Z.Y. Xu, J.J. Wang, H. Cai, T. Li, F. Chen, S.C. Tu, H.W. Huang, X.X. Xu, Efficient photocatalytic and piezocatalytic performance in oxygen-vacant $CdBiO_2Br$ with localized internal electric field, Sep. Purif. Technol. 361 (2025) 131460, https://doi.org/10.1016/j.seppur.2025.131460.
[140] D.W. Xu, Y. Liu, Y.H. Zhang, Z.Y. Shi, M.K. Yang, C. Zhang, B. Liu, Fabrication of pyramid-$BiVO_4$/CdSe composite with controlled surface oxygen vacancies boosting efficient carriers' separation for photocathodic protection, Chem. Eng. J. 393 (2020) 124693, https://doi.org/10.1016/j.cej.2020.124693.
[141] C.M. Deng, H.M. Xu, H.L. Qin, D.S. Xia, D.Y. Li, Q.L. Yu, D.H. Chen, Y. Zheng, Y. J. Wang, Enhancing the separation efficiency of photo-induced carriers in a Bi_2S_3/BiOCl heterostructure by cooperative influence of oxygen vacancies and the interfacial electric field, New. J. Chem. 46 (2022) 9195–9206, https://doi.org/10.1039/D2NJ00976E.
[142] F.X. Wang, R. Liu, Q.F. Xu, C.Y. Zhang, Flower-like Ag_2WO_4/CeO_2 heterojunctions with oxygen vacancies and expedited charge carrier separation boost the photocatalytic degradation of dyes and drugs, Dalton Trans. 51 (2022) 10179–10185, https://doi.org/10.1039/D2DT01420C.
[143] X.C. Liu, M.W. Wang, Y. Li, X.X. Li, J.J. Zhang, S. Yang, J. Wu, L.H. Wang, J.L. Li, F. Li, Bismuth titanate microplates with tunable oxygen vacancies for piezocatalytic hydrogen peroxide production, J. Colloid Interface Sci. 678 (2025) 246–255, https://doi.org/10.1016/j.jcis.2024.09.025.
[144] Z.N. Sha, C.Hu Wang, S.C. Tu, T. Li, F. Chen, H.W. Huang, Piezo-activating oxygen vacancy regulates quantum well effect and p-band center for exceptional photocatalysis, Nano Energy 139 (2025) 110919, https://doi.org/10.1016/j.nanoen.2025.110919.
[145] X.F. Zhou, J.Z. Liu, S.H. Ali, B. Shen, J.W. Zhai, N. Hedin, J.Y. Yuan, Efficient catalytic Production of Reactive Oxygen Species through Piezoelectricity in Bismuth Sulfide Rich in Sulfur Vacancies, Nano Lett. 429 115282 (2024), https://doi.org/10.1021/acs.nanolett.4c02795.
[146] H.P. Shi, Y.N. Liu, Y.B. Bai, H. Lv, W. Zhou, Y. Liu, D.G. Yu, Progress in defect engineering strategies to enhance piezoelectric catalysis for efficient water treatment and energy regeneration, Sep. Purif. Technol. 24 (2024) 13153–13161, https://doi.org/10.1016/j.seppur.2023.125247.
[147] Z.H. Kang, E.Z. Lin, N. Qin, J. Wu, D.H. Bao, Bismuth vacancy-mediated quantum dot precipitation to trigger efficient piezocatalytic activity of Bi_2WO_6 nanosheets, ACS Appl. Mater. Interfaces 14 (2022) 11375–11387, https://doi.org/10.1021/acsami.1c23282.
[148] J. Wang, J. Xie, Z.J. Lu, S.X. Yin, A.Z. Hao, J.D. Hu, Y.L. Cao, Bi vacancy-induced Bi_2O_2S nanosheets for remarkably boosting piezocatalytic degradation of dyes and antibiotic, Mater. Res. Bull. 190 (2025) 113483, https://doi.org/10.1016/j.materresbull.2025.113483.
[149] X.G. Wang, L.C. Chen, R.W. Huang, G.R. Li, X.Y. Pan, Boosting piezocatalytic hydrogen production via bismuth vacancy-engineered BiOCl–Bi_2S_3 heterojunctions fabricated by a light-induced deposition strategy, J. Mater. Chem. A 14 (2026) 10123–10133, https://doi.org/10.1039/D5TA09498D.
[150] J. Roy, S. Roy, D. Mondal, N. Bag, J.R. Chowdhury, S. Ghosh, S. Bardhan, R. Mondal, R. Basu, S. Das, Gd-doped bismuth ferrite nanocomposite: a promising candidate for piezocatalytic degradation of organic dyes and pathogenic *E. coli*, Surf. Interfaces 44 (2024) 103579, https://doi.org/10.1016/j.surfin.2023.103579.
[151] Y.K. Zheng, J.T. Xu, R.Y. Dong, X.C. Xu, J.N. Wang, Q.L. Qiu, K.Q. Wang, Y. Wu, Y.M. He, Zn-induced energy-level and polarization coupling enables highly efficient photo-piezocatalytic nitrogen fixation over layered $PbBiO_2Cl$, Chem. Eng. J. 537 (2026) 176435, https://doi.org/10.1016/j.cej.2026.176435.
[152] K. Zhou, W. Liu, P. Wang, J. Chen, H. Che, B. Liu, Y. Ao, Interfacial C-O covalent bonds improving the piezo-assisted photocatalytic performance of $Bi_4Ti_3O_{12}$@carbon schottky heterojunction, –478020, Chem. Eng. J. 480 (2024) 148012, https://doi.org/10.1016/j.cej.2023.148012.
[153] S.Y. Jiang, Q. Mai, H.M. Xu, Y.B. Ma, B.H. Jia, T.Y. Ma, Piezocatalysis and piezo-assisted catalysis in environmental remediation and energy conversion, Chem. Commun. 62 (2026) 3745–3760, https://doi.org/10.1039/D5CC06489A.
[154] P. Liu, L.M. Dong, Z.P. Zhang, J. Yu, Z. Li, Z.H. Qiao, L.G. Gong, S. Lu, X.X. Jin, F. M. Zhang, A review: recent progress of piezoelectric effect coupled photocatalytic reaction: diverse mechanisms, system/structure design, characterization and application, Catal 2 (2026), https://doi.org/10.1007/s44422-026-00025-x.
[155] L.H. Liu, M.N. Ruang, C.Y. Wang, Z.F. Liu, Optimization of the BiO_8 polar group of $BiVO_4$ by Cl—embedded modification to manipulate bulk-surface carrier separation for achieving efficient Piezo-PEC water oxidation, Appl. Catal. B Environ. 354 (2024) 124117, https://doi.org/10.1016/j.apcatb.2024.124117.
[156] S.Y. Wang, Y.J. Li, K. Lin, Z.F. Li, L. Xu, Z.Y. Yin, J.B. Qiu, Z.W. Yang, Z.G. Song, Enhancing the piezoelectric properties and carrier separation efficiency to improves Bi_2NdO_4Cl piezo-photocatalytic performance by Ce ion doping, Appl. Surf. Sci. 694 (2025) 162841, https://doi.org/10.1016/j.apsusc.2025.162841.
[157] C.R. Zhao, L.Y. Cai, K.Q. Wang, B.X. Li, S.D. Yuan, Z.H. Zeng, L.H. Zhao, Y. Wu, Y. M. He, Novel $Bi_2WO_6/ZnSnO_3$ heterojunction for the ultrasonic-vibration-driven piezocatalytic degradation of RhB, Environ. Pollut. 319 (2023) 120982, https://doi.org/10.1016/j.envpol.2022.120982.
[158] J.Y. Yue, R. Wu, Y. Zhang, N. Zhang, H.T. Jing, S.H. Wei, F.P. Ouyang, The piezoelectric field-induced rearrangement of free carriers unlocks the high redox ability of 1T@2H-MoS_2/Bi_2S_3 piezoelectric catalyst, Appl. Surf. Sci. 623 (2023) 157033, https://doi.org/10.1016/j.apsusc.2023.157033.
[159] K.L. Zhang, X.D. Sun, H.T. Wang, Y.L. Ma, H.W. Huang, T.Y. Ma, Interfacial engineering of Bi_2MoO_6-$BaTiO_3$ Type-I heterojunction promotes cocatalyst-free piezocatalytic H_2 production, Nano Energy 121 (2024) 109206, https://doi.org/10.1016/j.nanoen.2023.109206.
[160] J.W. Bai, J.M. Xiang, C.H. Chen, C.F. Guo, Piezoelectric-effect-enhanced photocatalytic performance in Cr/Nb modified $Bi_4Ti_3O_{12}$/g-C_3N_4 Z-scheme system, Chem. Eng. J. 456 (2023) 141095, https://doi.org/10.1016/j.cej.2022.141095.
[161] J.S. Liu, Y.F. Wu, C. Wang, Z.B. Sun, D.N. Wu, S.X. Gao, Y.B. Cheng, H.Z. Kang, H. L. Shen, K.J. Zhu, Piezo-photocatalysis enhanced separation of charge carriers and catalytic performance in the $Bi_2MoO_6/KNbO_3$ heterojunction, Appl. Catal. A-Gen. 697 (2025) 120224, https://doi.org/10.1016/j.apcata.2025.120224.
[162] Z.M. Yin, T. Liu, Z.S. Zheng, Y.L. Li, J.X. Duan, Efficient photocatalytic degradation of pollutants by piezoelectric effect in the flower sphere $BiTi_5NbO_{14}$/BiOCl heterojunction, Ceramint 51 (2025) 3510–3519, https://doi.org/10.1016/j.ceramint.2024.11.328.
[163] C.C. Zhou, J.S. Wei, Y. Li, H.X. Lin, J. Zhou, Y.Y. Li, Fibrous $MoS_2/Bi_2S_3/BiFeO_3$ ternary heterojunction boosts piezoelectric photocatalytic performance, J. Colloid Interface Sci. 683 (2025) 380–392, https://doi.org/10.1016/j.jcis.2024.12.151.
[164] D.M. Liang, M.X. Huang, W.H. Huang, Z.Q. Huang, H.Y. Hu, T. Gan, Y.J. Zhang, Polarized electric field-modulated growth and shared oxygen-bridged interfacial bonding to construct dual bismuth-based catalyst with atomic-scale interface for efficient piezo-photocatalysis, Chem. Eng. J. 526 (2025) 171026, https://doi.org/10.1016/j.cej.2025.171026.
[165] X.G. Wang, L.C. Chen, R.W. Huang, G.R. Li, X.Y. Pan, Boosting piezocatalytic hydrogen production *via* bismuth vacancy-engineered BiOCl–Bi_2S_3 heterojunctions fabricated by a light-induced deposition strategy, J. Mater. Chem. A 14 (2026) 10123–10133, https://doi.org/10.1039/D5TA09498D.
[166] Y. Yan, Z.P. Rao, W. Cai, X. Yang, Z.H. Wang, R.L. Gao, G. Chen, X.L. Deng, C. L. Fu, Enhanced piezo-photocatalytic performances of visible-light-driven $CdIn_2S_4/SrBi_2Ta_2O_9$ S-scheme heterojunction through ferroelectric polarization effect, J. Photoch. Photobio. A 470 (2026) 116646, https://doi.org/10.1016/j.jphotochem.2025.116646.
[167] Z.P. Rao, Y. Yan, W. Cai, R. Wang, Z.H. Wang, F. Long, Y.L. Ma, C.L. Fu, Achieving remarkable piezo-photocatalytic activity in $Sr_2Bi_4Ti_5O_{18}$/BiOCl sandwich ferroelectric heterojunction with continuous semi-coherent interfaces via selective etching of Aurivillius perovskite solid, J. Colloid Interface Sci. 694 (2025) 137705, https://doi.org/10.1016/j.jcis.2025.137705.
[168] N. Chandrakar, A. Kumar, R. Kumari, R. Singh, E.S. Kunnel, S. Trivedi, D. Guin, C. S.P. Tripathi, Improved piezo-catalysis through integration of dual-active semiconductors in a $NaNbO_3/MoS_2$ heterojunction for degradation of rhodamine B dye and ofloxacin antibiotic, and Cr (VI) reduction, J. Mater. Chem. A 14 (2026) 3391–3405, https://doi.org/10.1039/D5TA06616F.
[169] E.M. Jiao, D.Q. Jia, T. Yu, X.M. Wang, Y.F. Wei, Y. Jiang, M. Yang, M.Y. Xing, Scaling up Piezocatalytic Water Decontamination: Challenges and Opportunities, ACS EST Water 6 (2026) 1392–1402, https://doi.org/10.1021/acsestwater.5c01452.
[170] K.S. Hong, H.F. Xu, H. Konishi, X.C. Li, Piezoelectrochemical effect: a new mechanism for azo dye decolorization in aqueous solution through vibrating piezoelectric microfibers, J. Phys. Chem. C. 116 (2012) 13045–13051, https://doi.org/10.1021/jp211455z.
[171] R.H. Du, S.Y. Yu, L. Kang, L.Y. Li, C.L. Kang, Fabrication of $Bi_4Ti_3O_{12}/MoS_2$ heterojunctions for efficient piezocatalytic degradation of ciprofloxacin in water, Chem. Eng. J. 529 (2026) 173269, https://doi.org/10.1016/j.cej.2026.173269.
[172] L.L. Chang, W. Ma, Y. Yu, W. Gong, M.L. Li, B.Y. Cao, S. Xu, X.T. Wang, Interfacial piezoelectric potential-enhanced *Z*-scheme charge separation in ZnO/BiOCl heterojunctions for ultrafast antibiotic degradation, Chem. Eng. J. 530 (2026) 173484, https://doi.org/10.1016/j.cej.2026.173484.
[173] Q.Q. Huang, F.X. Zhu, F.Y. Xiao, G.L. Zhang, H.M. Hong, J.R. Bi, S. Yan, H.S. Hao, Construction of PVDF-HKUST-1/$BiVO_4$ hybrid electrospun flexible fiber membrane for enhanced piezo-photocatalytic reduction performance of Cr (VI),

Colloid Surf. A 693 (2024) 134046, https://doi.org/10.1016/j.colsurfa.2024.134046.
[174] R.S. Guo, L.H. Jin, Y. Zhang, Piezo-catalysis in $BiFeO_3$@In_2Se_3 Heterojunction for High-Efficiency Uranium Removal, Small 20 (2024) 2307946, https://doi.org/10.1002/smll.202307946.
[175] Y.Q. Xie, Z.Q. Zhang, J. Wang, J.J. Huang, D.Z. Shi, F. Chen, Piezoelectric-driven hydrogen peroxide production and in-situ utilization for organic wastewater decontamination and synchronous disinfection: Efficacy, mechanisms and comprehensive assessments, Water Res. 284 (2025) 123977, https://doi.org/10.1016/j.watres.2025.123977.
[176] L. Lin, Q. He, Y.X. Chen, B.L. Wang, L. Zhang, X.X. Dai, Y.Y. Jing, H. Chen, J. Q. Liao, Y.H. Mao, Y.S. Zhang, Y. Wang, MoS_2/polyaniline (PANI)/polyacrylonitrile (PAN)@$BiFeO_3$ bilayer hollow nanofiber membrane: Photocatalytic filtration and piezoelectric effect enhancing degradation and disinfection, J. Colloid Interface Sci. 644 (2023) 29–41, https://doi.org/10.1016/j.jcis.2023.04.069.
[177] M. Ali, H. Hussain, M. Ali, S. Aman, W.W. Yang, Z. Ali, L. Li, Y.Z. Jiang, M. Yousaf, Regulating a NaF-Rich SEI layer for dendrite-free sodium metal batteries using trifunctional halogenated covalent organic framework separators, Adv. Sci. 12 (2025) 03693, https://doi.org/10.1002/advs.202503693.
[178] Z. Ali, M.B. Shafqat, M.T. Ahsan, S.B. Li, W.T. Zhao, Y.L. Hou, Nucleophilic Sn seeding and interface engineering for highly stable sodium metal batteries, Small 21 (2025) 2406325, https://doi.org/10.1002/smll.202406325.
[179] K. Wang, J. Li, J. Qiu, J. Sunarso, S. Liu, The mechanism of piezocatalysis: energy band theory or screening charge effect? Angew. Chem. Int. Ed. 61 (2022) e202110429 https://doi.org/10.1002/anie.202110429.
[180] X. Ning, A. Hao, Y. Cao, R. Chen, J. Xie, Z. Lu, J. Hu, D. Jia, Construction of MXene/Bi_2WO_6 Schottky junction for highly efficient piezocatalytic hydrogen evolution and unraveling mechanism, Nano Lett. 24 (2024) 3361–3368, https://doi.org/10.1021/acs.nanolett.3c04959.
[181] C.Y. Wang, F. Chen, E. Chen, T. Chen, T.Y. Ma, H.W. Huang, Unveiling strong electric fields of ultrafine hollow nanotubes axially orienting asymmetric polar [Bi_5O_7] units for efficient piezocatalytic water splitting, ACS Nano 19 (2025) 22387–22401, https://doi.org/10.1021/acsnano.5c06046.
[182] P.W. Jia, J.M. Li, H.W. Huang, Piezocatalysts and piezo-photocatalysts: from material design to diverse applications, Adv. Funct. Mater. 34 (2024) 2407309, https://doi.org/10.1002/adfm.202407309.
[183] X.Y. Ma, R. Li, Z. Li, L. Zhang, Y.J. Gao, K. Nie, D. Zhou, Q. Ji, C. Wang, Z. H. Zhang, Y.T. Li, M.D. Que, J.Y. Qu, Piezoelectric polarization-induced photogenerated carriers transfer coupled with active electron transport Z-scheme heterojunction synergistic optimization of $BiFeO_3$/CdS composite photocatalysts for hydrogen production, J. Environ. Chem. Eng. 13 (2025) 115049, https://doi.org/10.1016/j.jece.2024.115049.
[184] K. Li, W. You, Y. Zhu, W. Wang, L. Wang, Y. Liu, Q. Ge, T. Wang, R. Wang, X. Ruan, H. Cheng, L. Zhang, Strong electric fields on water microdroplets enable near-unity selectivity in H_2O_2 photosynthesis, J. Am. Chem. Soc. 147 (2025) 36136–36145, https://doi.org/10.1021/jacs.5c06077.
[185] J.H. Zhang, Z.M. Ge, J. Wang, D.C. Zhong, T.B. Lu, Hydrogen-bonded organic frameworks for photocatalytic synthesis of hydrogen peroxide, Nat. Commun. 16 (2025) 2448, https://doi.org/10.1038/s41467-025-57939-8.
[186] Y.Y. Zhou, H.J. Dong, Z.F. Xu, Q.B. Zha, M.S. Zhu, Y. Meng, Carbon modification facilitates piezocatalytic H_2O_2 production over BiOCl nanosheets: correlation between piezoresponse and surface reaction, Appl. Catal. B Environ. 343 (2024) 123504, https://doi.org/10.1016/j.apcatb.2023.123504.
[187] M.Y. Zhang, Y.S. Jiang, F. Chen, Y.L. Zhang, Z. Li, F.M. Shi, B. Liu, X.Q. Huang, Y. F. Chen, Piezo-photocatalytic flowing synthesis of hydrogen peroxide in water using a piezoelectric heterojunction, ACS Sustain. Chem. Eng. 13 (2025) 2966–2977, https://doi.org/10.1021/acssuschemeng.4c10017.
[188] X.X. Li, S. Wang, Y.C. Bi, Z.J. Shen, J.T. Han, H.F. Li, Recent advances in 2D nanomaterials as photocatalysts for sustainable CO_2 reduction, Chem. Eng. J. 542 (2026) 178146, https://doi.org/10.1016/j.cej.2026.178146.
[189] Y.T. Ye, X. Zhou, Y.P. Chen, L.K. Wang, Q. Tang, The effect of electrolyte alkali cations on CO_2 electroreduction in atomically precise $Ag_{25}(SR)_{18}$ nanoclusters, Catal. Sci. Technol. 16 (2026) 3799, https://doi.org/10.1039/d6cy00350h.
[190] H.J. Yu, M. Wang, Y.H. Jiao, Y.X. Wu, R.F. Zhao, F. Guo, X.Q. Zhan, J. Han, Polarization modulated engineering via W doping in Bi_3TiNbO_9 nanosheets for enhancing synergistic piezo-photocatalytic CO_2 reduction, Colloid Surf. A 723 (2025) 137304, https://doi.org/10.1016/j.colsurfa.2025.137304.
[191] C.J. Li, J. He, T.L. Cai, X.L. Chen, H.C. Tao, Y.T. Zhou, M.S. Zhu, Surface oxygen vacancies of BiOBr regulating piezoelectricity for enhancing efficiency and selectivity of photocatalytic CO_2 reduction, Chin. J. Catal. 74 (2025) 130–143, https://doi.org/10.1016/S1872-2067(25)64649-3.
[192] X.Q. Wang, K. Li, W.Y. Xu, D.Y. Wang, Y. Wang, J.K. Feng, Y. Chen, X.Y. Liu, Z. S. Xu, X.J. Liu, S.H. Ge, H. Liu, J.H. Li, Leveraging piezo-augmented copper-induced bacterial death of sub-1 nm CuO-$SrTiO_{3-x}$ heterojunction nanosheets for osteomyelitis eradication, J. Nanobiotechnol 24 (2026) 464, https://doi.org/10.1186/s12951-026-04380-8.
[193] Y.Z. Gao, Y.C. Zhang, S.Y. Zhang, Z.W. Yang, W.J. Liu, J. Zhang, Z.P. Gu, X. C. Chen, Synergistic piezo-immunotherapy enabled by lithium-doped $SrTiO_3$ nanocatalysts for potent tumor ablation through ROS generation and immune activation, Regen. Biomater. 13 (2026) rbag030, https://doi.org/10.1093/rb/rbag030.
[194] L.X. Jing, F. Zhuang, W. Feng, H. Huang, Y. Chen, B.J. Huang, Doping-engineered piezoelectric ultrathin nanosheets for synergistically piezo-chemocatalytic antitumor and antibacterial therapies against cutaneous melanoma, Small 20 (2024) 2401171, https://doi.org/10.1002/smll.202401171.
[195] L. Yang, B.S. Tian, Y. Xie, S.M. Dong, M.Q. Yang, S.L. Gai, J. Lin, Oxygen-vacancy-rich piezoelectric Bio2-x nanosheets for augmented piezocatalytic, sonothermal, and enzymatic therapies, Adv. Mater. 35 (2023) 2300648, https://doi.org/10.1002/adma.202300648.
[196] C.R. Xiao, R.X. Wang, R.M. Fu, P. Yu, J.X. Guo, G.P. Li, Z.G. Wang, H.G. Wang, J. J. Nie, W.F. Liu, J.X. Zhai, C.H. Li, C.L. Deng, D.F. Chen, L. Zhou, C.Y. Ning, Piezo-enhanced near infrared photocatalytic nanoheterojunction integrated injectable biopolymer hydrogel for anti-osteosarcoma and osteogenesis combination therapy, Bioact. Mater. 34 (2024) 381–400, https://doi.org/10.1016/j.bioactmat.2024.01.003.
[197] Y.B. Chen, X.F. Wan, Y. Yue, S. He, J. Cao, W.X. He, T.T. Tai, D. Wang, Z.K. Zhou, Y. Deng, Low-intensity ultrasound-activated cavitation effect triggers piezoelectric catalysis coordinating respiratory chain interference tactics against bacterial infection, Adv. Funct. Mater. 35 (2025) 2419426, https://doi.org/10.1002/adfm.202419426.
[198] C. Peng, W.T. Wu, H.X. Huo, J. Li, E. Wang, Defect-boosted piezoelectric and nanozymatic synergetic catalysis for deep bacterial abscess therapy, ACS Nano 19 (2025) 21830–21843, https://doi.org/10.1021/acsnano.5c05806.
[199] Q.P. Zhang, J. Tu, Y.Q. Jiang, H.H. Wang, W.X. Xue, C.Y. Dong, R.Z. Ouyang, Y. Q. Miao, Bismuth based nanomaterials, Des. Synth. Appl. Tumor Ther. Colloid Surf. B 256 (2025) 114992, https://doi.org/10.1016/j.colsurfb.2025.114992.
[200] V. Vijayakanth, T. Viswanathan, R. Shalini, A. Manohar, N.K. Sahu, M. R, B.A. Al-Asbahi, K. Chintagumpala, Superparamagnetic hyperthermia and cytotoxicity properties of $BiFeO_3$ nanoparticles, Appl. Phys. A 130 (2024), https://doi.org/10.1007/s00339-023-07151-6.
[201] X.Y. Zhang, F.N. Gao, Y.Z. Dai, M.G. Wang, J. Liu, Safe-by-design strategies towards bismuth-based nanomaterials in tumor diagnosis and therapy, Nano Today 62 (2025) 102714, https://doi.org/10.1016/j.nantod.2025.102714.
[202] M.V. Cosme, P.L. Oliveira, C.C.L. Arruda, N.F. Vasconcelos, M. Navarro, A. M. Benko-Iseppon, D.V. Freitas, A.C. Brasileiro-Vidal, Aqueous glutathione-capped Bi2S3-GSH nanocrystals: electrosynthesis and biological toxicity assessment, J. Drug. Deliv. Sci. Tec. 124 (2026) 108627, https://doi.org/10.1016/j.jddst.2026.108627.